Technische Universität München
TUM School of Medicine and Health

Selecting individualized therapeutic targets using a CRISPR/Cas9 screening pipeline in an *in vivo* PDX leukemia model

Diana M. Amend

Vollständiger Abdruck der von der TUM School of Medicine and Health der Technischen Universität München zur Erlangung des akademischen Grades einer

Doktorin der Naturwissenschaft (Dr. rer. nat.)

genehmigten Dissertation.

Vorsitz: Prof. Dr. Julian Grünewald

Prüfer der Dissertation:

1. Prof. Dr. Marc Schmidt-Supprian
2. apl. Prof. Dr. Arnd Kieser

Die Dissertation wurde am 30.08.2023 bei der Technischen Universität München eingereicht und durch die TUM School of Medicine and Health am 20.12.2023 angenommen.

Table of Contents

Abstract

Precision medicine is an innovative approach that involves tailoring medical treatments to the specific needs of individual patients and revolutionized cancer treatment with many targeted therapies. However, suitable biomarkers for predicting patient-individual targeted drugs are missing. The currently used biomarkers are mostly descriptive, while functional tests for biomarker prediction are just starting, so far restricted to drug testing *in vitro*. Functional tests are of particular interest as numerous anti-cancer drugs cannot be assigned to a specific descriptive biomarker so far.

The present proposal aimed to evaluate whether CRISPR/Cas9 dropout screens might represent a suitable tool to prioritize therapeutic targets in individual leukemic patient samples using patient-derived xenograft (PDX) models *in vivo*. The aim of the CRISPR/Cas9 screens was to identify patient-specific dependencies by knocking out specific genes for patient-individual drug prediction. We designed a sgRNA library targeting druggable and cancer-relevant genes; while most published CRISPR/Cas9 screens targeted the whole genome *in vitro* in cell lines, we tested small customized screens in an *in vivo* model. To ensure the quality of our screen, we implemented several thresholds and quality measures. We started with ten different PDX models, five from acute lymphoblastic leukemia (ALL) and five from acute myeloid leukemia (AML) samples. All ALL samples passed the quality control, while three of the five AML PDX models had to be excluded at this step.

Through the *in vivo* CRISPR/Cas9 screening, we discovered 24 commonly depleted genes, shared between several, but not all PDX models and thus represent patient-individual gene dependencies. Several dropout genes participate in epigenetic pathways and chromatin remodeling via the SWI/SNF complex. The strongest depleted genes for which targeted drugs are available were *XPO1, HDAC3, NEDD8, MCL1,* and *BCL2.* In future work and as an outlook, others will now use my results and target these genes with the respective targeted drugs in preclinical trials in PDX models *in vivo*.

All in all, I established CRISPR/Cas9 screens in PDX models *in vivo* as an attractive functional tool for precision medicine and showed that the screens identify patient-individual gene dependencies. Warranting further research, our CRISPR/Cas9 tool might add to the precision medicine pipeline to predict patient-individual drug responses.

Zusammenfassung

Personalisierte Medizin ist ein innovativer Ansatz um eine Therapieform auf das spezifische und individuelle Bedürfnis eines Patienten anzupassen. Zielgerichtete Therapie ist solch ein Ansatz und hat die Krebsbehandlung in den letzten Jahren immer mehr personalisiert. Jedoch sind die dafür verwendeten Biomarker meist deskriptiv und funktionale Tests für die Bestimmung neuer Biomarker sind noch selten und auf *in vitro* Tests beschränkt. Funktionale Test sind aber daher wichtig, da es viele Krebs Medikamente gibt, die keinem spezifischen, deskriptiven Biomarker zugeordnet werden können.

In der vorliegenden Arbeit haben wir untersucht, ob CRISPR/Cas9-Dropout-Screens ein geeignetes Tool zur Priorisierung therapeutischer Targets in einem *in vivo* Patienten-abgeleiteten Xenograft-Modell (PDX) der akuten Leukämien sind. Das Ziel des CRISPR/Cas9 Screens war, durch Knockouts Patienten-spezifische Abhängigkeiten zu identifizieren, welche dann eine personalisierte Therapie Vorhersage ermöglichen. Wir haben eine sgRNA Library entworfen, die auf krebsrelevante Gene, mit einem assoziierten Medikament abzielt. Während die meisten veröffentlichen Screens *in vitro* und in Ziellinien durchgeführt wurden, haben wir eine kleine, spezifische Library in einem *in vivo* Model getestet. Um die Qualität unserer Screens sicherzustellen, haben wir mehrere Schwellenwerte und Qualitätsmaßstäbe eingeführt. Wir sind insgesamt mit zehn verschiedenen PDX Proben gestartet (fünf ALL und fünf AML Proben). Nach dem Durchlaufen der Qualitätskontrollen mussten jedoch zwei AML Proben exkludiert werden.

Mit den *in vivo* Screens in den restlichen sieben Proben haben wir 24 generelle Abhängigkeiten identifiziert, welche in mehrerer aber nicht allen Proben gefunden wurden und somit Patienten-spezifische Abhängigkeiten darstellen. Mehrere dieser Gene sind über den SWI/SNF Komplex an epigenetischen Signalwegen und der Chromatin Umstrukturierung beteiligt. Die Gene mit der signifikantesten Abhängigkeit, und für die spezifische Medikament verfügbar sind, waren *XPO1, HDAC3, NEDD8, MCL1* und *BCL2*. In Folgeexperimeten und als Ausblick werden meine Ergebnisse verwendet um die PDX Proben mit den entsprechenden zielgerichteten Medikamenten in präklinischen *in vivo* Versuchen zu therapieren.

Zusammengefasst habe ich *in vivo* CRISPR/Cas9-Screens in PDX-Modellen als attraktives funktionelles Tool für die personalisierte Medizin etabliert und gezeigt, dass die Screens patientenindividuelle Genabhängigkeiten identifizieren können. Unser

CRISPR/Cas9-Tool könnte die Pipeline der personalisierten Medizin ergänzen, um ein patientenindividuelles Ansprechen auf spezifische Medikamente vorherzusagen.

List of Abbreviations

°C	Degree Celsius
AL	Acute leukemia
ALL	Acute lymphoblastic leukemia
AML	Acute myeloid leukemia
APC	Allophycocyanin
BCL2/Bcl-2	B-cell lymphoma 2
BM	Bone marrow
BSA	Bovine serum albumin
Cas9	Human codon-optimized Streptococcus pyogenes Cas9
CNS	Central Nervous System
cPPT	central polypurine tract
CRISPR	Clustered regularly interspaced short palindromic repeats
CSF	Cerebrospinal fluid
d	day
DMEM	Dulbecco's modified Eagle's medium
DMSO	Dimethylsulfoxid
DNA	Deoxyribonucleic acid
dNTP	Desoxyribonucleosid triphosphate
E. coli	Escherichia coli
Edta	Ethylenediaminetetraacetic acid
EF1α	Human elongation factor-1 alpha
eFFly	Enhanced Firefly
eGFP	Enhanced green fluorescent protein
f	Female
FACS	Fluorescence-activated cell sorting
FBS	Fetal bovine serum
FDA	Food and drug administration
FDR	False discovery rate
Fig.	Figure
FLT3	Recombinant human FMS-like tyrosine kinase 3 ligand
FSC	Forward scatter
Fwd.	forward
g	Relative centrifugal force
gDNA	Genomic DNA
h	Hour
HF	High fidelity
i.v.	Intravenous
IL3	Recombinant human interleukin 3
InO	Inotuzumab ozogamicin
LDTA	Limiting dilution transplantation assay
LIC	Leukemia initiating cell
LTR	Long terminal repeat
m	Male
MACS	Magnetic cell separation
MAGeCK	Model-based Analysis of Genome-wide CRISPR/Cas9 Knockout
min	Minute
mTagBFP	Monomeric blue fluorescent protein
NGS	Next generation sequencing
NOD	Non-obese diabetic
ns	Not significant
Oligo	Oligonucleotide
P/S	Penicillin/Streptomycin
P2A	Porcine teschovirus-1 2A
PBS	Phosphate buffered saline
PCR	Polymerase chain reaction
PDX	Patient-derived xenograft
PE	Phycoerythrin

Rev	reverse
RNA	Ribonucleic acid
RRA	Robust rank aggregation
RT	Room temperature
SCF	Recombinant human stem cell factor
SCID	Severe combined immunodeficiency
sec	Second
sgRNA	Single guide RNA
SNV	Single nucleotide variant
SSC	Side scatter
SSFV	Spleen focus-forming virus
T2A	Thosea asigna virus 2A
TKI	Tyrosine Kinase Inhibitor
VAF	Variant allele frequency
w/o	without
WPRE	Woodchuck hepatitis virus post-transcriptional regulatory element

List of Tables

List of Figures

1. Introduction

1.1 Acute leukemia

Leukemia is a disease of the hematopoietic system, once thought to be a single disease and first described in the 4th century (MD et al. 2020). A more detailed classification was done at the end of the 19th century, dividing leukemia into four subgroups based on the altered cell type and their rate of growth: acute myeloid leukemia (AML), acute lymphoblastic leukemia (ALL), chronic myeloid leukemia (CML) and chronic lymphoid leukemia (CLL) (Blackburn, Bender, and Brown 2019; Siegel et al. 2022).

Acute leukemia is the most common cancer in children, with most patients diagnosed with ALL, whereas only 15-20% of children suffer from AML (Quessada et al. 2021). On the other hand, AML predominates in adults with a median age of 68 at diagnosis (Blackburn, Bender, and Brown 2019).

The cancer statistics 2022 revealed 60 650 new leukemia cases per year in the United States, including 6 660 acute lymphoid leukemia cases and 20 050 acute myeloid leukemia cases (Siegel et al. 2022). A closer look at their origins is needed to understand better the differences between the mentioned leukemias.

1.1.1 Acute myeloid leukemia

AML is described as a heterogeneous disease of the hematopoietic system. AML is defined by the abnormal growth and differentiation failure of hematopoietic stem cells (HSCs), resulting in an accumulation of myeloblasts (myeloid precursors) in the bone marrow and peripheral blood. In healthy individuals, an HSC gives rise to myeloid or lymphoid progenitors. Myeloid progenitor cells differentiate into mature types of blood cells like erythrocytes, granulocytes, granulocytes and platelets, whereas lymphoid progenitors give rise to B- and T- lymphocytes (Figure 1) (Duan and Mukherjee 2016).

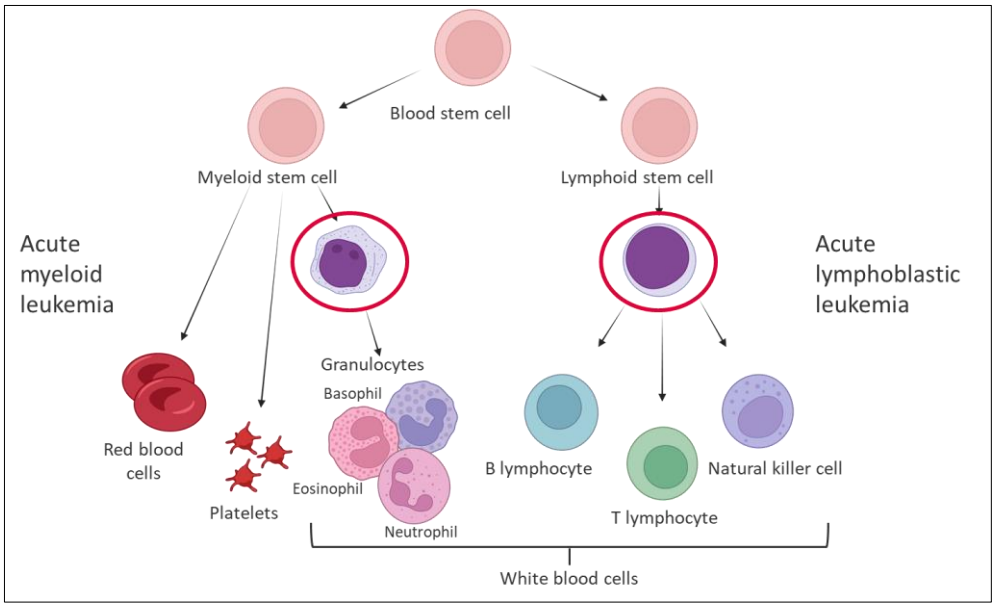

Figure 1: Differentiation arrest causing AML or ALL
Differentiation block results in an accumulation of blast cells (red circles) (Created with BioRender).

The block of differentiation and accumulation of non-functional myeloblasts in AML leads to the typical but unspecific symptoms of bone marrow failure: fatigue, bleeding, recurrent infections and shortness of breath (Khwaja et al. 2016). Patients with those symptoms are diagnosed with AML when myeloblast counts are higher than 20% in the peripheral blood. Additionally, molecular characterization, cytogenetics, cytochemistry and immunophenotyping are used to strengthen the diagnosis further. After the characterizations mentioned above, the AML subtype can be determined. The World Health Organization defined seven different subtypes of AML based on chromosomal translocations, mutations, and cytogenetic parameters (Hwang 2020).
The cytogenetic analysis allows the identification of changes at the chromosomal level. Cytogenetic abnormalities are recognized in 75 to 80% of pediatric AML cases. In *de novo* AML in adults, the rate of chromosomal abnormalities is lower by approximately 56% (Bendari et al. 2020).
The most frequently detected karyotypic abnormality in AML is the t(8;21)(q22;q22.1) rearrangement, occurring in up to 12% of all patients (P. Lin et al. 2008). This translocation is defined by a fusion between the *AML1* gene on chromosome 21 and the ETO gene on chromosome 8, resulting in the two fusion genes: AML1-ETO and ETO-AML1 (Bendari et al. 2020). Patients with t(8;21) have an overall favorable prognosis, defined by a higher response to treatment and a longer median survival compared to other types of AML (Bendari et al. 2020; P. Lin et al. 2008). Opposing this, more complex karyotypes (≥3 cytogenetic abnormalities) or specific chromosomal

aneuploidies are considered to have a poor prognosis due to their more chemoresistant phenotype (Short et al. 2020).

Besides cytogenetics, the advances in genomic techniques improved the understanding of the mutational landscape of AML. The AML genome shows a significantly lower number of mutations than most solid tumors, with an average of five mutations per genome (Short et al. 2020). Despite this small number of mutations, in around 98% of the patients with *de novo* AML, one driver mutation can be identified, with 86% of them harboring ≥ two driver mutations (Papaemmanuil et al. 2016; 'Genomic and Epigenomic Landscapes of Adult De Novo Acute Myeloid Leukemia' 2013).

Therefore, the most frequent mutations and clinically relevant genetic markers in AML are *FLT3, KIT, TP53* and *RAS* mutations (Hou and Tien 2020). Besides these mutations, several genes involved in epigenetic modification such as *IDH, TET2, DNMT3A, ASCL1, EZH2* and *KMT2A* are frequently mutated in AML patients (Hou and Tien 2020).

The prognostic impact of most of the identified mutations is still uncertain. Currently, only some can be correlated to a clear prognosis, like mutations in the FMS-like tyrosine kinase 3 (*FLT3*), the most frequent genetic alteration in AML patients. Those patients are known to have a poor prognosis. There are two major types of *FLT3* mutations: internal tandem duplication (ITD) mutations in the juxtamembrane domain (*FLT3*-ITD) or a deletion or point mutation in the tyrosine kinase domain (*FLT3*-TKD) (Kiyoi, Kawashima, and Ishikawa 2020).

Nevertheless, the knowledge about frequently occurring mutations, chromosomal aberrations and karyotypes lays a foundation to understand better the disease and its underlying mechanisms, a pitfall to refine and invent therapeutics.

1.1.2 Current treatment strategies in AML

Although the recent advances in the genetic characterization of AML, the standard of care has mostly stayed the same since its development in 1970.

The combination of Anthracycline and Cytarabine, known as the "7 + 3" regimen, is used as induction therapy in young adults (age < 60) and fit elderly patients to achieve complete remission (CR) preferably without the measurable residual disease (MRD). MRD describes a small number of leukemic cells that remain after and during treatment. Complete remission is achieved in 60-80% of the young, *de novo* AML patients (Blackburn, Bender, and Brown 2019; Medinger, Lengerke, and Passweg

2016a). The rate of CR is strongly reduced to 38-62% in elderly patients (>60 years) (Medinger, Lengerke, and Passweg 2016a). The poor complete remission rate in elderly patients is caused by a lower tolerance of high-dose chemotherapeutics and a higher likelihood of an adverse cytogenetic risk profile (De Kouchkovsky and Abdul-Hay 2016).

After successful induction therapy, it is essential to eradicate residual disease by following consolidation therapy. There are two main options for consolidation therapies: further chemotherapy or hematopoietic stem cell transplantation (HSCT) (Medinger, Lengerke, and Passweg 2016b). In younger adults with a favorable prognosis, the follow-up chemotherapy successfully prolongs remission and improves survival. Patients with intermediate or high risk instead receive high doses of chemotherapy followed by HSCT (Medinger, Lengerke, and Passweg 2016a). Especially in fit patients with an intermediate or high-risk AML, who achieve CR during induction therapy, the HSCT is the most effective long-term treatment with a cure rate of 50-60% (Medinger, Lengerke, and Passweg 2016a; Passweg et al. 2016).

Nevertheless, most treated patients relapse (40-50% in younger and the majority in elderly patients). Patients that do not reach complete remission after two cycles of induction therapy are diagnosed with a refractory AML (Thol and Ganser 2020). The high percentage of relapse or refractory patients and the poor treatment options of elderly patients show the need for new treatment options.

The progress of genetic technologies led to a better description and understanding of the mutational profile of AML and several new agents for AML treatment. Between 2017 and 2019, the Food and Drug Administration (FDA) approved eight new agents for treating AML (DiNardo and Perl 2019). The development of targeted therapies for some of the common genetic mutations has led for example to the approval of *FLT3* and *IDH1/2* inhibitors (Short et al. 2020).

Although new treatment options became available, therapy resistance and relapse remain major clinical challenges. This problem became more pronounced when the first patients developed resistance to the targeted therapies (Scholl et al. 2020).

1.1.3 Acute lymphoblastic leukemia

A differentiation block in the lymphoid lineage defines acute lymphoblastic leukemia (ALL). This block in differentiation results in an accumulation of lymphoid progenitor cells in the bone marrow and peripheral blood. ALL is seen in children and adults, while 80% of ALL occurs in children (Terwilliger and Abdul-Hay 2017). Pediatric ALL is

curable in 90% of the cases, whereas in adults diagnosed with ALL the cure rate drops below 40% (Samra et al. 2020). This dismal prognosis originates from a poor prognosis biology and lower tolerance of intensive chemotherapy.

The World Health Organization differentiates between ALL as B-lymphoblastic leukemia/lymphoma (B-ALL9 or T-lymphoblastic leukemia/lymphoma (T-ALL) with T-ALL summing up to 10-15% of diagnosed cases (Arber et al. 2016; Teachey and Pui 2019). Patients diagnosed with T-ALL are mainly older, show a poorer tolerance of chemotherapy, are in general more resistant to chemotherapy and are known to have a worse outcome prediction than B-ALL patients do (Teachey and Pui 2019). B-ALL is divided into two subgroups for further classification: B-ALL not otherwise specified and B-ALL with recurrent genetic abnormalities (Terwilliger and Abdul-Hay 2017).

Patients with ALL mainly present with nonspecific symptoms and signs of bone marrow failure and “B-symptoms” like night sweats, fever and weight loss (Terwilliger and Abdul-Hay 2017). ALL is diagnosed by 20% or more lymphoblasts in the peripheral blood or bone marrow (Alvarnas et al. 2015). Following the blast count, flow cytometry complemented by cytogenetics and immunophenotyping are used for further risk evaluation and diagnosis. Since involvement of the central nervous system (CNS) occurs in 5-8% of ALL patients a cerebrospinal fluid (CSF) analysis is the standard of care to detect migrated blasts in the CSF (Terwilliger and Abdul-Hay 2017; Deak et al. 2021).

Chromosomal alterations are the hallmark of ALL patients and are therefore described for decades. In patients with B-ALL chromosomal alterations are defined by hyperdiploidy with a gain of at least five chromosomes, hypodiploidy with less than 44 chromosomes and recurrent chromosomal translocations like the Philadelphia chromosome (Ph) t(9;22)(q34;q11). This translocation encodes the BCR-ABL1 protein, leading to a constitutively active tyrosine kinase (Inaba, Greaves, and Mullighan 2013). Rearrangements of *KMT2A* (also known as mixed lineage leukemia, or *MLL*), a histone methyltransferase, involving 11q23 with different fusion partners are an additional possible translocation (Inaba, Greaves, and Mullighan 2013). T-ALL is characterized by chromosomal aberrations that activate different oncogenes like *TAL1, LMO2, TLX1, TXL3* and *HOXA* (Mroczek et al. 2021). The most common pathway abnormality observed in 70-80% of all T-ALL patients is found in the Notch1 pathway, often together with a loss of the *CDKN2A* locus, which encodes tumor suppressors like p16INK4A and p14ARF (Mroczek et al. 2021; Teachey and Pui 2019). In general, there is much

more knowledge about B-ALL's genetic abnormalities than T-ALL due to its rare occurrence and higher heterogeneity (Mroczek et al. 2021).
The increase in the genetic profiling capabilities of patient cells during the last years utilizes the technological progress of innovative technologies like next-generation sequencing (NGS). This made several more precision treatment options available and enhanced risk stratification.

1.1.4 Current treatment strategies in ALL

The standard chemotherapy treatment procedure in ALL patients consists of induction, consolidation and maintenance therapy steps. Induction therapy aims to achieve CR together with normal hematopoiesis. Induction therapy includes chemotherapeutics like Vincristine, Corticosteroids and Anthracycline (Terwilliger and Abdul-Hay 2017). For patients diagnosed with a Philadehia-positive leukemia, tyrosine kinase inhibitors (TKI) like Imatinib and Dasatinib are included as targeted therapy (De Kouchkovsky and Abdul-Hay 2016). For CNS treatment or prophylaxis, chemotherapy is directly injected into the cerebrospinal fluid (intrathecal chemotherapy) (Thastrup et al. 2022). After the induction therapy and achieving remission, consolidation treatment follows. Generally, consolidation and maintenance treatment aim to remove any remaining leukemic cells and maintain this status. Depending on the risk, genetic background and MRD status, there are several further treatment options. Patients may receive more chemotherapy in higher doses and more cycles, adding immunotherapy and targeted therapy or as a last option a HSCT.
With these treatment strategies, the cure rate of pediatric ALL patients reached 90% (Samra et al. 2020; Rose-Inman and Kuehl 2014), whereas adults diagnosed with ALL have a dismal prognosis and a cure rate below 40% (Samra et al. 2020; Rose-Inman and Kuehl 2014). Noteworthy, the adaption of pediatric-inspired intense chemotherapy for the treatment of young adults (<40 years) led to an improvement in the overall survival rate of 65-80% (Stock et al. 2019; Wieduwilt et al. 2021).
Before TKIs became available in 2000, Philadelphia-positive patients' outcomes were very poor. Nevertheless, the combinatory treatment of TKIs and chemotherapeutics led to complete remission rates of 90-95% and long-term survival of 40-50% in Philadelphia-positive patients (Salvaris and Fedele 2021). The application of TKIs showed the power of targeted therapy. These numbers contribute to the notion that targeted therapies can elevate cure rates to new heights, as shown for other agents. Patients with *KMT2A* rearrangements are associated with a poor prognosis and the

arrangement indicates HSCT. KMT2A-fusion proteins are known to bind DNA and chromatin which results in an aberrant gene expression pattern, promoting leukemogenesis. Menin, a *KMT2A* cofactor is the most promising target for the treatment of *KMT2A*-rearranged leukemias (Salvaris and Fedele 2021).

Besides those targeted agents that target only disease-specific mutations there are additional immunotherapeutic approaches for targeting more general vulnerabilities in ALL. The CD19/CD3 bispecific T-cell engager Blinatumomab, the anti-CD22 antibody-drug conjugate Inotuzumab ozogamicin (InO) and the chimeric antigen receptor (CAR) T-cell therapy are new treatment options for patients with B-ALL (Salvaris and Fedele 2021). Especially for patients with relapsed or refractory ALL the treatment with Blinatumomab and InO improved the remission and survival rate, regardless of the patient's age when compared to the standard chemotherapy regimen (H. M. Kantarjian et al. 2016; H. Kantarjian et al. 2017). Anti-CD19 CAR-T cell therapy for the treatment of B-cell malignancies was approved by the US Food and Drug Administration (FDA) in 2017 (Schuster et al. 2017). A treatment study of children and young adults (3 to 23 years) with second generation anti-CD19 CAR-T cells led to an overall remission rate of 81% (Maude et al. 2018). An additional advantage of the anti-CD19 CAR-T therapy cells is their reported presence within the cerebrospinal fluid of treated ALL patients, resulting in a clearance of the CNS from leukemic cells (Grupp et al. 2013; He et al. 2019). But besides its great potential to improve the survival of B-cell malignancies there are some serious challenges such as cytotoxicity, cytokine release syndrome and immune effector cell-associated neurotoxicity syndrome (ICANS) (Sheykhhasan, Manoochehri, and Dama 2022).

The development of new therapies improved the cure rate as well as the survival rate of patients diagnosed with ALL. Besides these treatment advances there remain several challenges and needs for new approaches e.g. treatment of T-ALL cells and older patients.

1.1.5 Remaining challenges

After induction therapy, a chemotherapy-surviving leukemia cell population remains in some patients. This cell population gives rise to relapse of the disease and is defined as MRD. The detection of those chemotherapy-surviving leukemia cells is important for the outcome prediction and the selection of further therapy strategies in both ALL and AML patients (Heuser et al. 2021; Kruse et al. 2020; Saygin et al. 2022). Therefore, targeting the MRD is crucial for long-term survival. The recent years improved its

detection by sensitizing the evaluation method and by the enhanced knowledge about the genetic landscape of patients. New approaches helped eradicate MRD in patients with B-ALL whereas approaches to target MRD in T-ALL are urgently needed (Saygin et al. 2022). The detection of MRD in AML patients is more challenging due to the genetic and immunophenotypic heterogeneity of AML and needs further investigation (Blachly, Walter, and Hourigan 2022).

Besides MRD, drug resistance is a huge challenge and the main reason for treatmentfailure. Resistance can either be primary or acquired. Primary resistance describes the phenomena of being resistant to treatment before the usage of any anti-tumor drug whereas tumor cells with acquired drug resistance are first sensitive to the treatment and develop resistance during induction therapy (J. Zhang, Gu, and Chen 2019).

Certain types of gene mutations, aberrant activation of PI3K/AKT and autophagy pathways as well as abnormal expression of miRNAs are known to be related to drug resistance in AML patients (J. Zhang, Gu, and Chen 2019). By accessing the status of these risk factors, it is possible to predict an individual patient's risk for developing treatment resistance, nevertheless, it is still unclear how to use those discovered mechanisms to reverse resistance. Resistance not only occurs upon standard chemotherapy but also after targeted treatment. The knowledge on how to overcome resistance to targeted therapies is mainly restricted to *in vitro* and mice findings and needs further patient-closer investigation (Mecklenbrauck and Heuser 2022).

Resistance towards the standard therapy or targeted therapy is also observed in ALL patients. In the majority of cases the resistant patient cells are treated by using a different combination of drugs, without knowing the resistant-causing mechanism (Follini, Marchesini, and Roti 2019). For example, research on resistance mechanisms in ALL patients revealed certain point mutations in the BCR::ABL1 gene resulting in resistance towards TKIs (Jędraszek et al. 2022).

To achieve complete remission in the majority of patients and to be able to treat a relapsing patient successfully, more research on the underlying mechanisms is needed, as well as strategies to provide an even more individually tailored treatment approach.

1.2 Precision medicine

Hematology is a field where the concepts of precision medicine are implemented successfully by several approved targeted therapies. In general, the idea of precision

medicine is the prediction of the right treatment, for the right patient at the right time. The most prominent example is the approval of imatinib (TKI) for the treatment of Philadelphia-positive CML patients. Due to their BCR::ABL1 rearrangement, Philadelphia-positive patients are characterized by a constitutively activated tyrosine kinase. The treatment with a TKI shifted the prognosis of Philadelphia-positive patients from a severe outcome to a favorable prognosis. Besides the TKIs, the development of several small-molecule inhibitors of *FLT3, IDH1/IDH2* and *BCL-2* for the treatment of AML improved those patients' outcomes, too (Döhner, Wei, and Löwenberg 2021).
Although these precision medicine tools often result in treatment improvement, their implementation in the health care systems is difficult and as well as their affordability (Valent et al. 2021). Besides the challenge of providing precision medicine to all leukemia patients, only a small fraction of these patients harbor mutations that can be targeted, even fewer respond to the assigned treatment and several develop resistance (Malani et al. 2022). This shows that not every detected mutation is a dependency for the patient's leukemogenesis. This highlights the need for more functional screening tools for the prediction of a personalized treatment strategy.

1.2.1 Characterization of patient cells for treatment prediction

Although there are disadvantages as described above, precision medicine is increasingly used for therapy decision with descriptive omics-based methods. Omics informally describes different molecular methods like genomics, transcriptomics, proteomics and metabolomics in a large-scale approach.
Several studies and research groups designed clinical trials to access the predictive potential of different sequencing methods for effective drugs.
The 'Individualized Therapy for Relapsed Malignancies in Childhood' (INFORM) is an example of a precision medicine study in Germany. The study includes children with high-risk relapsed/refractory malignancies and aims at predicting individual therapeutic targets. The used descriptive methods for these predictions are whole-exome, low-coverage whole-genome and RNA sequencing together with methylation and expression microarray analyses (Worst et al. 2016; van Tilburg et al. 2021). The 2016 published pilot study characterized 52 patients with an average turnaround time from sampling to the first report of 28 days, identifying potential druggable alterations in 50% of the cohort (Worst et al. 2016). The follow-up study, published in 2021, included a total of 519 pediatric patients with 38 patients suffering from acute leukemias. In 43% of the screened patients, a genetically altered target was identified. Those alterations

were then used to determine the target priority level and patients were sorted into the following priority groups: very high, high and moderate. 42 patients were sorted into the highest target priority group. Out of these patient 42 patients, 20 patients received an individual targeted therapy which resulted in a significantly longer progression-free survival when compared to all other patients (van Tilburg et al. 2021).

A collaborative precision medicine study for AML patients is the BEAT AML trial taking place in the United States, initiated by the Leukemia & Lymphoma Society (LLS). Until then, genetic data of AML patients were predominately used for prognostic measures or treatment decisions after induction therapy, but not for the initial induction therapy decision itself (besides the additional use of *FLT3* inhibitors to standard chemotherapy) (Stone et al. 2017; Uy et al. 2017). Genetic profiling is used to categorize AML patients (≥60 years) into molecularly defined, subtype-specific therapies within 7 days (Burd et al. 2018). The central treatment decision is based on NGS and cytogenetics. A huge achievement of this study is the 7-day window for genetic characterization and treatment since an earlier study showed that a treatment delay of 8 days after diagnosis has no effect on the overall survival of AML patients (Bertoli et al. 2013). In an efficacy update in 2021, 395 suitable patients were enrolled in the study. For 95% of those patients, the genetic and cytogenetic analysis was completed within the 7-day window. 224 patients were assigned to sub-study groups like *KMT2A*-rearranged, TP53 mutated and hypermethylation, defined by the *TET2/WT1* mutations. The 30-day mortality rate was less frequent accompanied by a significantly longer overall survival in patients receiving the targeted treatment in comparison to patients treated with standard chemotherapy (Burd et al. 2018). Overall the BEAT AML study showed a successful precision medicine strategy that is feasible within 7 days, allowing a rapid inclusion of the genomic data into the treatment decision (Burd et al. 2018).

A recently emerging field for better matching of patients to drugs is artificial intelligence, using machine learning. As input these approaches rely on genome-wide expression profiles and *ex vivo* drug screens, leading to therapeutic strategies and disease prediction (S.-I. Lee et al. 2018; Gimeno et al. 2022). This field carries great potential but until now suffers from limited available data sets.

A remarkable fact in the above-described trials is the number of patients that cannot be assigned to a certain group due to lack of identified genetic alterations. For those patients, there is a high need to add more functional tools for the prediction of individualized therapy options. Additionally, there are many therapies that do not have a confirmed biomarker. This also shows the need for a more functional way to predict

individual therapies. A 2022 published study by Malani et al. established a functional precision medicine tumor board (FPMTB) where they generated ex-vivo drug response data and multiomics profiling for 186 AML patients. Actionable drugs were found in 97% of all patients and finally 37 patients were selected for treatment with the predicted drugs. They report a 59% response rate to individual therapies. Additionally this study was able to associate IL-15 overexpression with resistance to *FLT3* inhibitors through combining functional drug response data with multiomics data (Malani et al. 2022).
In January 2023 a group from the St. Judes Hospital in the USA published a similar study, analyzing samples from pediatric patients with ALL (S. H. R. Lee et al. 2023). Performing pharmacogenetic read-outs they accessed the drug response rates of 805 patients, followed by genomics to search for the biological basis of the patien's' drug sensitivity. The study tested the sensitivity of primary leukemia cells to 18 different drugs, from patients representing 23 genetics-defined molecular subtypes. The trial revealed various drug sensitivities across different ALL subtypes. For example, they identified a varying sensitivity of BCR-ABL1 (Ph) and BCR-ABL1 like (Ph-like) leukemic cells to Dasatinib, Mercaptopurine and Prednisolone although their transcriptional profile and somatic genomic composition are comparable.
This work marks a big step to make precision medicine more functional and helps identify the right drug for the right patient at the right time or stage of the disease.

1.2.2 Additional tools to make personalized medicine more functional

The above-mentioned diagnostic methods to make precision medicine more functional are all based on *ex vivo* cultivation of patient cells. Primary patient cells are often hard to culture *in vitro* and limited to a two-dimensional culture. Ongoingly these models are unable to represent the *in vivo* microenvironment and cannot precisely predict drug performance *in vivo* (Dozzo et al. 2022). Despite progresses in the development of three-dimensional cell culture models and the attempt to mimic the bone marrow niche and microenvironment in these models, the use of patient-derived cells in animal models represents a powerful preclinical tool to study leukemogenesis and perform drug screens (Lau et al. 2022).

1.2.3 The patient-derived xenograft (PDX) model for studying leukemia *in vivo*

Mice are a popular mammalian model in research due to their genetic similarity to humans, their small size, short breeding time and low costs for maintenance (Kohnken, Porcu, and Mishra 2017). There are different strategies to study leukemia in mice and

classification is as spontaneous, xenograft, syngeneic mouse models, genetically engineered mouse models and humanized models(Almosailleakh and Schwaller 2019).

The engraftment of patient-derived cells in immune-compromised mice was first described in 1990 and improved lately by using NOD/scid IL2 receptor gamma chain knockout (NSG) mice (Agliano et al. 2008). These model systems are called patient-derived xenograft (PDX) models and are known to be biologically stable and reflect the patient's tumor regarding histopathology, gene expression, genetic mutations and inflammations accurately (Lai et al. 2017). Therefore PDX models are a powerful tool for the investigation of human tumor biology, the identification of therapeutic targets as well as their utilization as preclinical models (Lai et al. 2017; Hidalgo et al. 2014). Although the PDX model brings improvements to cancer research, there remain several limitations like a long engraftment period as well as engraftment failure(Hidalgo et al. 2014).

Our lab established an *in vivo* leukemia model system, allowing serial transplantation that provides a continuous supply of patient-derived xenograft (PDX) cells which can be used for several further studies (Figure 2). Our model system is not limited to ALL samples, but also includes AML samples, which makes it unique worldwide. These repetitively transplanted cells can be genetically engineered by using lentiviral transduction (Vick et al. 2015).

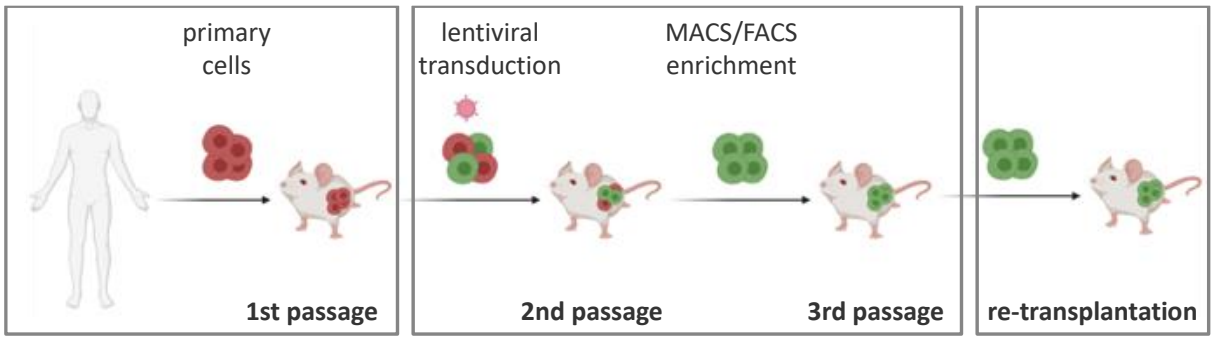

Figure 2: The patient-derived xenograft (PDX) model
Xenotransplantation of primary patient cells generates either AML or ALL PDX models. Transduction and enrichment of PDX cells with lentiviral constructs result in transgenic PDX cells that can be used for further experiments (Created with BioRender).

The establishment and improvement of this leukemia *in vivo* model made several options available and allows research on primary patient material in a suitable microenvironment. To study these patient cells, for example, by introducing specific

knockouts, a genetic engineering tool would be helpful. This was found with the described CRISPR/Cas9 system.

1.2.4 CRISPR/Cas9 system as a functional tool

In 1987 researchers from Osaka University in Japan discovered unusual repetitive sequences, later named CRISPR (clustered regularly interspaced short palindromic repeats), together with their gene of interest, the *iap* gene from the genome of *Escherichia coli* (Y Ishino et al. 1987). Years later, in 1993 a group of Spanish researchers described similar repetitive sequences in an archaeal genome which was followed by more detections in an increasing number of bacteria and archaea (F. J. M. Mojica, Juez, and Rodriguez-Valera 1993). In 2005 the same Spanish researcher identified similarities between the found sequences and sequences of bacteriophages, from which he concluded CRISPR could be an adaptive immune system (Francisco J.M. Mojica et al. 2005). A major addition to the discovery of CRISPR sequences came with the finding of a set of homologous genes, encoding CRISPR-associated (Cas) proteins (Jansen et al. 2002). In 2007 Philippe Horvath and colleagues experimentally showed that the CRISPR system indeed is an adaptive immune system(Barrangou et al. 2007). Following this, in 2012 the CRISPR system was first used to cleave a determined target DNA in an *in vitro* experiment. This experiment, using the CRISPR system as a gene editing tool by Jennifer Doudna and Emmanuelle Charpentier revolutionized molecular life science. The importance of this adaption was honored in 2020 by the Nobel Prize in Chemistry (‘The Nobel Prize in Chemistry 2020’ n.d.).

The most widely used gene editor is the CRIPSR/Cas9 protein, belonging to the CRISPR/Cas Class 2 system, subtype II. The Cas9 system is defined by just one effector protein, a CRISPR RNA (crRNA) having a sequence homologous to the target site and a trans-activating CRISPR RNA (tracrRNA) together forming a functional guide RNA (gRNA) (Yoshizumi Ishino, Krupovic, and Forterre 2018) (see Figure 3).

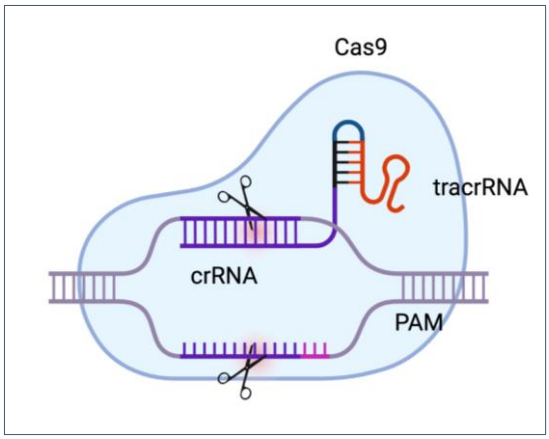

Figure 3: The CRISPR/Cas9 system as a tool for genomic engineering
The system has three components: the endonuclease Cas9, the crRNA, and a tracrRNA. The 20-nucleotide-long crRNA complements the target DNA site and must be followed by a PAM sequence. Guided Cas9 finally introduces a double-strand break of three nucleotides upstream of the PAM sequence (Created with BioRender).

Besides this and due to its origin, the CRISPR system relies on the recognition of self versus non-self sequences. These short foreign motifs, called protospacer adjacent motif (PAM) vary in their sequence and position across the different CRISPR/Cas system types. In the *Staphylococcus pyogenes* Type II system (effector protein = Cas9) the PAM sequence corresponds to a NGG consensus sequence (Gleditzsch et al. 2018).

After the DNA target site was identified by the Cas9 complex, the Cas9 nuclease introduces DNA Double Strand Breaks (DSBs). The activated intrinsic DNA repair machinery then repairs those breaks with one of the two available repair mechanisms in mammals: non-homologous-end-joining (NHEJ) or homology-directed repair (HDR) (Lieber 2010). NHEJ, as the major repair process, reconnects the two ends of the DSBs and by doing so this frequently leads to small insertions or deletions (called indels) which results in a frameshift and therefore to gene knockout.

Due to this mechanism, the CRISPR/Cas9 system is widely used as a genome engineering tool to generate knockouts in different model systems. Besides this, its establishment also enables a fast creation of knockout animals, and multiplex editing in plants and thanks to further improvements the possibility to perform single base editing (J. Y. Wang and Doudna 2023). CRISPR base editors, using a dead Cas9 (lacking nuclease activity) fused to a deaminase, allow changes of single nucleotides without introducing double-strand breaks (Komor et al. 2016).

Besides the mentioned applications, the CRISPR system can also be used to perform functional genetic screens. CRISPR screens allow the simultaneous testing of thousands of individual knockouts in a single experiment and were first performed in

2014 by three different groups. The first performed CRISPR/Cas9 screens were done in cell lines using sgRNA libraries targeting the whole genome, resulting in a library size of around 70 000 sgRNAs and showed its potential as a powerful tool for genetic analysis (Shalem et al. 2014; T. Wang et al. 2014; Koike-Yusa et al. 2014).
Thanks to this potential the Cancer Dependency Map (DepMap) project emerged. This project aims at identifying genes essential for the proliferation/survival of cancer cells by performing genome-wide loss of function screens (Tsherniak et al. 2017). These screens already revealed hundreds of potential cancer vulnerabilities.
Many *in vitro* cell line screens were performed, but the desire to screen in models with a proper *in vivo* microenvironment makes *in vivo* screens particularly interesting. But also, *in vivo* screens reveal several additional challenges like the number of cells that engraft and subsequently contribute to the tumor and the need to determine the cell number over the screen time (Doench 2018). These limitations allow no genome-wide *in vivo* screens and require screens with smaller customized sgRNA libraries.
Recently our group and others described the feasibility of a CRISPR/Cas9 screen using a small library in a human leukemia xenograft model (Wirth et al. 2022; S. Lin et al. 2022; Ghalandary et al. 2023; Bahrami et al. 2023). Although technical still challenging, this development brought CRISPR/Cas9 screens closer to clinical applications.

1.3 Aim of the project

Precision medicine has become an increasingly popular approach for treating patients, focusing on identifying and targeting patient-specific dependencies. Lots of targeted therapies already exist or are in clinical trials and development. However, the lack of biomarkers that predict which targeted drugs will work for specific patients remains a challenge. The current workflow for identifying biomarkers is mainly descriptive and lacks functional testing. Researchers have just begun using functional tests, such as *ex vivo* drug screens in patient cells, to address this issue. In addition, new technologies like the CRISPR/Cas9 system offer a powerful tool for identifying functional biomarkers and developing new drugs.
In this work, we used CRISPR/Cas9 screens to determine biomarkers in an *in vivo* patient-derived xenograft model of acute leukemia. By identifying patient-specific dependencies, this approach can help predict which patients are most likely to respond to a specific drug.

Overall, precision medicine holds great promise for improving patient outcomes, but continued investment in new technologies and tools is critical to fully realize its potential.

2. Material

2.1 Animals, cell lines and bacterial strains

Table 1: Animals, cell lines and bacterial strains

Category	Name	Provider
Bacterial strain	E.coli DH5α	Thermo Fisher Scientific (Waltham, USA)
Bacterial strain	Endura electrocompetent cells	Lucigen (Middleton, USA)
human embryonic kidney cell line	HEK-293T	DSMZ (Braunschweig, Germany)
human B cell precursor leukemia cell line	Nalm-6	DSMZ (Braunschweig, Germany)
human AML cell line	OCI-AML3	DSMZ (Braunschweig, Germany)
human AML cell line	MOLM13	DSMZ (Braunschweig, Germany)
Laboratory animal	NOD.Cg-Prkdc^{scid} Il2rg^{tm1Wjl}/SzJ (NSG) mice	Jackson Laboratory (Bar Harbor, USA)

2.2 Plasmids, enzymes and primers

Table 2: Plasmids, enzymes and primers

Plasmid name	Provider
pCDH-H1-CD19sgRNA 1-EF1α-mTagBFP	cloned by Martin Becker
pCDH-H1-CD33sgRNA-EF1α-mTagBFP-mutBbsI-Puromycin	cloned by Diana Amend
pCDH-H1-sgRNA-iScaffold-EF1α-mTagBFP-mutBbsI-Puromycin	cloned by Diana Amend
pCDH-H1-stuffer-Druggables3_all-sgRNA_iScaffold-EF1a-H2K-k-BFP	cloned by Diana Amend
pCDH-H1-stuffer-Druggables3_all-sgRNA_iScaffold-EF1-mTagBFP-P2A-Puro	cloned by Diana Amend
pCDH-H1-stuffer-Druggables3_sublibrary1-sgRNA_iScaffold-EF1-mTagBFP-P2A-Puro	cloned by Diana Amend
pCDH-H1-stuffer-Druggables3_sublibrary2-sgRNA_iScaffold-EF1-mTagBFP-P2A-Puro	cloned by Diana Amend
pCDH-H1-stuffer-sgRNA_iScaffold-EF1a-H2K-k-BFP	cloned by Martin Becker
pCDH-H1-stuffer-sgRNA_iScaffold-EF1-mTagBFP-P2A-Puro	cloned by Martin Becker
pMD2.G	Addgene (Cambridge, USA)
pMDLg/pRRE	Addgene (Cambridge, USA)
pRSV-Rev	Addgene (Cambridge, USA)
pCDH-SFFV-YN-N-Cas9-N-Intein	cloned by Martin Becker
pCDH-SFFV-C-Intein-C-Cas9-P2A-CC	cloned by Martin Becker
pCDH-EF1a-H2Kk-T2A-NGFR-DNABC (Version-2017-01-24)-eBC(Version-2017-04-20) (w/o NheI, with AvrII)	cloned by Daniel Richter

Oligo pool with all sgRNA sequences was designed using the published CLUE pipeline (Becker et al. 2020) at www.crispr-clue.de and ordered from Twist Bioscience (South San Francisco, USA).

Table 3: Enzymes

Enzyme	Company
BbsI-HF	New England Biolabs (Frankfurt am Main, Germany)
FastDigest BpiI	Thermo Fisher Scientific (Waltham, USA)
GoTaq Polymerase	Promega (Madison, USA)
T4 DNA Ligase	Thermo Fisher Scientific (Waltham, USA)

Table 4: Primers

Sequence	Application
TGCGGATCATTCAATACGG	Initial oligo pool amplification (PCR1_fwd)
CGCCATAACGATGTTTGAG	Initial oligo pool amplification (PCR1_rev)
GCGTGTTTGAATTCCACT	Sublibrary amplification (PCR2.1_fwd)
GAGCCGACGAGGAAATTT	Sublibrary amplification (PCR2.1_rev)
AGGATCTCTAGCCTCAAA	Sublibrary amplification (PCR2.2_fwd)
CAGTTACGATGCTTCATC	Sublibrary amplification (PCR2.2_rev)
AACTGCGATCGCTAATGT	Sublibrary amplification (PCR2.3_fwd)
AATAAGGCACTGGAGAAC	Sublibrary amplification (PCR2.3_rev)
CTGTATGAGACCACTCTTTCCC	PCR for cloning-ready fragments (PCR3_fwd)
TGTTTCCAGCATAGCTCTTAAAC	PCR for cloning-ready fragments (PCR3_rev)
CAAGCAGAAGACGGCATACGAGATNNNNNNNNGTCTCGTGGGCTCGGAGATGTGTATAAGAGACAGGAGCGGATAACAATTTCACACAGG	NGS rev primer for TOPO pool_1 (TOPO_rev1)
CAAGCAGAAGACGGCATACGAGATNNNNNNNNGTCTCGTGGGCTCGGAGATGTGTATAAGAGACAGGTTTTCCCAGTCACGACGTTG	NGS rev primer for TOPO pool_2 (TOPO_rev2)
AATGATACGGCGACCACCGAGATCTACACNNNNNNNNTCGTCGGCAGCGTCAGATGTGTATAAGAGACAG[N]GTATGAGACCACTCTTTCCCG	NGS fwd. primer for TOPO pool and cloned Library (NGS_fwd)
CAAGCAGAAGACGGCATACGAGATNNNNNNNNGTCTCGTGGGCTCGGAGATGTGTATAAGAGACAGAAAAAGGCGGAGCCAGTACA	NGS rev primer for cloned library (NGS_rev)
CGATCTGCAATATTTGCATGTCGC	NGS fwd Primer nested PCR from gDNA (610)
ATTCGAATTCGCTAGCTCTAGAGTAGGCGC	NGS rev Primer nested PCR from gDNA (663

[N] NGS barcodes, [N] nucleotides for staggers

Table 5: Illumina adapter sequences

P5 barcode	Sequence	P7 barcode	Sequence
N503	TATCCTCT	D701	CGAGTAAT
N504	AGAGTAGA	D702	TCTCCGGA
N505	GTAAGGAG	D703	AATGAGCG
N506	ACTGCATA	D704	GGAATCTC
N507	AAGGAGTA	D705	TTCTGAAT

N508	CTAAGCCT	D706	ACGAATTC
A501	TGAACCTT	D707	AGCTTCAG
A502	TGCTAAGT	D708	GCGCATTA

2.3 Oligonucleotides and sgRNAs

Table 6: sgRNAs

sgRNA sequence	Application
AAACCGGTGCTCATAATCACCCCAC	Oligonucleotide for sgCD33 cloning (-)
TCCCGTGGGGTGATTATGAGCACCG	Oligonucleotide for sgCD33 cloning (+)
TGGGGTGATTATGAGCACCG	sgRNA targeting CD33
TTCACCACTAGAGGTTCCTC	sgRNA targeting CD19

2.4 Antibodies and MACS beads

Table 7: Antibodies

Antibody	Company
anti-human CD19-APC (HIB19)	BioLegend (San Diego, USA)
anti-human CD33-PE	BD Biosciences (San Jose, USA)
anti-human CD38-PE	BD Biosciences (San Jose, USA)
anti-mouse CD45-APC (30-F11)	BioLegend (San Diego, USA)
anti-mouse H2K-k-APC	Miltenyi (Bergisch Gladbach, Germany)

Table 8: MACS beads

MACS beads	Company
Dead Cell Removal Kit	Miltenyi (Bergisch Gladbach, Germany)
MACSelect Kk MicroBeads	Miltenyi (Bergisch Gladbach, Germany)

2.5 Reagents and chemicals

Table 9: Reagents and chemicals

Name	Company
100bp/1 kb DNA ladder	Thermo Fisher Scientific (Waltham, USA)
2-propanol	Merck Millipore (Darmstadt, Germany)
Acetic acid	Carl Roth (Karlsruhe, Germany)
Agar-Agar Kobe I	Carl Roth (Karlsruhe, Germany)
Agarose	Invitrogen (Carlsbad, USA)
Ampicillin	Sigma Aldrich (St. Louis, USA)
Annexin V Binding Buffer	Miltenyi (Bergisch Gladbach, Germany)
BSA	Carl Roth (Karlsruhe, Germany)
$CaCl_2$	Carl Roth (Karlsruhe, Germany)
DMEM	Gibco (San Diego, USA)
DMSO	Sigma Aldrich (St. Louis, USA)
DNA loading dye	Thermo Fisher Scientific (Waltham, USA)
DNase I	Thermo Fisher Scientific (Waltham, USA)
DPBS	Gibco (San Diego, USA)
EDTA (0.5 M)	Lonza (Basel, Switzerland)
Endura recovery medium	Lucigen (Middleton, USA)
Enrofloxacin	Bayer (Leverkusen, Germany)
Ethanol	Carl Roth (Karlsruhe, Germany)

FACS buffer	BD Bioscience (Heidelberg, Germany)
FACS Lysing solution	BD Bioscience (Heidelberg, Germany)
Fast Digest Buffer	Thermo Fisher Scientific (Waltham, USA)
FBS	Gibco (San Diego, USA)
Ficoll	GE Healthcare (Solingen, Germany)
Glycerin 98%	Carl Roth (Karlsruhe, Germany)
GlycoBlue Coprecipitant	Thermo Fisher Scientific (Waltham, USA)
GoTaq reaction buffer	Promega (Madison, USA)
Heparin	Ratiopharm (Ulm, Germany)
K-Acetate	Sigma Aldrich (St. Louis, USA)
Kanamycin	Thermo Fisher Scientific (Waltham, USA)
KCl	Merck Millipore (Darmstadt, Germany)
L-Glutamine	Gibco (San Diego, USA)
LB-Medium (Luria/Miller)	Carl Roth (Karlsruhe, Germany)
MEM α	Thermo Fisher Scientific (Waltham, USA)
Midori Green	Biozym Scientific (Hessisch Oldendorf, Germany)
$MnCl_2$	Sigma Aldrich (St. Louis, USA)
MOPS	Sigma Aldrich (St. Louis, USA)
NaCl	Carl Roth (Karlsruhe, Germany)
Penicillin/Streptavidin (P/S)	Gibco (San Diego, USA)
Polybrene	Sigma Aldrich (St. Louis, USA)
Polyethylenimine	Polysciences (Warrington, USA)
Puromycin	Invivogen (San Diego, UAS)
recombinant human FMS-like tyrosine kinase 3 ligand (FLT3L)	R&D Systems (Minneapolis, USA)
recombinant human interleukin 3 (IL3)	Thermo Fisher Scientific (Waltham, USA)
recombinant human stem cell factor (SCF)	Thermo Fisher Scientific (Waltham, USA)
recombinant human thrombopoietin (TPO)	Thermo Fisher Scientific (Waltham, USA)
RPMI-1640	Gibco (San Diego, USA)
StemPro-34 Medium	Thermo Fisher Scientific (Waltham, USA)
StemSpan SFEM II	Stemcell Technologies (Vancouver, Kanada)
T4 DNA Ligase Buffer	Thermo Fisher Scientific (Waltham, USA)
Tris-HCl	Carl Roth (Karlsruhe, Germany)
Trypan blue	Sigma Aldrich (St. Louis, USA)
Trypsin	Gibco (San Diego, USA)
β-Mercaptoethanol	Sigma Aldrich (St. Louis, USA)

2.6 Buffer and media

Table 10: Buffer

Buffer	**Composition**
Annealing buffer	T4 DNA Ligase Buffer diluted 1:8
TAE buffer	40 mM Tris-base, 1 mM EDTA, 20 mM acetic acid
TFB I	100 mM KCl, 10 mM $CaCl_2$, 30 mM K-Acetate, 50 mM $MnCl_2$, 15% Glycerin, pH 5.8
TFB II	10 mM KCl, 75 mM $CaCl_2$, 10 mM MOPS, 15% Glycerin, pH 7.0

Table 11: Medium

Medium	Company
Freezing medium	FBS + 20% DMSO
HEK-293T culture medium	DMEM supplemented with 10% FBS and 2 mM glutamine
Nalm-6 and MOLM13 culture medium	RPMI-1640 supplemented with 10% FBS and 2 mM glutamine
OCI-AML3 culture medium	MEM α supplemented with 20% FBS and 2 mM glutamine
PDX-ALL culture medium	StemSpan SFEM II supplemented with 1% P/S
PDX-AML culture medium	StemPro-34 medium including Nutrient Supplement supplemented with 2mM glutamine, 1% P/S, 10ng/mL FLT3L, 10ng/mL SCF, 10 ng/mL IL3 and 10ng/mL TPO

2.7 Commercial Kits

Table 12: Kits

Kit	Company
DNeasy Blood & Tissue Kit	Qiagen (Hilden, Germany)
KAPA HiFi PCR Kit	Roche (Basel, Switzerland)
NEBuilder HiFi DNA Assembly Master Mix	New England Biolabs (Frankfurt, Germany)
NucleoBond Xtra Maxi Kit	Macherey-Nagel (Düren, Germany)
NucleoBond Xtra Midi Kit	Macherey-Nagel (Düren, Germany)
NucleoSpin Gel and PCR Clean-Up Kit	Macherey-Nagel (Düren, Germany)
NucleoSpin Plasmid Easy Pure	Macherey-Nagel (Düren, Germany)
Zero Blunt TOPO PCR Cloning Kit	Invitrogen (Carlsbad, USA)

2.8 Consumables

Table 13: Consumables

Consumable	Company
6-/24- and 96-Well PCR Plates	BioRad (Hercules, USA)
Amicon-Ultra centrifugal filter units	Merck Millipore (Darmstadt, Germany)
Bacterial tubes	Corning (Corning, USA)
Cell culture EasyFlask T75	Thermo Fisher Scientific (Waltham, USA)
Cell culture flasks (T25, T75)	Greiner bio-one (Kremsmünster, Germany)
Cell scraper	Sarstedt (Nürmbrecht, Germany)
Cell strainer (45 mm, 70 mm)	Greiner bio-one, Frickenhausen, Germany
Cryotubes	Thermo Fisher Scientific (Waltham, USA)
Disposable serological pipettes	Greiner bio-one (Kremsmünster, Germany)
Electroporation Cuvettes, 0.1 cm gap,	BioRad (Hercules, USA)
FACS tubes (with and without filter)	Corning (Corning, USA)
Freezing container	Corning (Corning, USA)
Glass beads	VWR International (Radnor, USA)
LS columns	Miltenyi (Bergisch Gladbach, Germany)
Microcentrifuge tube, DNA LoBind	Sigma Aldrich (St. Louis, USA)
Microvette	Sarstedt (Nürmbrecht, Germany)
Neubauer Counting Chamber	Optik Labor, Lancing, United Kingdom
Nunc Square BioAssay Dishes	Thermo Fisher Scientific (Waltham, USA)
PCR plate seal	BioRad (Hercules, USA)
PCR tubes	Sigma Aldrich (St. Louis, USA)
Petri dishes	Greiner bio-one, Frickenhausen, Germany
Pipette tips (with and without filter)	Starlab (Hamburg, Germany)
Well plates for tissue culture	Corning (Corning, USA)

2.9 Equipment

Table 14: Equipment

Equipment	Company
Cell sorter BD FACS AriaIII	BD Biosciences (San Jose, USA)
Flow cytometer BD LSRFortessa X20	BD Biosciences (San Jose, USA)
Gel documentation station E-box VX5	Peqlab (Erlangen, Germany)
Gene Pulser Xcell Electroporation Systems	BioRad (Hercules, USA)
Illumina HiSeq 2000	Illumina (San Diego, USA)
Illumina NextSeq 1000	Illumina (San Diego, USA)
Nanodrop OneC	Thermo Fisher Scientific (Waltham, USA)
PCR Theromcycler	Thermo Fisher Scientific (Waltham, USA)
Quietek CO2 Induction Systems	Next Advance (Troy, USA)

2.10 Software

Table 15: Software

Software	Provider
BioRender	Biorender, Toronto, Canada
FlowJo 10	FlowJo LLC (Ashley, USA)
Genious 11.1.5	Biomatters Ltd, Auckland, New Zealand
GraphPad Prism 8	Graphpad Prism (La Jolla, USA)
Microsoft Office 2016	Microsoft Corporation (Tulsa, USA)
MyIMouse	Python Software Foundation (Wilmington, USA)
Python (version 3.7.11)	Python Software Foundation (Wilmington, USA)
RStudio (R version 3.6.1)	Rstudio, Inc. (Boston, USA)
Zotero	George Mason University, Washington DC, USA

3. Methods

3.1 Ethical statement

3.1.1 Patient material

Fresh AL patient material was collected from bone marrow aspiration or peripheral blood obtained in the Department of Internal Medicine III, LMU Munich; Dr. von Hauner Children's Hospital, Munich; University Hospital Tübingen and the Charité University Hospital, Berlin. Written informed consent was obtained from all patients or parents/caregivers/legal guardians when patients were minors. The study was performed in accordance with the ethical standards of the responsible committee on human experimentation (written approval by Ethikkommission des Klinikums der Ludwig-Maximilians-Universität Munich, number 068–08 and 222–10) and with the Helsinki Declaration of 1975, as revised in 2000.

3.1.2 Animal work

NSG mice were kept under the pathogen-free condition on a 12 h light-dark rhythm, with constant temperature, food, and water *ad libitum* in the research animal facility of the Helmholtz Zentrum München.

All animal trials were performed in accordance with the current ethical standards of the official committee on animal experimentation (written approval by Regierung von Oberbayern, tierversuche@reg-ob.bayern.de; May 2016, ROB-55.2Vet2532.Vet_02–16-7 and August 2016, ROB-55.2Vet-2532.Vet_03–16-56, ROB-55.2-2532.Vet_02-20-159, ROB-55.2-2532.Vet_03-21-9).

3.2 Xenograft mouse model of acute leukemia

AL cells were amplified and studied in NSG mice using the established individualized PDX mouse model (Vick et al. 2015).

3.2.1 Engraftment of PDX cells

Up to 10^7 fresh or thawed cells were re-suspended for engraftment in 100 µL sterile-filtered PBS and injected intravenously into the tail vein of 6-20 weeks old NSG mice. To prevent an infection followed by injection, 2.5% Enrofloxacin was added to the drinking water for seven days. The growth of human cells was monitored by flow cytometry measurement in peripheral blood (see 3.2.2). Mice were sacrificed (see

3.2.3) at defined time points, at signs of advanced leukemia or any clinical signs of illness (rough fur, hunchback, reduced mobility). Engrafted cells were isolated from bone marrow and spleen (see 3.2.4 and 3.2.5).

3.2.2 Quantification of human cells in murine peripheral blood

The growth of leukemic cells was monitored by measuring human cells in the peripheral blood using flow cytometry. Around 50 µL blood from the tail vein was collected in a heparin-coated glass capillary and transferred to a reaction tube with 5 µL heparin. For staining of human cells, the samples were incubated with 1:100 anti-human CD38-PE (ALL specific marker) or anti-human CD33-PE (AML specific marker) and 1:100 anti-human CD45-APC for 30 min at RT. Followed by erythrocytes lysis with 1 mL FACS Lysing solution for 15min at RT. Samples were washed twice with 3 mL FACS Buffer (5 min, 300 g, RT) and measured by flow cytometry (see 3.3.7). Analysis was done using the FlowJo software.

3.2.3 Sacrificing mice by cervical dislocation

Mice were sacrificed by cervical dislocation. Reflex movements verified clinical death, and organs were isolated for further analysis.

3.2.4 Isolation of PDX cells from bone marrow

Bone marrow, femora, hip, sternum, and spine are dissected and crushed using a mortar and pestle to isolate PDX cells. Cells were suspended in PBS, and bone remains were removed using a 70 µm cell strainer. After washing (400 g, 5 min, RT), cells were re-suspended in the needed buffer or medium depending on the following application.

3.2.5 Isolation of PDX cells from spleen

The dissected spleen was homogenized by squashing through a 70 µm cell strainer, and isolated cells were suspended in PBS. To separate the certain cell types 10 mL Ficoll was added, and a density gradient was created by centrifugation (400 g, 30 min, RT, no brake). The desired mononuclear cells are located in the interphase layer of the gradient and were carefully removed. After washing twice (400 g, 5 min, RT), the cells were re-suspended in the needed buffer or medium depending on the following application.

3.3 Cell culture methods

3.3.1 Maintenance of PDX cells *ex vivo*

Fresh or thawed PDX cells were washed once with PBS (400 g, 5 min, RT) and re-suspended in the appropriate medium (AML or ALL PDX culture medium). AML PDX cells were seeded with a 1 x 10^6 cells/mL medium density in 6-well plates or T75 flasks and incubated at 37 °C and 5% CO_2. ALL PDX cells were seeded with a density of 5 x 10^6 cells/mL medium in 6-well plates and incubated at 37 °C and 5% CO_2.

3.3.2 Maintenance of cell lines

HEK-293T cells were cultured with a density of 0.5 – 2 x 10^6 cells/mL in DMEM supplemented with 10% FBS and 1% glutamine at 37 °C and 5% CO_2. Cells were passaged every 2-3 days by washing with PBS and using 0.05% trypsin-EDTA for dissociation. Cells were diluted 1:10 with the appropriate medium and seeded in a T75 flask.

MOLM13 were passaged 1:2 or 1:3 and Nalm-6 cells 1:10 every 2-3 days and therefore maintained at a density of 0.5 – 2 x 10^6 cells/mL in RPMI supplemented with 10% FBS and 1 % glutamine at 37 °C and 5% CO_2.

OCI-AML3 cells were passaged 1:2 or 1:3 every 2-3 days and maintained in MEM α supplemented with 20% FBS and 1 % glutamine at 37 °C and 5% CO_2.

3.3.3 Cell counting

PDX cells and cell lines were counted using a Neubauer chamber. An aliquot of cells was diluted 1:10 - 1:1000 and stained 1:10 with trypan blue for counting. Cell numbers were calculated using the following formula:

$$Cells\ per\ mL = mean\ of\ counted\ cells * 10^4 * dilution\ factor$$

3.3.4 Cryopreservation of PDX cells and cell lines

Freshly isolated PDX cells from bone marrow, spleen, or cultivated cell lines were pelleted and re-suspended in FBS. The freezing medium was added carefully 1:2 to the cell suspension. 0.5 – 1 x 10^7 cells/mL were quickly transferred to cryopreservation tubes, and the tubes were placed into a freezing container that ensured slow cooling of 1 °C/min in a -80 °C freezer. For long time storage, the cells were transferred to -196 °C.

ALL PDX cells and cell lines were thawed quickly in a 37 °C water bath. Cell suspensions were immediately diluted and washed with 10 mL PBS (400 g, 5 min, RT) and afterward diluted in a culture medium or the needed buffer.
AML PDX cells were thawed quickly in a 37 °C water bath, and 0.1 mg/mL DNase was added dropwise. After 1 min incubation, the cells were transferred to a 50 mL tube, and FBS was added dropwise in a 1:2 ratio. After 1 min incubation, 10 mL PBS + 2% FBS was added slowly and incubated for 1 min. Up to 30 mL PBS + 2% FBS was added slowly, and cells were filtered (70 µm cell strainer) and centrifuged (200 g, 5 min, RT). The cell pellet was re-suspended in a culture medium or the needed buffer.

3.3.5 Lentivirus production

HEK-293T cells with a 50-80% density were transfected to produce third-generation lentiviral particles. Packaging plasmids, transfer plasmids, and transfection reagents were mixed, as shown in the following table:

Table 16: Transfection for lentivirus production

Reagent/Plasmid	Volume/amount
DMEM	1 mL
PEI 1mg/mL	34 µL
pRSV-Rev	2.5 µg
pMDLg/pRRE	5 µg
pMD2.G	1.25 µg
pCDH transfer plasmid	2.5 µg

After 20 min incubation at RT, HEK-293T cells were transfected with the plasmid mix and incubated for three days at 37 °C and 5% CO_2. After incubation, the supernatant was transferred to a 50 mL tube, and cell debris was removed by centrifugation (400 g, 5 min, RT) and filtering (0.45 µm filter). The filtered supernatant was concentrated by ultrafiltration using Amicon-Ultra 15 mL (2000g, 30 min, RT). The concentrated virus was stored in aliquots at 80 °C.

3.3.6 Lentiviral transduction

Before experimental usage of lentiviruses, the virus titer was determined by transducing Nalm-6 cells. For transduction, Nalm-6 cells were seeded with a density of 1 x 10^6 cells/mL in a 24-well plate, transduced with several amounts of virus (e.g., 0.3 µL, 1 µL, and 3 µL) together with 8 µg/mL polybrene. After overnight incubation (37

°C and 5% CO_2.), cells were washed three times with PBS (400 g, 5 min, RT), and transgene expression was analyzed using flow cytometry (see 3.3.7).
For sgRNA library transduction, 10^8 PDX cells were transduced at a low multiplicity of infection (0.3-0.5) to ensure each cell contained a single sgRNA (Doench 2018).
For transduction of PDX cells, cells were seeded in a 6-well plate at a density of 10^7 cells/mL using the appropriate PDX medium (AML or ALL PDX culture medium) together with 8 µg/mL polybrene. The needed amount of virus was added, and cells were incubated overnight (37 °C and 5% CO_2.). Cells were washed three times with PBS the next day (400 g, 5 min, RT) and re-suspended in the needed volume of medium or buffer (see 3.3.1).

3.3.7 Flow cytometry staining

The expression of human markers (CD33, CD19, CD38, and CD45) or transgenes like H2Kk were analyzed by antibody staining. 0.1 – 1 x 10^6 cells/mL were re-suspended in 100 µL PBS, and the antibody was added in the respective dilution (1:25 or 1:50) and incubated (20 min, RT, dark). Cells were washed twice with PBS (400 g, 5 min, RT) and analyzed by flow cytometry (see 3.3.8).

3.3.8 Flow cytometry

Flow cytometry was performed using a BD LSR Fortessa X-20. The analysis was based on gating for viable lymphocytes (FSC, SSC) and expression of fluorochromes (eGFP, mTagBFP) or antibody-conjugated fluorochromes (APE, PE) using the following laser and filter settings:

Table 17: Filter setting LSRFortessa X-20

Laser	Long pass filter	Bandpass filter	Parameters/Fluorochromes
Blue (488 nm)	none	488/10	SSC
	505	530/30	eGFP
Violet (405 nm)	none	450/50	mTagBFP
Red (640 nm)	none	670/30	APC
Yellow/Green (561 nm)	600	610/20	mCherry
	none	586/15	PE

Analysis of flow cytometry data was done using the FlowJo software. The gating strategy is shown in Figure 4.

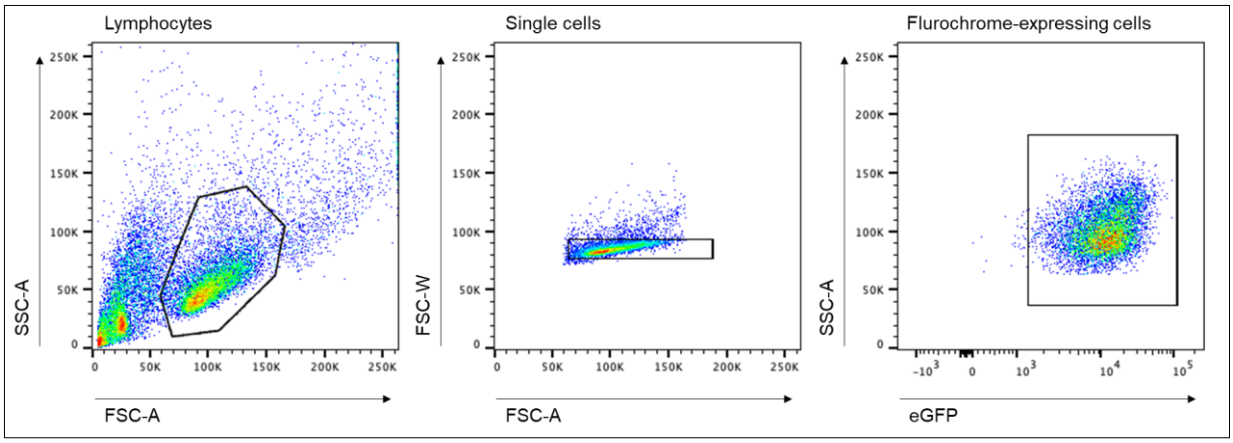

Figure 4: Exemplary gating strategy on fluorochrome expressing cells.
Gating on lymphocytes in SSC-A/FSC-A followed by exclusion of doublets. Next, cells were gated on fluorochrome.

3.3.9 Enrichment of PDX cells by magnetic cell separation (MACS)

Magnetic cell separation (MACS) enriched living or transduced PDX cells. Living cells were enriched when viability post-puromycin selection was below 10%. H2Kk-MACS selection was used after the transduction of sgRNA libraries.

The enrichment of living cells was done using negative selection by a dead cell removal kit (Miltenyi, Bergisch Gladbach, Germany). PDX cells were re-suspended in 100 µL dead cell removal beads per 1 x 10^7 cells (15 min, RT). LS columns were placed into a magnet and prepared by washing with Binding Buffer. Cells were filled to 500 µL with Binding buffer and loaded onto the column. Columns were washed four times with Binding buffer, and flow-through containing living PDX cells was collected and washed (400g, 5 min, RT) and re-suspended in a desired buffer.

ALL-PDX cells transduced with an H2Kk expressing transgene were enriched by positive selection using MACSelect K^k System (Miltenyi, Bergisch Gladbach, Germany). On day four post-transduction, PDX cells were suspended in 2 mL PBS + 0.5% BSA, filtered (70 µm cell strainer), and 20 µL MACSelect K^k beads per 1 x 10^7 cells were added, and the mix was incubated (15 min, RT, dark, rotating). LS columns were placed into a magnet and prepared by washing once with PBS + 0.5% BSA. The cell suspension was loaded onto the column and washed with PBS + 0.5% BSA four times. The positive fraction was eluted by adding 5 mL PBS + 0.5% BSA, removing the column from the magnet, and flushing the enriched cells using a plunger.

3.3.10 Enrichment of PDX cells by puromycin selection

AML-PDX cells transduced with a puromycin resistance transgene, co-expressing mTagBFP for monitoring, were enriched using puromycin for two to four days. On day

four post-transduction, the selection was started by adding 1.5 µg/mL puromycin to the culture medium. From now on, cells were monitored for enrichment every second day by flow cytometry (see 3.3.8). When the enrichment reached over 90%, cells were prepared for injection into NSG mice.

3.3.11 Enrichment of PDX cells by fluorescent-activated cell sorting

PDX cells were enriched based on the expression of a fluorochrome marker (eGFP, mTagBFP) using the BD FACS AriaIII (BD Bioscience, Heidelberg, Germany) cell sorter. Cells were prepared for sorting by filtering (70 µm cell strainer), washing with PBS (400g, 5min), and resuspension in PBS. Gating was performed based on viable lymphocytes and transgene expression (Figure 4).

Table 18: Configurations of BD FACS AriaIII

Laser	Long pass filter	Bandpass filter	Parameters/Fluorochromes
Violet (405 nm)	none	450/40	mTagBFP
Blue (488 nm)	488	530/30	eGFP
		488/10	SSC

3.3.12 Reducing clonal heterogeneity of AML PDX samples

The clonal composition of AML is known to be heterogeneous. This background could have a negative impact on a CRISPR/Cas9 screen, as sgRNAs may integrate into clones that are dominantly outgrowing. To minimize this risk, we aimed at generating AML PDX samples with a reduced clonal heterogeneity. Therefore, we aimed at injecting a small number of cells into NSG mice. The frequency of leukemia-initiating cells (LICs) was used to calculate this small number of cells. The frequency of LIC for our PDX samples was earlier determined by limiting dilution transplantations assays (Ebinger et al. 2020). For PDX with a known frequency, we defined injecting less than ten times the frequency of LICs (AML388, AML393, and AML602).

For the AML356, one sample without data, we proceeded without limiting the number of injected cells. However, because of the low transduction efficiency of the Split-Cas9 constructs in this sample, the minimum number of cells injected was 60,000.

Due to time issues and since no mutations were annotated after performing the standard AML sequencing panel, the AML346 sample was handled without limiting the number of injected cells. The lowest injected number was 250 000 cells, representing 100 times the LIC frequency.

3.3.13 *In vitro* cell line screen procedure

For the cell line *in vitro* test screen, 6 x 10^6 cells with and without Cas9 were transduced with the sgRNA library plasmid. On day four post-transduction cells were selected for transduced cells by adding 1.5 µg/mL puromycin to the medium. Puromycin was removed two days later (d4 post-transduction) when cells showed more than 90% mTagBFP expression. 2 x 10^6 cells were taken as an input control. Cells were passaged 1:2 every 2-3 days to ensure a library coverage of at least 500 per sgRNA and high cell viability. 14 days after successful selection, the screen was ended by sampling DNA for the final read-out (see 3.5.12, 3.6.2).

3.3.14 *In vivo* and *in vitro* PDX screen procedure

Per PDX sample, around 1 x 10^8 fresh PDX cells, with or without Cas9 construct, were isolated from bone marrow and spleen (see 3.2.4,3.2.5), filtered (70 µm cell strainer) and transduced (see 3.3.6) with library virus. During washing the next day, 2 x 10^6 cells were taken as the first input sample (Input_1). At day four, cells are selected with puromycin (see 3.3.10) or enriched using K2Kk-MACS (see 3.3.9). To ensure each cell contains a single sgRNA, the enrichment was started when transduction efficiency did not exceed 30-50%. MACS-selected cells were directly prepared for injection, aiming at 1 x 10^7 cells per mouse in three mice and around 2 x 10^6 as Input_2. If possible, an *in vitro* screen was started by seeding 2 x 10^6 cells in a 6-well plate three times. Endpoint DNA was collected depending on the cell viability at d7 and/or d14.

Puromycin selection was defined as finalized when cells reached an enrichment level of over 90%. Cells that did not recover well and showed viability below 10% were MACS enriched for living cells (see 3.3.9). After taking around 2 x 10^6 cells as Input_2, 1 x 10^7 cells per mouse in three mice were injected. If possible, an *in vitro* screen was started by seeding 2 x 10^6 cells in a 6-well plate three times. Endpoint DNA was collected depending on the cell viability at d7, d14, d21, and the endpoint of mice.

Mice were taken down at signs of advanced leukemia or any clinical signs of illness. For further analysis, 2-4 x 10^6 bone marrow cells per PDX sample were taken for gDNA isolation (see 3.5.8) and prepared for NGS (see 3.5.12, 3.6.2). In parallel, an aliquot was used for flow cytometry to analyze the expression of the library, Cas9, and the number of human cells (see 3.3.8).

3.4 Microbiology methods

3.4.1 Generation of competent E.coli DH5α

100 mL LB medium was inoculated with 1 mL E.coli DH5α overnight culture. At an OD of 0.4-0.5 nm, bacteria suspension was cooled down and centrifuged down (4000 g, 5 min, 4 °C). Bacteria pellets were re-suspended in 15 mL TFB I buffer followed by incubation (5 min, 4 °C) centrifugation (4000 g, 5 min, 4 °C) and re-suspended in 4 mL TBF II buffer. Bacteria were aliquoted and stored at -80 °C.

3.4.2 Heat shock transformation

For the amplification of plasmid DNA in E.coli, the heat shock method was used. Therefore 5 µL ligation product was added to 50 µL DH5α and incubated (30 min, on ice), followed by heat shock (90 s, 42 °C) and an incubation (2 min, on ice). 400 µL pre-warmed LB medium was added, and the bacteria culture was incubated (60 min, 37 °C, shaking). Around 250 µL were plated on LB_{Amp} agar plates and incubated overnight at 37 °C. Single colonies were picked the next day and further expanded in LB_{Amp} (overnight, 37 °C, shaking). The cell suspension was collected for plasmid DNA isolation (see 3.5.9 and 3.5.8).

3.4.3 Transformation using electroporation

sgRNA library plasmids were amplified by electroporation into Endura electrocompetent bacteria. 2 µL DNA was mixed with 25 µL Endura electrocompetent cells. Bacteria suspension was transferred to a pre-chilled electroporation cuvette and electroporated using the following settings: 1.8 kV, 600 Ohm, 10 µF. Bacteria were re-suspended with 975 µL Endura recovery medium, transferred into a tube, and incubated (37 °C, 1 h shaking). The suspension was plated onto 245 mm square dishes with LB Agar containing either Ampicillin for the pCDH backbone or Kanamycin for the Topo plasmid backbone and incubated overnight at 37 °C. To determine electroporation efficiency, 1:10 000 and 1:100 000 dilutions were plated on small LB Agar plates containing Kanamycin or Ampicillin. Bacterial colonies on 245 mm square dishes were scratched and floated off using LB medium and collected for isolation of plasmid DNA (see 3.5.8)

3.5 Molecular biology methods

3.5.1 Annealing of oligonucleotides

To clone sgRNAs into a lentiviral backbone, single-stranded oligonucleotides (oligos), including sgRNA sequence and adjacent nucleotides to enable cloning, were ordered from Sigma-Aldrich (St. Luis, USA). Complementary oligos were annealed using the following protocol:

Reagent	Volume
Forward oligo	1 µL
Reverse oligo	1 µL
Annealing buffer	16 µL

The reaction was incubated at 95 °C for 5 min and cooled to 25 °C (ramp down with 0.1 °C per s). Annealing created double-stranded oligos with 5' and 3' overhangs compatible with BpiI restriction digestion overhangs.

3.5.2 Restriction digestion of backbone

The backbone plasmids were digested at 37 °C overnight.

Reagent	Volume/Amount
Plasmid	5 µg
FastDigest BpiI	10 U
10x FastDigest Buffer	5 µL
H_2O	ad 50 µL

Digested DNA fragments were separated by agarose gel electrophoresis (see 3.5.7) and cleaned up using NucleoSpin Gel and PCR Clean-up Kit (Macherey-Nagel, Düren, Germany) according to the manufacturer's instructions.

3.5.3 Golden Gate cloning

Annealed oligos were ligated into digested lentiviral backbones with compatible overhangs. The ligation was performed as indicated.

Reagent	Volume/Amount
Plasmid backbone	100 ng
Annealed oligos	2 µL
FastDigest BpiI	10 U
T4 Ligation Buffer	2 µL
T4 Ligase	5 U
H_2O	ad 20 µL

Temperature	Time	Cycles
37 °C	5 min	20
16 °C	10 min	
55 °C	5 min	1
80 °C	5 min	1

3.5.4 Design and cloning of sgRNA libraries

Design and cloning of sgRNAs libraries were done as previously described (Becker et al. 2020). Five sgRNAs sequences per target gene and control gene as well as non-targeting sgRNAs, were chosen based on published genome-wide libraries (T. Wang et al. 2015; Doench et al. 2016) and the Project Achilles (https://depmap.org/portal/achilles/). For each library, the sgRNA sequences were prolonged with adapters to amplify the oligo pool, specific library adapters, and an H1 promoter and sgRNA scaffold sequence. The generated oligo pool containing all library sequences and additional libraries was ordered from Twist Bioscience (South San Francisco, USA) as a lyophilized pool of double-stranded DNA oligos. In the first step, the reconstituted oligo pool was amplified using a universal PCR primer, amplifying all libraries, followed by cloning into a TOPO vector to enable unlimited amplification (see 3.5.5). The library composition of the generated Topo library plasmid was checked by NGS (see 3.5.11). Next, library-specific primers were used to amplify individual sgRNA libraries from the generated TOPO library plasmid (see 3.5.6). The resulting PCR products were purified and used as input for the following PCR, generating fragments ready for cloning into lentiviral sgRNA expression backbones. For both PCRs, several reactions were run in parallel to ensure sufficient coverage of all oligos of the different libraries. In parallel, the lentiviral sgRNA expression backbone was digested using BpiI (see 3.5.2). Digested backbone and sgRNA inserts were cloned using Gibson assembly (see 3.5.6), transformed into bacteria using electroporation (see 3.4.3), and re-isolated by Maxi prep (see 3.5.8). The distribution of sgRNAs in every generated library was controlled by NGS (see 3.5.11).

3.5.5 Oligo Pool amplification and Topo cloning

Reconstituted oligo pool DNA with a concentration of 10 ng/µL was amplified using PCR1 primer and the following settings:

Reagent	Volume/Amount
Oligo pool DNA	10 ng
Primer PCR1_fwd (10 µM)	0.75 µL
Primer PCR1_rev (10 µM)	0.75 µL
5X KAPA HiFi Buffer	5 µL
KAPA dNTP Mix (10 mM)	0.75 µL
KAPA HiFi Polymerase (1 U/µL)	0.5 µL
H_2O	ad 25 µL

Temperature	Time	Cycles
98 °C	3 min	1
98 °C	30 sec	15
62 °C	30 sec	
72 °C	15 sec	
72 °C	2 min	1

Next, the PCR product was cloned using Zero Blunt TOPO PCR Cloning Kit (Invitrogen, Carlsbad, USA) with the following setup:

Reagent	Volume
PCR product	2 µL
TOPO plasmid	1 µL
Salt Solution	1 µL
H_2O	2 µL

To ensure sufficient library coverage, two reactions were performed in parallel, incubated (30 min, RT), pooled, DNA was precipitated (see 3.5.10), and finally electroporated for amplification (see 3.4.3). Electroporation efficiency was checked by counting colonies on the small dilution plates. After Maxi prep of plasmid DNA (see 3.5.8), the generated TOPO library plasmid was verified by NGS (see 3.5.11).

3.5.6 Amplification and cloning of specific sgRNA libraries

To amplify specific libraries from the TOPO library plasmid, individual library-specific primer pairs were used. The optimal annealing temperature for each primer pair was determined by gradient PCR. PCR was performed with the following protocol:

Reagent	Volume/Amount
TOPO library plasmid	50 pg
Primer PCR2.1-3_fwd (10 µM)	0.75 µL
Primer PCR2.1-3_rev (10 µM)	0.75 µL
5X KAPA HiFi Buffer	5 µL
KAPA dNTP Mix (10 mM)	0.75 µL
KAPA HiFi Polymerase (1 U/µL)	0.5 µL
H_2O	ad 25 µL

Temperature	Time	Cycles
98 °C	2 min	1
98 °C	20 sec	20
52-65 °C	15 sec	
72 °C	1 sec	
72 °C	2 min	1

Per library, eight PCR reactions were done in parallel, pooled, and the correct PCR product size was verified by agarose gel electrophoresis (see 3.5.7) of an aliquot. The remaining PCR product was purified using NucleoSpin Gel and PCR Clean-up Kit (Macherey-Nagel, Düren, Germany) according to the manufacturer's instructions. DNA quantity was determined by NanoDrop (Thermo Fisher Scientific, Waltham, USA).
The PCR product was diluted to 50 pg/µL and used for Gibson cloning with the following PCR settings:

Reagent	Volume/Amount
amplified sgRNA library	50 pg
Primer PCR3_fwd (10 µM)	0.75 µL
Primer PCR3_rev (10 µM)	0.75 µL
5X KAPA HiFi Buffer	5 µL
KAPA dNTP Mix (10 mM)	0.75 µL
KAPA HiFi Polymerase (1 U/µL)	0.5 µL
H_2O	ad 25 µL

Temperature	Time	Cycles
98 °C	2 min	1
98 °C	20 sec	30
62 °C	15 sec	
72 °C	1 sec	
72 °C	2 min	1

Per library, eight PCR reactions were done in parallel, pooled, and the correct PCR product size was verified by agarose gel electrophoresis (see 3.5.7) followed by DNA precipitation (see 3.5.10).
The products were cloned into digested lentiviral sgRNA expression backbones using Gibson assembly (50 °C, 1h).

Reagent	Volume/Amount
sgRNA Library fragments	100 ng
linearized sgRNA expression backbone	100 ng
NEBuilder HiFi DNA Assembly Master Mix	5 µl
H_2O	ad 10 µL

The product was DNA precipitated (see 3.5.10) and electroporated into Endura electrocompetent cells and the sgRNA distribution of every library was checked by NGS (see 3.5.11).

3.5.7 Agarose gel electrophoresis

Agarose gel electrophoresis was performed to separate and determine DNA fragments by size. Agarose gels were prepared by heating 1-2% Agarose solved in TAE buffer. For DNA detection, 0.01% Midori Green was added before the gel was poured into a gel chamber for polymerization. DNA samples were mixed with loading dye and loaded onto the gel next to a 1 kb DNA ladder to determine fragment size. Gel electrophoresis was performed in TAE buffer (45 min, 85V), and DNA fragments were visualized using a gel documentation station. The desired DNA fragments were cut from the gel and purified for cloning based on restriction digestion using NucleoSpin Gel and PCR Clean-up Kit (Macherey-Nagel, Düren, Germany) according to the manufacturer's instructions.

3.5.8 Isolation of plasmid DNA

Depending on the amount of bacterial suspension or plates, plasmid DNA was isolated using NucleoSpin Plasmid Easy Pure, NucleoBond Xtra Midi, or NucleoBond Xtra Maxi Kit (all Macherey-Nagel, Düren, Germany) according to the manufacturer's instructions.

3.5.9 Isolation of genomic DNA

According to the manufacturer's instructions, genomic DNA from up to 10^7 cells was isolated using the DNeasy Blood & Tissue Kit (Qiagen, Hilden, Germany). The quantity and quality of the isolated DNA were checked using the NanoDrop (Thermo Fisher Scientific, Waltham, USA).

3.5.10 DNA precipitation

During sgRNA library cloning, plasmid DNA and PCR fragments were precipitated for purification. DNA was mixed 1:1 with 2-Propanol, 1% 5 M NaCl, and 0.5% Glycoblue was added additionally. Mix was incubated (15 min, RT) and centrifuged (full speed, 15 min, RT). The DNA pellet was washed twice with 70% Ethanol (full speed, 5 min, RT). The DNA pellet was re-suspended in H_2O.

3.5.11 Amplification of plasmid DNA for NGS

The composition of libraries in the TOPO library plasmid and the distribution of sgRNAs in the individual libraries were analyzed by NGS like previously described (Becker et al. 2020). Due to the blunt end-based cloning of the TOPO library plasmid, two PCR reactions were necessary to cover both insert directions. NGS PCR of the sgRNA library plasmid was performed using one primer pair. PCRs were set up with primers containing Illumina adapters and barcodes to facilitate sequencing using the following protocol:

Reagent	**Volume/Amount**
TOPO library plasmid/sgRNA library plasmid	50 ng
NGS_fwd (10 µM)	0.75 µL
TOPO_rev1 or rev2 or NGS_rev (10 µM)	0.75 µL
5X KAPA HiFi Buffer	5 µL
KAPA dNTP Mix (10 mM)	0.75 µL
KAPA HiFi Polymerase (1 U/µL)	0.5 µL
H_2O	ad 25 µL

Temperature	**Time**	**Cycles**
98 °C	2 min	1
98 °C	30 sec	25
62 °C	15 sec	
72 °C	20 sec	
72 °C	2 min	1

Correct PCR product size was checked by agarose gel electrophoresis (see 3.5.7) and purified using NucleoSpin Gel and PCR Clean-up Kit (Macherey-Nagel, Düren, Germany) according to the manufacturer's instructions and utilized for NGS (see 3.6.2).

3.5.12 Amplification of genomic DNA for NGS

To analyze *in vivo* and *in vitro* screens by NGS, genomic DNA (gDNA) was isolated from collected cells (see 3.5.9), and integrated sgRNA sequences were amplified using nested PCR. To ensure sufficient coverage of the sgRNA library the gDNA input was calculated:

$$mass\ (template\ DNA) = library\ size\ x\ coverage\ \left(\frac{cells}{sgRNA}\right) x\ mass\ \left(\frac{gDNA}{cell}\right)$$

$$mass(template\ DNA) = 811\ or\ 408\ x\ 500\ x\ 6.6\ pg = 2.68\ \mu g\ or\ 1.35\ \mu g$$

Two reactions per sample were performed for the first PCR of samples screened with the drug_sub1/2 library (408 sgRNAs) to ensure sufficient coverage of individual sgRNA sequences. Three reactions were set up for samples screened with the drug-all library containing 811 sgRNAs. The first PCR run was done using the following conditions:

Reagent	**Volume/Amount**
Template DNA	1 µg
610 or NGS:fwd (10 µM)	1.5 µL
663 or NGS_rev (10 µM)	1.5 µL
5X KAPA HiFi Buffer	10 µL
KAPA dNTP Mix (10 mM)	1.5 µL
KAPA HiFi Polymerase (1 U/µL)	1 µL
H_2O	ad 50 µL

Temperature	**Time**	**Cycles**
98 °C	2 min	1
98 °C	20 sec	30
62 °C	15 sec	
72 °C	30 sec	
72 °C	1 min	1

The PCR product was checked by agarose gel electrophoresis (see 3.5.7) and purified using NucleoSpin Gel and PCR Clean-up Kit (Macherey-Nagel, Düren, Germany) according to the manufacturer's instructions. The second PCR was set up using the same protocol with 100 ng PCR product from the first PCR and primers containing sample-specific Illumina sequence barcodes for multiplexed NGS. PCR product size was again checked by agarose gel purification (see 3.5.7), purified as described above, and submitted for NGS (see 3.6.2).

3.5.13 Identification of PDX samples

To check the identity of PDX samples across several *in vivo* passages, sample-specific single nucleotide variants (SNVs) were analyzed like previously published (Hutter et al. 2004). Isolated gDNA from PDX cells (see 3.5.9) was used to amplify Hypervariable Region1 of mitochondrial DNA:

Reagent	Volume/Amount
gDNA	300 ng
Forward Primer (10 pmol/µL)	5 µL
Reverse Primer (10 pmol/µL)	5 µL
5X GoTaq reaction buffer	10 µL
dNTPs (10 mM)	1 µL
GoTaq Polymerase	0.25 µL
H_2O	ad 50 µL

Temperature	Time	Cycles
95 °C	2 min	1
94 °C	30 sec	35
60 °C	30 sec	
72 °C	30 sec	
72 °C	5 min	1

The PCR product was checked by agarose gel electrophoresis (see 3.5.7) and purified using NucleoSpin Gel and PCR Clean-up Kit (Macherey-Nagel, Düren, Germany) according to the manufacturer's instructions and analyzed by Sanger Sequencing (see 3.6.1). Sequences were compared to reference sequences of the analyzed PDX sample.

3.6 Sequencing methods

3.6.1 Sanger sequencing

PCR products were sequenced by Microsynth (Balgach, Switzerland) using 30 ng/µL purified product and 10 pmol/µL primer. Sequences were analyzed using Genious version 11.1.5.

3.6.2 Next Generation Sequencing

The composition of sgRNA libraries in cloned plasmids and cells transduced with libraries was analyzed by NGS. Generated PCR products (see 3.5.11, 3.5.12) with sample-specific Illumina Sequencing barcodes were sequenced at the Laboratory of Functional Genome Analysis (LaFuGa, LMU, Munich). Sequencing was performed using either an Illumina HiSeq 2000 (Illumina, San Diego, USA) with 50 bp single-end reads or an Illumina NextSeq 1000 (Illumina, San Diego, USA) with 60 bp paired-end reads. At least 500 reads per sgRNA were requested to ensure sufficient sequencing coverage. Demultiplexing of samples was done either by LaFuGa or on the Galaxy server using a provided tool by LaFuGa. Readcount tables, including counts per individual sgRNA, were generated using a customized Python script like previously

described (Becker et al. 2020). This script generated a readcount file, a bar graph, a histogram, and a density plot, all showing the sgRNA distribution and the calculated Gini index to measure even sgRNA distribution. Readcount files were used to further analyze cloning efficiency or dropouts from *in vivo* and *in vitro* screens (see 3.7.1). For a detailed analysis of readcounts and comparison between different samples, the readcount of every sgRNA in a sample was normalized to the total number of reads in this sample.

3.7 Statistics and analysis

All statistical analyses were performed using GraphPad Prism 8.2.0 or MAGeCK 0.5.9. Statistical information is shown in figure legends.

3.7.1 Analysis of CRIPSR/Cas9 screens using MAGeCK

Significant dropouts of *in vivo* and *in vitro* CRISPR/Cas9 screens were identified using the Model-based Analysis of Genome-wide CRISPR/Cas9 Knockout (MAGeCK) method (Li et al. 2014). MAGeCK ranks genes using a robust ranking aggregation (RRA) algorithm, which assumes a uniform distribution of sgRNAs targeting a gene that does not affect selection. The final gene ranking tests how much the distribution of sgRNAs per gene differs from all sgRNAs in the library. The MAGeCK pipeline was processed using Python 3.7.11 on a MAC system. When starting from raw readcounts, the following command line was used:

mageck test -k readcountfile_name.txt -t sample1,sample2,... -c Input1, Input2 -n filename

-k: provided readcount file
-t: treatment sample (bone marrow 1-3)
-c: control sample (Input1+Input2 or just Input1)
-n: individual prefix of the output file

For AML PDX, Input_1 was used as a control sample, whereas for the ALL PDX, both inputs were used. The bone marrow samples were used as test samples. MAGeCK generates two output files: “gene summary” (ranking of genes by RRA score) and “sgRNA summary” (showing individual sgRNA data). A significant dropout was defined

by an RRA score below 0.003, representing a p-value below 0.05 and a maximum FDR of 0.15.

3.7.2 Calculation of the Gini index as a measure of an even sgRNA distribution

To calculate the evenness of sgRNAs in the library pool plasmids and Cas9 negative control samples, the Gini index was calculated (D. Wang 2018):

$$GINI\ Index = \frac{area\ under\ the\ curve\ (measured)}{area\ under\ the\ curve\ (perfect\ distribution)}$$

The calculation results in Gini indices between 0 and 1, whereas a Gini index of 0 reflects perfect equality and a higher index indicates greater inequality.

4. Results

As we move toward the future of medicine, precision medicine has become an increasingly important field. With many targeted therapies available, it is crucial to identify the right treatment for each patient. Biomarkers can help identify patient-individual therapies and descriptive omics are frequently used to identify them and make treatment decisions, as evidenced by the INFORM study (Worst et al. 2016). However, since more drugs exist than biomarkers, additional tools are required.

Functional genomics has the potential to enhance drug-gene relationships. In this project, we plan to use CRISPR/Cas9 *in vivo* screening in PDX cells to evaluate the potential of a functional tool for identifying biomarkers and determining patient-specific treatment (see Figure 5).

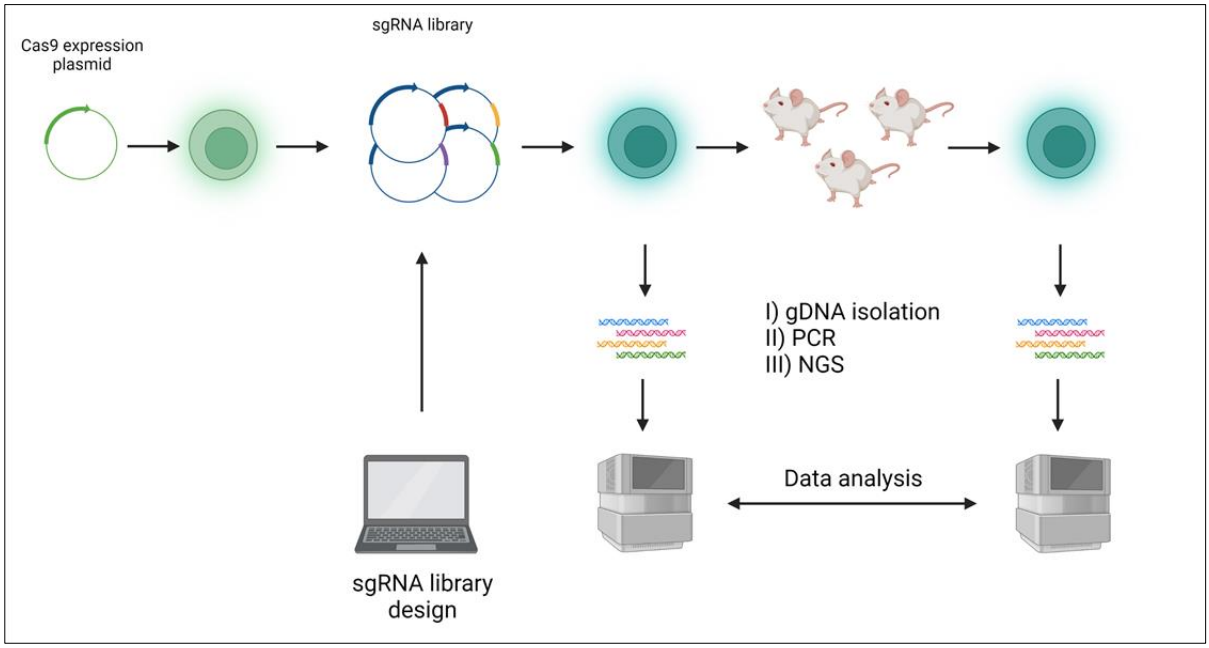

Figure 5: CRISPR/Cas9 screening pipeline enables *in vivo* screening in AML and ALL PDX samples
Including the generation of PDX cells stably expressing a Split Cas9/eGFP construct followed by the in-silico design of a targeted library. Transduction of PDX cells with sgRNA-library labeled with mTagBFP for monitoring, collection of DNA samples prior to injection, injection into NSG mice, and collection of DNA after *in vivo* time. Final NGS analysis of the collected samples allows a statement on depleted genes (Created with BioRender).

To screen multiple PDX samples, a small sgRNA library was created with druggable targets. All genes in the library have known direct or indirect drugs. The CRISPR/Cas9 screen was conducted *in vivo* to identify essential genes for *in vivo* growth. Depleted genes (dropouts) are potential therapeutic targets and are believed to be essential for *in vivo* growth. To confirm the identified dependency of an AL PDX sample on a gene,

we plan to treat the PDX sample with the gene-associated drug *in vivo*. This *in vivo* drug treatment was part of Katharina Hunt's doctoral studies.

4.1 Generation and testing of PDX cells for *in vivo* CRISPR/Cas9 screening

Establishing a robust screening process to provide a tailored drug recommendation based on a CRISPR dropout screen was crucial. This involved creating PDX cells that expressed a functional Cas9. To ensure the effectiveness of Cas9, we conducted a test by transducing the PDX samples with a sgRNA targeting a well-known surface marker.

4.1.1 Generation of Cas9-expressing PDX cells

Our laboratory has encountered difficulties in transducing PDX cells. To address this issue, we utilized a Split-Cas9 construct that reduces plasmid size and potentially enhances transduction efficiency (see Figure 6A) (Truong et al. 2015). Both constructs were transduced simultaneously, with Cas9 proteins reconstituted via intein-mediated trans-splicing and GFP proteins via Leucin-Zipper-directed protein reassembly. eGFP expression was utilized as a surrogate marker for Cas9 expression and to enable the identification and enrichment of cells via flow cytometry.

Transduced cells were enriched by flow cytometry and transplanted into NSG mice for amplification. This process was repeated until over 90% of the PDX cells displayed a stable Cas9/eGFP expression. Figure 6B+C show an exemplary generation of AML388 cells expressing the Cas9/eGFP construct. The initial transduction efficiency was 15.1%, but with two rounds of flow cytometry-based enrichment and *in vivo* amplification, more than 90% of the cells expressed Cas9/eGFP. Although we followed a standardized protocol for transduction, the initial transduction efficiency varied for different PDX samples, with some requiring more rounds of sorting and transplantation. We repeated the experiment twice if the initial transduction showed no Cas9/eGFP expression to ensure accuracy. If there was still no visible Cas9/eGFP expression after the third experiment, we excluded the PDX sample from this work as it was defined as not transducible for Cas9.

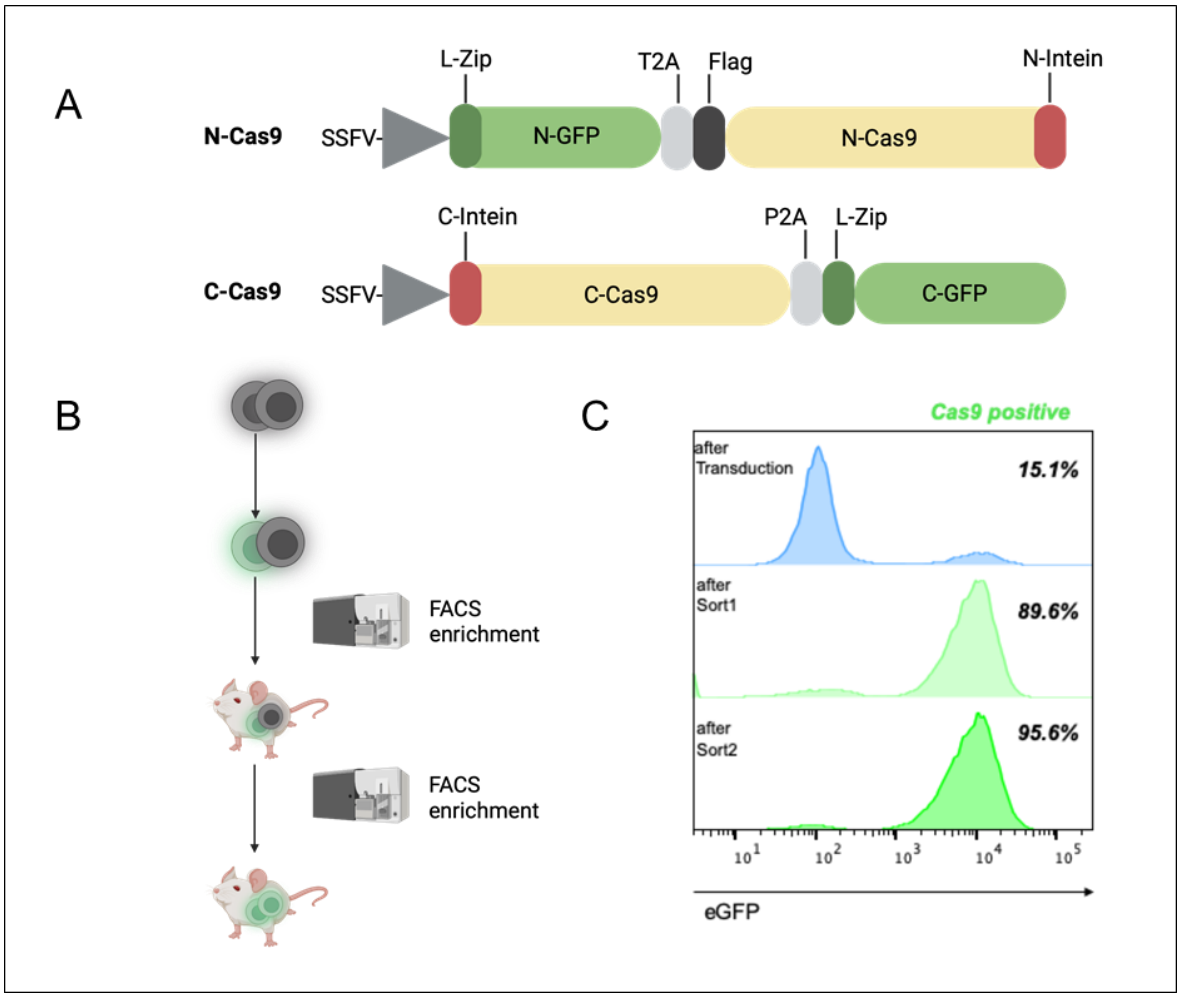

Figure 6: Generation of Cas9 expressing PDX cells using a Split-Cas9 construct
A: Split-Cas9 constructs are made of N- and C-terminal domains of either Cas9 or eGFP. **B:** Serial transplantation of PDX cells into NSG mice allows cultivation and engineering using lentiviral constructs and FACS enrichment**. C:** Representative generation of a PDX sample stably expressing Cas9/eGFP. Initial transduction efficiency of the AML388 is shown in the upper part, the enrichment after the two sorting steps below (Created with BioRender).

Ultimately, the generation of Cas9-transgenic PDX cells was successful for ten PDX samples, five of them AML and five ALL PDXs. The genetic background and patient information are shown in Table 19 and Table 20.

All generated ALL PDX samples with Cas9 originate from B-ALL patients; most alterations are based on chromosomal rearrangements.

Table 19: ALL PDX samples used in this work

PDX sample	Age	Sex	Disease stage	Mutations
ALL1034	20	M	relapse	ETV6::ABL1 (Ph-like)
ALL199	7	F	relapse	germline +21; somatic homozygous 9p deletion (CDKN2A); P2RY8::CRLF2
ALL265	5	F	relapse	High hyperdiploidy
ALL50	7	F	diagnosis	t(1;19) TCF3::PBX1
ALL502	9	F	relapse	IGH::DUX4

The point mutations display the genetic aberrations of the AML PDX samples, and the variant allele frequency (VAF) of each mutation is shown in brackets behind.

Table 20: AML PDX samples used in this work

PDX sample	Age	Sex	Disease stage	Mutations
AML346	1	F	relapse	no hits found with NGS panel
AML356	5	M	relapse	U2AF1 S34Y (0.5), KRAS A146T (0.5)
AML388	57	M	diagnosis	KRAS Q61H (0.4), KMT2A::AF6
AML393	47	F	relapse	KRAS G12A (0.5), BCOR P1012Lfs*8 (0.5), KMT2A::AF10
AML602	40	F	relapse	FLT3-ITD positive (0.2), TET2 N281* (0.4), TET2 S1369* (0.3), NPM1 W288Cfs*12 (0.5), CEBPA D262Rfs*59 (0.5)

4.1.2 Cas9 functionality proven by knockout of AML and ALL specific surface molecules

To assess the functionality of Cas9 in the generated cells, Cas9-expressing cells were transduced with a sgRNA targeting a surface marker. We used a sgRNA to target CD33 in AML PDX cells, as this protein is present on over 90% of AML myeloblasts (Ehninger et al. 2014). ALL PDX cells were transduced with a sgRNA that targets CD19, a marker found on all B-ALL cells (He et al. 2019). A surface marker ensures an easy read-out by antibody staining of the CD marker, followed by flow cytometry.

The two sgRNAs were cloned into a lentiviral backbone (cloning of CD19 sgRNA performed by Martin Becker). The identical backbones were later used for the CRISPR/Cas9 screening experiments. The used backbones for AML and ALL differ in the selection marker (see Figure 7).

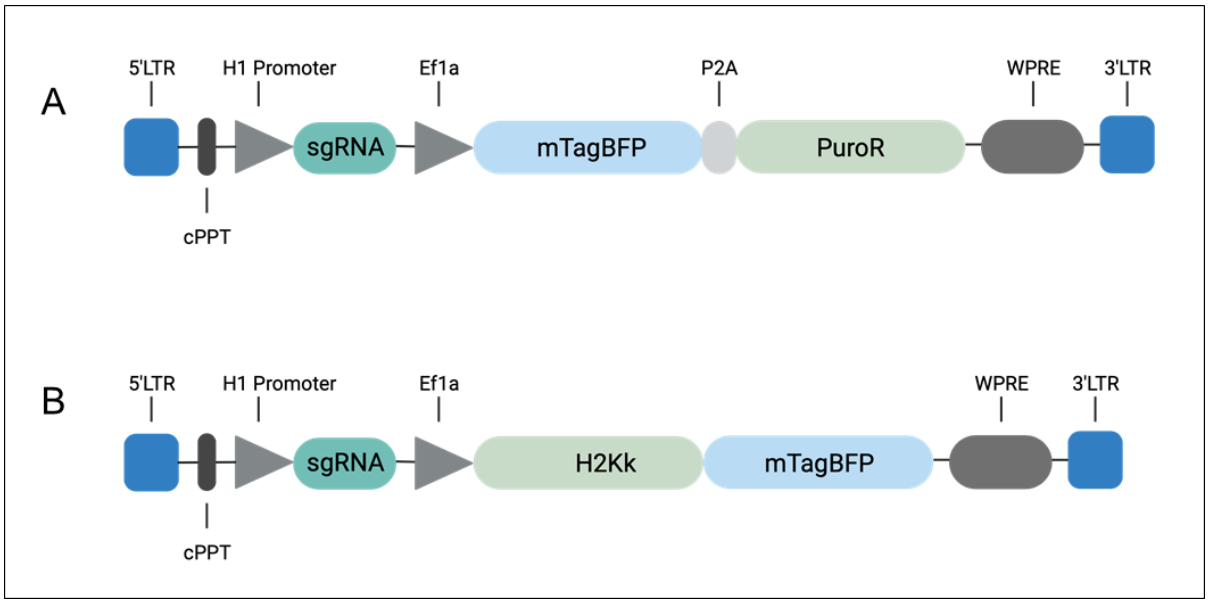

Figure 7: sgRNA/library expressing constructs
A: Construct with H2Kk-mTagBFP fusion for transduction of ALL PDX. **B:** Construct with puromycin resistance gene and mTagBFP as fluorochrome to monitor expression level used for AML PDX (Created with BioRender).

In previous experiments, we observed that H2Kk-MACS effectively enriched transduced ALL cells, while AML PDX cells undergo cell death upon MACS enrichment. In conclusion, we have decided to utilize puromycin to select AML cells and H2Kk-MACS to select ALL cells.

Therefore, sgRNAs targeting CD33 were cloned into a backbone expressing a puromycin-resistant gene, whereas sgRNAs targeting CD19 were cloned into an H2Kk-expressing backbone. Additionally, every sgRNA plasmid encoded the fluorophore marker mTagBFP under the control of the human EF1a promoter, allowing monitoring by flow cytometry. The H2Kk construct was designed to express an H2Kk-mTagBFP fusion protein, whereas the puromycin selection gene was cloned downstream of a mTagBFP and P2A self-cleavage peptide sequence. We transduced every Cas9-expressing PDX sample with a CD33 or CD19-expressing sgRNA with the suitable selection marker. After 4-14 days, we analyzed the expression of CD33 or CD19 using flow cytometry (Figure 8).

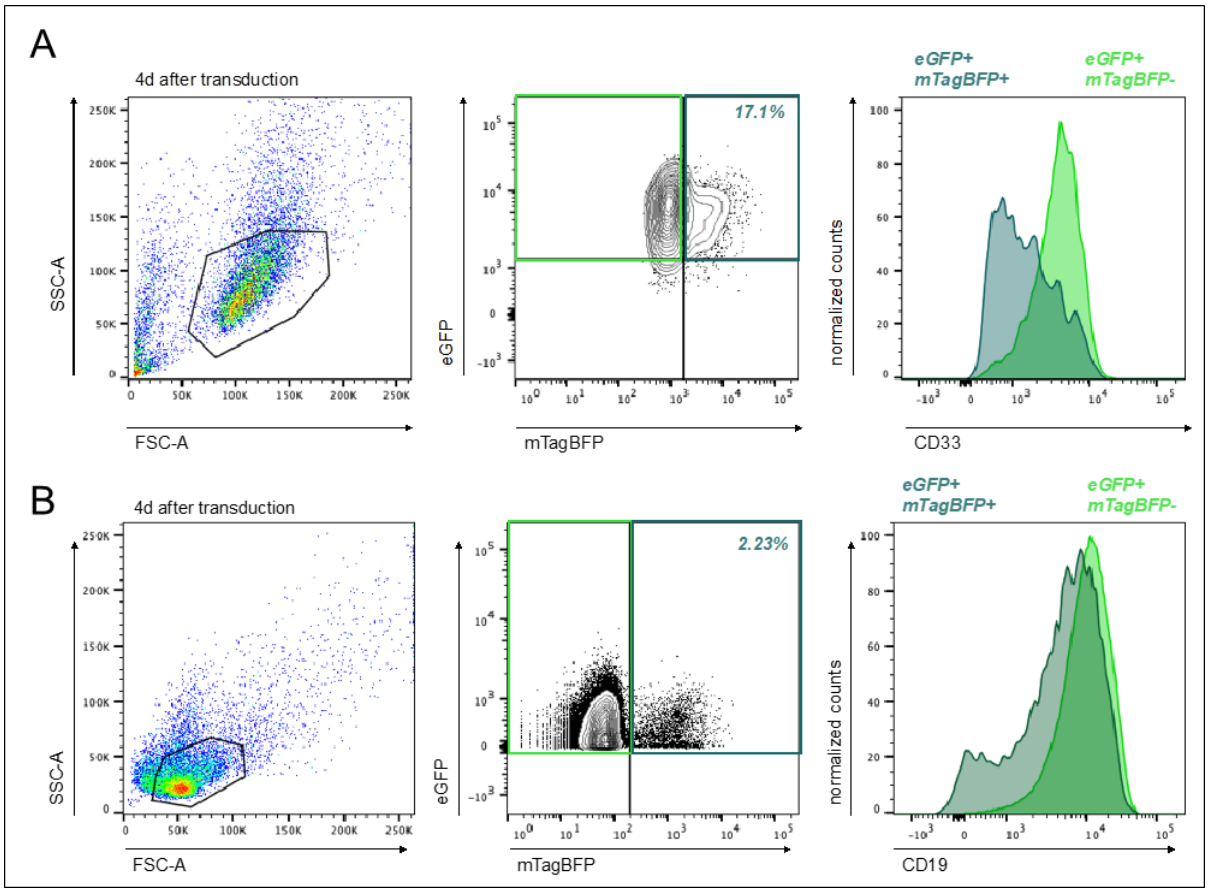

Figure 8: Functionality of Cas9 in AML and ALL PDX cells
A: Representative analysis of PDX AML388 four days post-transduction. Showing a CD33 knockout in the Cas9/eGFP and sgRNA/mTagBFP double-positive population compared to the Cas9/eGFP-only population. **B:** Representative CD19 knock out in ALL50 four days after transduction. A CD19 knockout can be seen in the double-positive population compared to the Cas9/eGFP-only population.

Gating was performed based on lymphocytes and pre-existing Cas9/eGFP expression. eGFP-positive cells were analyzed for sgRNA expression using mTagBFP as a marker. mTagBFP negative cells were used as an internal control of CD marker expression. Staining of CD19 or CD33 in the internal control showed the expected high expression, while the expression of CD33 or CD19 was strongly reduced in the eGFP/mTagBFP double positive cell fraction. Since the gene knockout of the CD19 and CD33 locus was successful, the Cas9 nuclease was defined as functional in all PDX cells.

4.2 Design, cloning and quality controls of CRISPR/Cas9 KO library

After testing the functionality of Cas9 in all PDX cells, the sgRNA library was designed and cloned. Previous experiments conducted in our laboratory have revealed that the size of a sgRNA screening library is restricted when screening *in vivo* (Wirth et al. 2022;

Bahrami et al. 2023; Ghalandary et al. 2023). The maximum estimated size for each library is 200 target genes.

For this project, we based our target decisions on a list of drug-target pairs from the INFORM project, which contained 371 genes. We narrowed our focus to 146 specific genes through a series of selection processes. The *in-silico* design of all sgRNA sequences and the cloning were done according to the published CLUE pipeline (Becker et al. 2020). With CLUE, it's possible to create an oligo pool that includes multiple libraries, each specified by its adapter sequence. This work included optimizing the PCR process to amplify specific libraries. (PCR2 in Figure 11). As a final quality check of all cloning steps, the sgRNA library plasmid was sequenced using next-generation sequencing. After completing quality control, two Cas9-expressing AML cell lines were transduced with the cloned library plasmid for a test screen *in vitro*. To ensure that the library size was suitable for each PDX sample, all samples were transduced with the library plasmid, and the distribution of sgRNAs was checked after *in vivo* time. An even distribution of sgRNAs indicates an appropriate library size for *in vivo* screening in the tested sample, as these cells did not express Cas9.

4.2.1 Design of a CRISPR/Cas9 library targeting druggable genes

All target selection steps were done in collaboration with Katharina Hunt.

Our goal was to create a library comprising a maximum of 200 genes, each of which would be targeted by five sgRNAs, including positive and negative controls. This project aims to predict individual targets using a CRISPR/Cas9 screening pipeline in AL PDX and subsequently validate the target-specific drug *in vivo*. We used a drug-target list of 371 cancer-related genes and over 800 drugs (unpublished data) obtained from the INFORM project in Heidelberg as the basis for selecting the targets. However, given the size limitations of the library, we had to narrow down the list of possible target genes (Figure 9).

First, we excluded leukemia-irrelevant targets and all kinases. This decision was made based on the fact that there are cheaper and easier ways to screen for relevant kinases like LC-MS/M (Abdelhameed, Attwa, and Kadi 2017), ATP assays(Singh et al. 2004) and kinase-assay linked phosphoproteomics (Xue et al. 2012).

Additionally, we excluded immunotargets from our model as we are working with an immunodeficient mouse model, making these targets unsuitable for our purposes. After excluding all targets where we were unable to purchase the drug, we narrowed down

our list to 146 target genes. These genes can be linked to 240 drugs, with 48 of them being FDA approved.

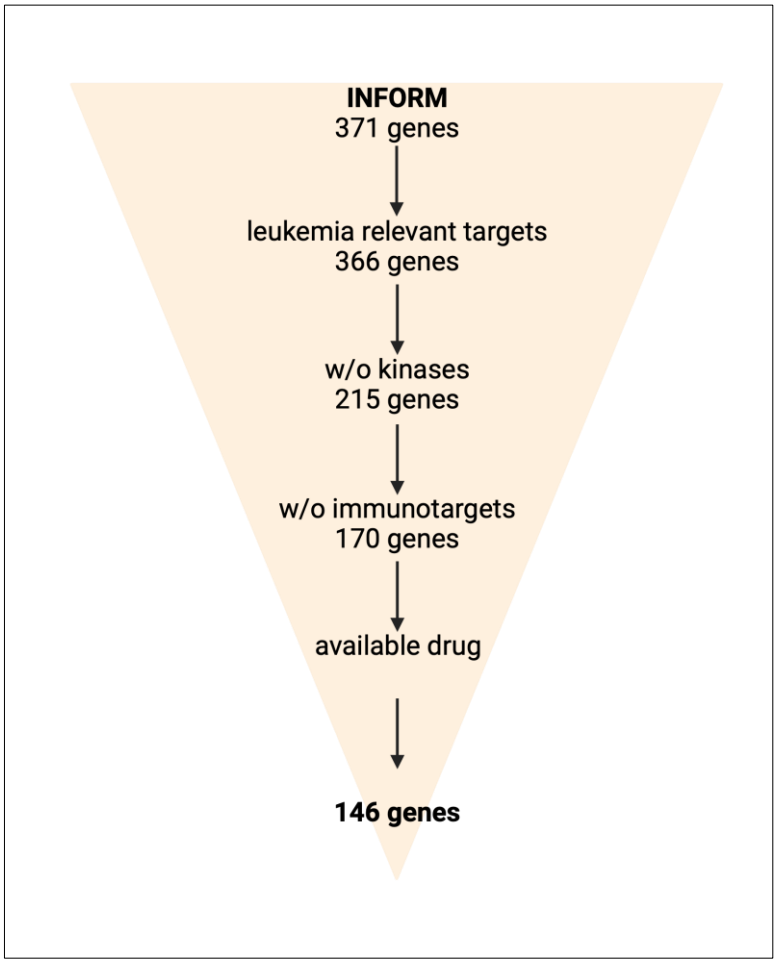

Figure 9: Generation of sgRNA library leading to 146 target genes
Exclusion of kinases, immunotargets and focus on leukemia-relevant targets as well as the availability of the gene-associated drug result in 146 target genes (Created with BioRender).

Previous experiments indicated that the maximum library size for AML PDX is lower than that of ALL PDX (Wirth et al. 2022; Bahrami et al. 2023; Ghalandary et al. 2023). To adjust the library size while working with AML PDX, we split the 148 targets into two smaller libraries. As a result, we created two smaller libraries, each consisting of 73 target genes, which modulate all 146 targets. To ensure the quality of our planned in vivo screens and finalize the library design, we added approximately 10% controls (see Table 21). Our positive controls, listed as pan-essential genes, came from the Achilles project (Table 22). This dataset contains the results of genome-scale CRISPR knockout screens for over 18,000 genes in over 600 cancer cell lines (Dempster et al. 2019). For our negative controls, we chose several non-targeting sgRNAs from the Brunello Whole Genome Library (Doench et al. 2016). Our final library size, which

includes all controls, was 811 sgRNAs (Drug_all). We adjusted the number of controls when we divided the library into two smaller parts (Drug_sub1 and Drug_sub2), and each small library was made up of 408 sgRNAs.

Table 21: Library compositions

Library	genes	sgRNAs	positive controls (genes)	positive controls (sgRNAs)	negative controls (sgRNAs)	total size (sgRNAs)
Drug_all	146	730	11	55	26	811
Drug_sub1	73	365	6	30	13	408
Drug_sub2	73	365	6	30	13	408

Table 22: List of pan-essential genes used as positive controls

Positive controls
CDK7
HSPE1
POLR2L
PSMB3
RAN
RPL12
RPL37
RRM2
SARS
SNRNP200
SS18L2

4.2.2 Cloning of CRISPR/Cas9 library using CLUE

Large commercial sgRNA libraries can be difficult to handle and require high cell numbers to ensure proper coverage during each screening step. However, a customized small library can be used for more complex and limited environments, such as a PDX model. The CLUE pipeline, which allows for easy generation and cloning of customized libraries, was utilized for this purpose (Becker et al. 2020). By using CLUE, a single oligo pool containing all necessary sgRNA libraries could be designed. Each sgRNA library has different adapter sequences that are used for specific PCR amplification. Additionally, the easy-to-use web interface of CLUE aids in designing a customized library and generating oligos for all subsequent cloning steps. For more information on CLUE, visit (www.crispr-clue.de).

The CLUE wet lab work is defined by three PCRs (see Figure 10). The first PCR amplifies the whole oligo pool and the product is used for cloning into a TOPO plasmid for long-time storage. The second PCR amplifies the specific sgRNA library as defined

by the library-specific PCR primers. Lastly, the third PCR prepares the generated PCR fragments for the final Gibson cloning into a lentiviral sgRNA expression backbone.

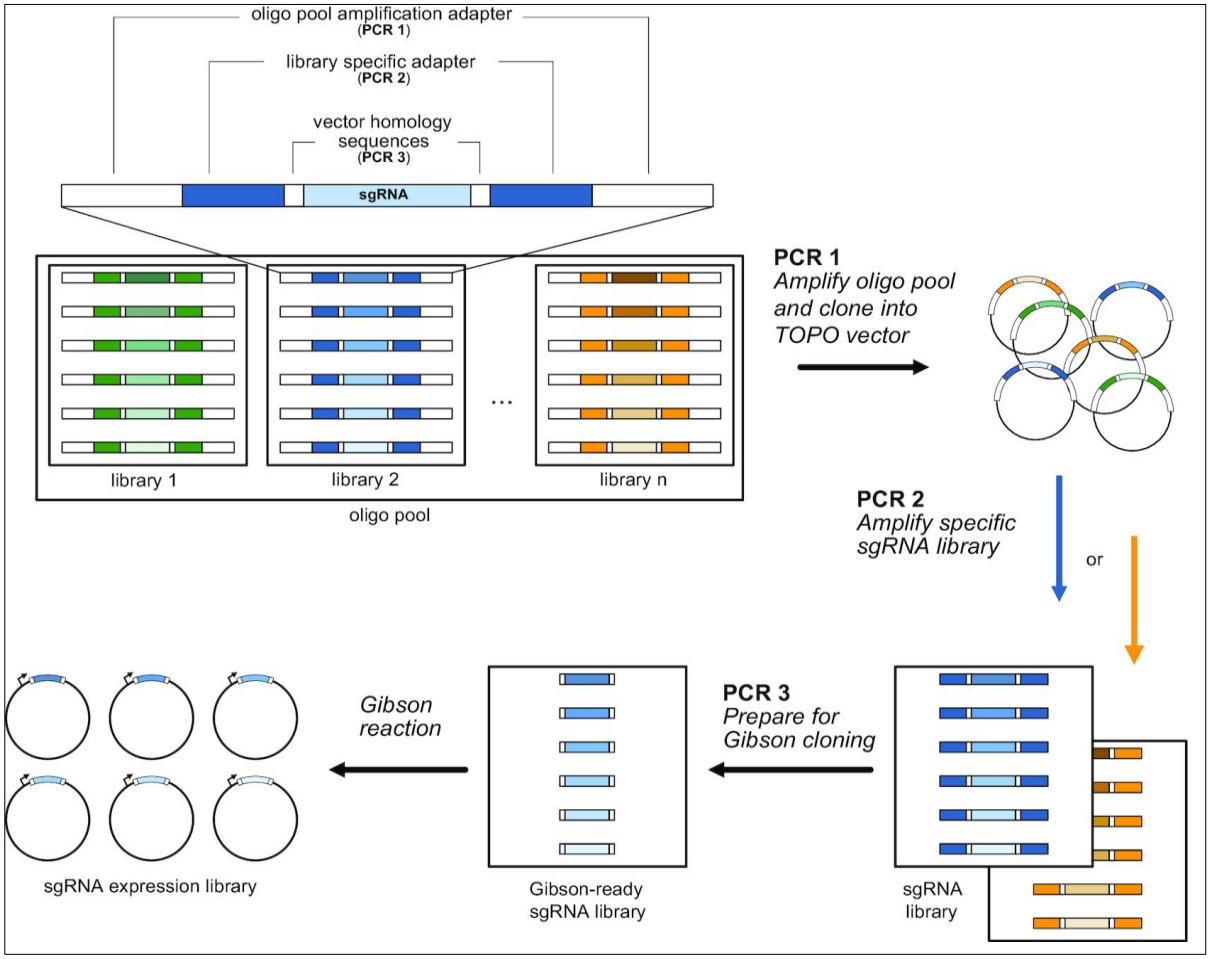

Figure 10: Utilization of the CLUE protocol allowed parallel cloning of all sgRNA libraries
Starting from an oligo pool with many different sgRNA libraries, defined by library-specific adapter sequences, to the final sgRNA fragments ready for cloning into a sgRNA expression plasmid (Becker et al. 2020).

As the paper was a joint effort between our lab and another, we conducted some optimization under the guidance of the first author, Martin Becker. The original paper recommended a relatively high number of cycles, 30, for amplifying the library (PCR2). To enhance this amplification process and guarantee an unbiased and precise DNA target amplification, we conducted tests on various cycles and assessed the evenness of sgRNA distribution using NGS and the Gini Index.

We optimized the PCR using 20, 23, 26, and as a control 30 cycles, and then followed the methods as described (see 3.5.6 and 3.5.12). Afterward, we submitted the plasmids for NGS and analyzed the data using the methods outlined in 3.6.2. We calculated the Gini index as described in 3.7.1. The generated density plots can be found in Figure 11. Unfortunately, the NGS quality of the data for the 23-cycle sample

was not high enough, so we had to exclude it from our final analysis. However, all three remaining attempts successfully restored the entire size of the library, and none of the sgRNA was missing, as shown by the density plots. The lower the cycle number, the lower the Gini index, which means that the sgRNA distribution is more equal. Concluding, we utilized the lowest cycle number (20 cycles) for all further experiments.

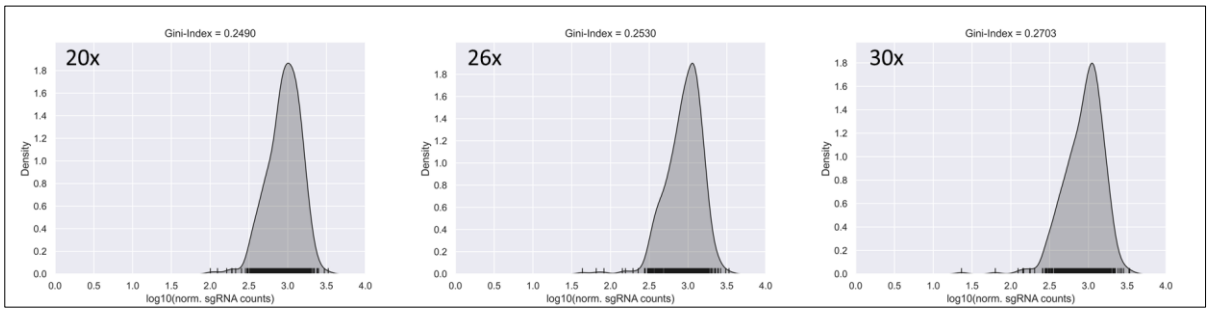

Figure 11: Reduction of PCR cycles improved evenness of sgRNA distribution
Gini index is indicated above every density plot.

For the screening purpose of the project, we cloned Drug_all, Drug_sub1, and Drug_sub2 in the AML-specific sgRNA expressing backbone with puromycin serving as the selection marker. For screening the ALL PDX samples, we used the H2Kk-BFP expression plasmid to clone the Drug_all library. All libraries underwent parallel cloning using the optimized procedure outlined in chapters 3.5.5 and 3.5.6. The resulting plasmids were prepared and sent for NGS to assess the quality of the cloned libraries, as described in 3.5.11. The NGS data was analyzed as described in 3.6.2, and the Gini indices and density plots (Figure 12) revealed an even distribution of sgRNAs and no loss of sgRNAs during any cloning step.

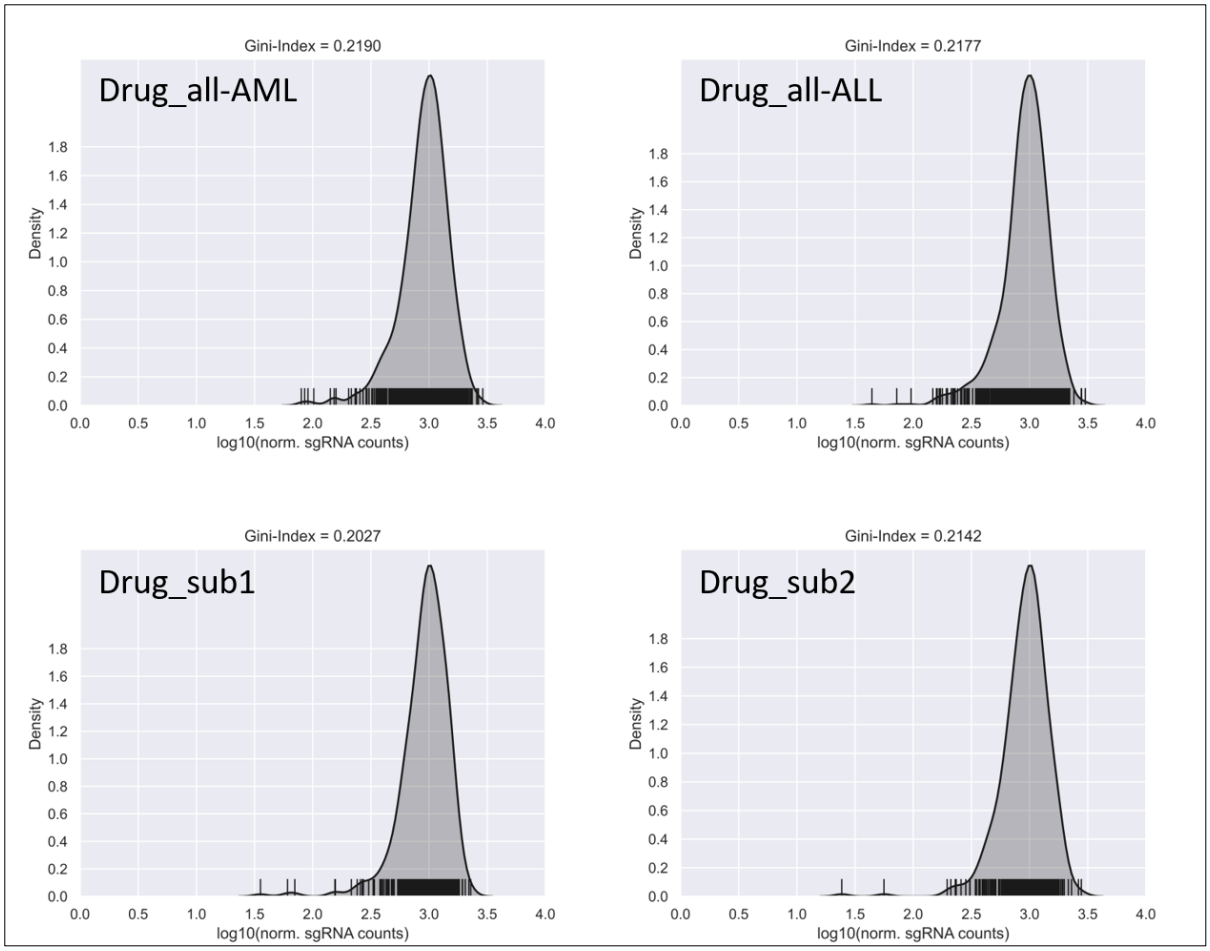

Figure 12: Cloning according to CLUE protocol generated a narrow sgRNA distribution
Gini index is indicated above every density plot.

After successfully cloning and conducting quality checks, the sgRNA expression constructs are ready for both *in vivo* and *in vitro* screening.

4.2.3 I*n vitro* screen test in AML cell lines shows functional sgRNA library

The successful cloning of the sgRNA libraries was ensured through NGS. To now confirm their functionality, we conducted an *in vitro* screening in two AML cell lines.
We transduced Cas9-negative cells to observe how the library was distributed during in vitro passaging. The sgRNA sequences served as "barcodes," so we anticipated that the input and endpoint distribution would be similar. We used the Gini index to represent the distribution, as shown in Figure 13. As expected, there was no significant difference in the distribution between the two time points.

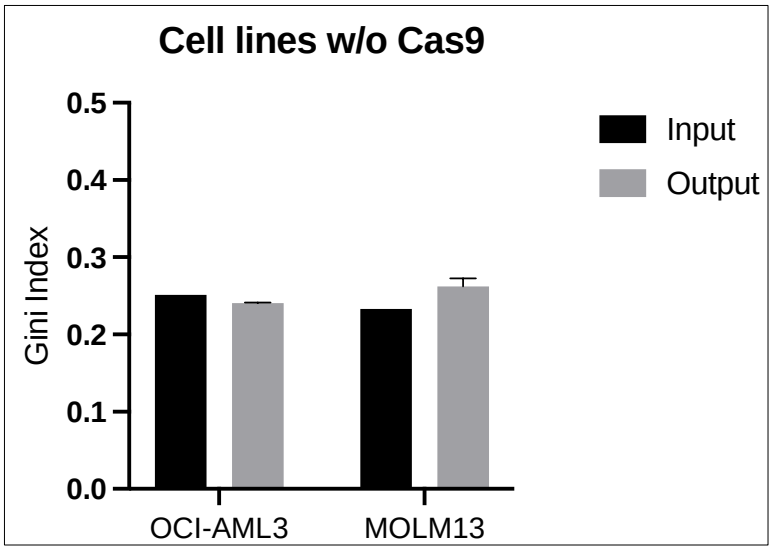

Figure 13: Even sgRNA distribution after 14 days in Cas9 negative cell lines

The *in vitro* screen using Cas9-expressing cells was performed as described in 3.3.13. We prepared input and output samples for NGS and analyzed the received data using the MAGeCK algorithm (as described in 3.7.1). The algorithm produces RRA scores for every gene, and we used these scores to rank the dropouts for both cell lines. Figure 14 displays the ranking of these dropouts, where a score smaller than 0.003 indicates a significant dropout, marked by a dotted line.

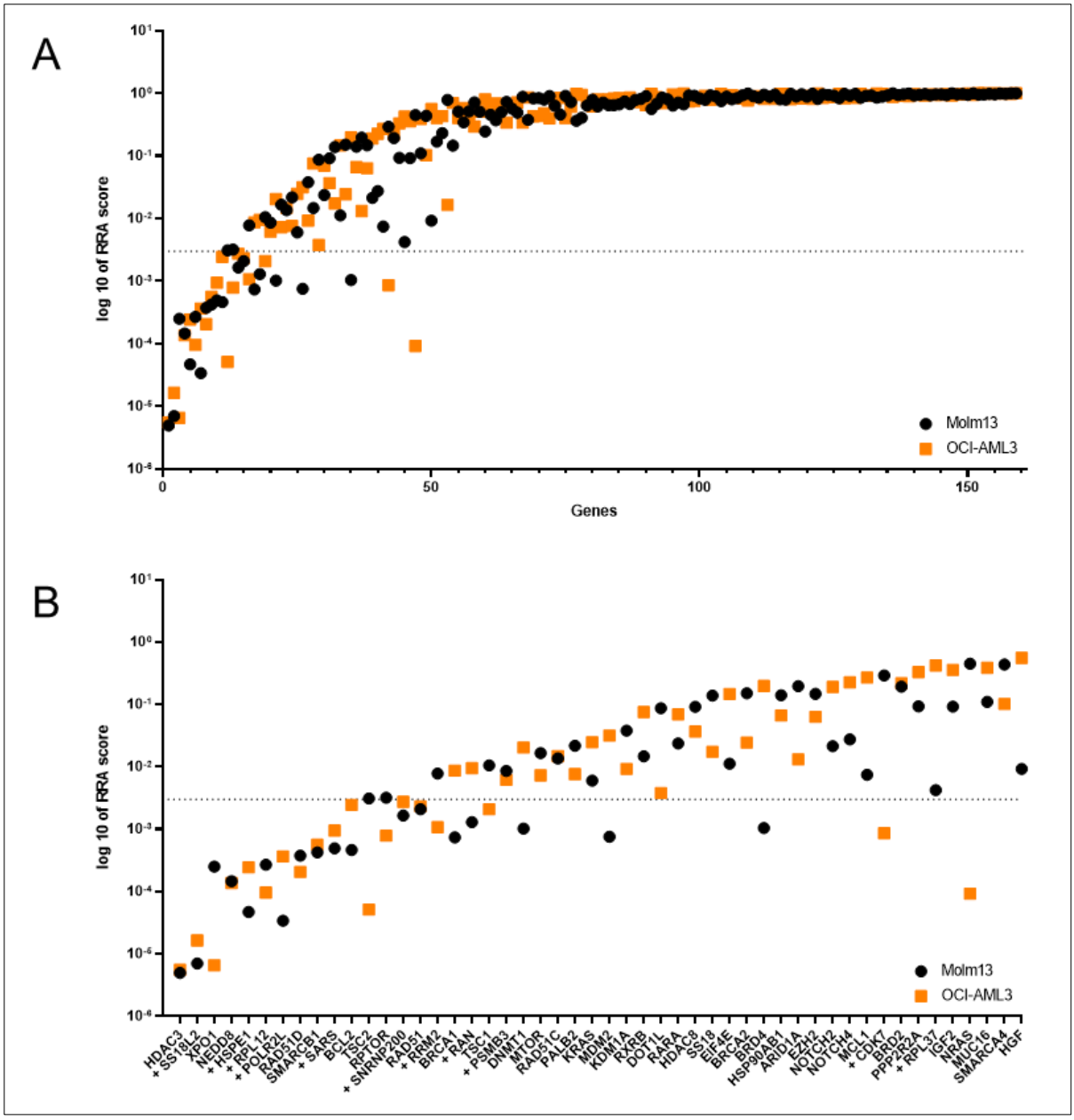

Figure 14: CRISPR/Cas9 test screen in two cell lines showed a functional sgRNA library
Dropouts are depicted by RRA score. The dotted line represents the threshold of significance of 0.003. A: Overview of all dropouts and non-dropouts. B: Depiction of 50 strongest depleted genes. Positive controls are marked by "+".

Our analysis of the AML cell lines revealed several dropouts, with HDAC3 being the main one. To strengthen our findings, we compared the five strongest dropouts to the open-access data of the Cancer Dependency Map (DepMap) portal (www.depmap.org). DepMap is an ongoing project that identifies gene essentialities across hundreds of cancer cell lines using whole genome CRISPR knockout screens (Meyers et al. 2017b). The bioinformatic analysis of the DepMap screen data is done using CHRONOS (Dempster et al. 2021). A gene effect score with a value of -1 is defined by the median of all common essential genes and therefore indicates a substantial dependency. In each cell line screen, the top five most significant dropouts

produced a total of seven genes. Out of these, six genes exhibited significant dropouts in both cell lines. Only *NRAS* showed a dependency in the OCI-AML3 cells but not in the Molm13 cells.

When we compared the dropouts from our cell line screen with the DepMap data, we found that 13 out of 14 dropouts were identified by both methods, as shown in Figure 15.

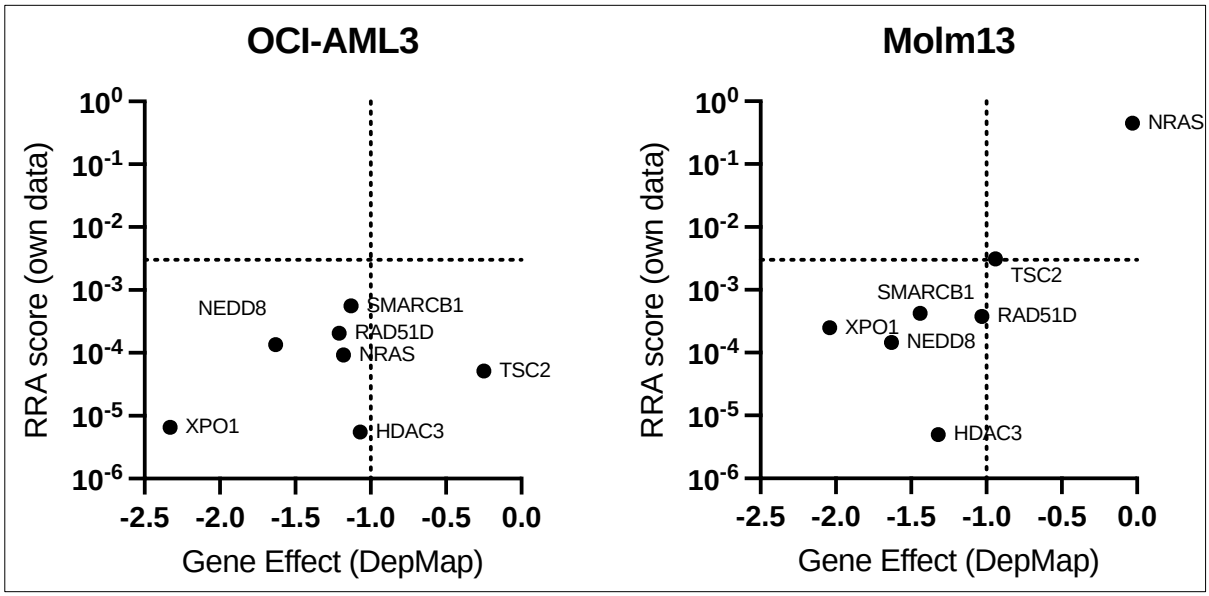

Figure 15: High overlap between own and DepMap data reinforced functionality of the sgRNA library

Dropouts from DepMap are represented by gene effect, originating from the Chronos algorithm. The dotted line marks the significance. Significant RRA score: < 0.003. Significant gene effect: < -1.

The gene *TSC2* was the only one that differed between the two data sets. Based on our analysis, OCI-AML3 shows a dropout in *TSC2*. However, DepMap does not identify this dependency.

Nevertheless, our data was supported and confirmed by the identified overlaps, which further demonstrated the effectiveness of the cloned sgRNA library.

Further, we tested the quality of the screens by analyzing the dropout significance of the positive controls and checking the non-targeting controls. The selected positive control genes are expected to dropout due to their essentiality. Of 11 positive controls, ten displayed a significant dropout in both cell lines. To analyze this further, the average readcount for each gene was determined. Then, the average of the input and output samples was calculated (as shown in Figure 16) revealing a decrease in normalized readcounts for the output samples compared to the input samples in both cell lines.

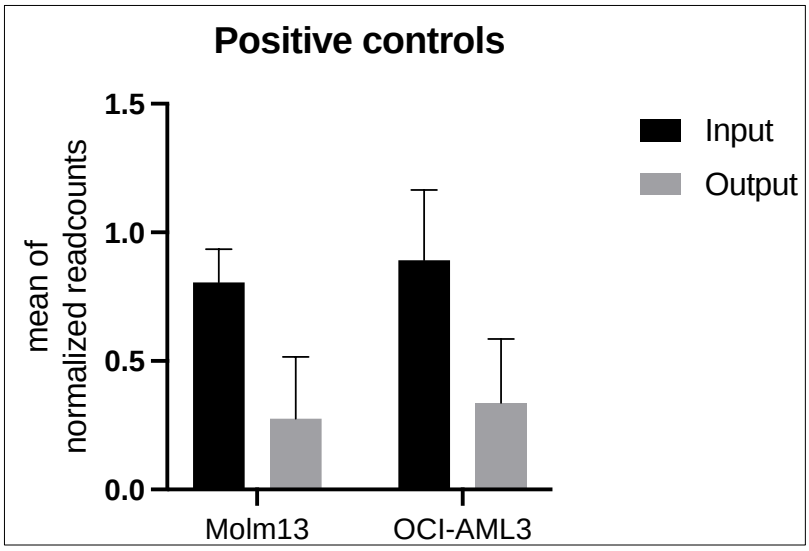

Figure 16: Depletion of positive controls showed the functionality of Cas9 during the screening process

The non-targeting controls remained consistent or seemed to have increased because the cells with a non-targeting sgRNA were not affected by Cas9 cutting and therefore did not experience any DNA damage.

Based on the fact that both screens passed the quality controls and most dropouts were confirmed by the DepMap data, we have defined the test screens as successful. As a result, the library is now ready to be used in the upcoming *in vivo* screens.

4.2.4 Transduction of a Cas9 negative PDX sample to control suitability of *in vivo* library size

As we anticipated a limited maximum library size for an *in vivo* screen, we planned a control experiment. We tested the libraries by transducing PDX samples without Cas9. As the libraries were transduced in a Cas9-negative background, the distribution of all sgRNAs should remain unchanged in the output samples.

Cas9-negative PDX samples were transduced and processed for screening as described in chapters 3.3.6, 3.3.9, 3.3.10 and 3.3.14. We injected two mice each with 1 x 10^7 cells intravenously and ended the experiments once the mice showed the first signs of disease. We collected samples from the bone marrow and spleen (if possible) and used them for gDNA isolation (3.5.9) and preparation for NGS (3.5.12). The data was analyzed like the Cas9 negative samples in the cell line test screen chapter 4.2.3. The Gini index for every PDX sample was calculated and can be seen in Figure 17.

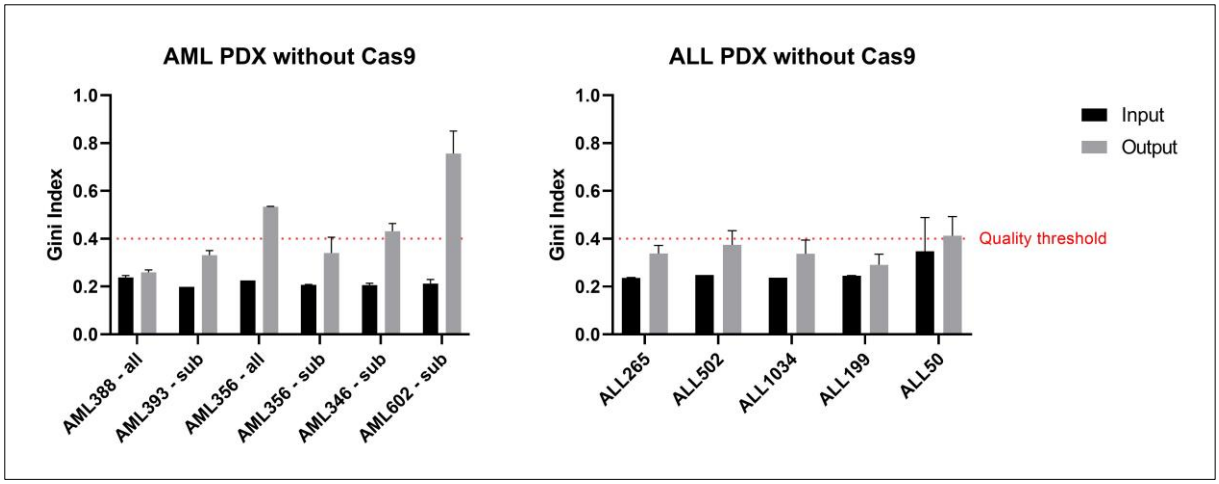

Figure 17: The analysis of the sgRNA distribution after *in vivo* growth of cells without Cas9 led to the exclusion of two AML PDX samples
A: Distribution of sgRNAs of AML PDX cells depicted by the Gini index.Including the follow-up experiment of the AML356 samples using the smaller sub-library **B:** sgRNA distribution of ALL PDX samples. The dotted line represents the quality threshold of a Gini index of 0.4.

We used the Gini index of the cloned libraries, as shown in Figure 12, to determine the maximum Gini index that a sgRNA distribution should reach when transduced in cells without a Cas9 construct. Based on this analysis, we decided to double the Gini index value by 0.2 and use it as a threshold. Therefore, any PDX screened with a specific library size in a Cas9 negative background that generated a Gini index below 0.4 is considered screenable with the tested library size or any smaller library.

Previous *in vivo* screening experiments with the AML388 sample suggested that this sample be screened with the Drug_all library (unpublished data). As PDX sample AML356 had not been screened before, we also decided to use the Drug_all library. However, data from previous experiments indicated that a smaller library size would be suitable for the three remaining AML PDX samples, so we used the Drug_sub1/2 sub-libraries for these (unpublished data).

After analyzing the control experiment, we found that the Gini index of the AML388 and AML393 samples was below 0.4. Therefore, we classified those samples as screenable with the tested libraries. The Gini index of AML602, AML346, and AML356 exceeded the threshold. We found that AML602 and AML346 were not screenable with our smallest library, Drug_sub, and were therefore excluded. On the other hand, AML356 was initially tested with the larger Drug_all library, and since it also exceeded the threshold, the test was repeated with the smaller Drug_sub library (as shown in Figure 17A). This confirmed that the AML356 sample can be screened using the Drug_sub libraries.

As some of the ALL PDXs were previously screened *in vivo* (Wirth et al. 2022; Bahrami et al. 2023), using an even larger library, we chose to utilize the Drug_all library for all screenings. Of the five ALL PDX samples tested, four had a Gini index below the threshold and are considered screenable using the Drug_all library.

The ALL50 sample had a higher Gini index in the output than other samples, but even the input samples had a higher Gini index than any other ALL input sample. The second input sample had a single Gini index value of 0.4475. We suspected that a handling step post-injection reduced the number of cells, leading to a coverage problem and an uneven sgRNA distribution. This coverage problem was also observed in the output samples. As a result, we concluded that it was a technical issue rather than a biological one, and therefore, we used the ALL50 sample for screening with the Drug_all library.

4.3 Technical setup and quality controls of screen data

We created a CRISPR/Cas9 library, specifically targeting druggable genes. With this, we aim to determine whether an *in vivo* screen in PDX samples can be used to predict patient-specific drugs. We cloned and tested the library and confirmed its suitability in three out of five AML PDX samples (AML388, AML356, and AML393) and all five ALL PDX samples (ALL265, ALL199, ALL502, ALL1034, and ALL50) as depicted in Figure 17.

To ensure quality control throughout the entire screening process, we conducted various tests such as checking the percentage of mapped reads, coverage of sgRNA in the NGS procedure, and number of zero reads in the read count file. Additionally, we analyzed the positive and non-targeting controls in the sgRNA libraries as further quality control for the *in vivo* screen.

4.3.1 Screening procedure in AML PDX cells

In order to conduct a knockout screen, it is necessary to introduce a Cas9 nuclease and a sgRNA library that targets specific genomic loc. For this purpose, freshly isolated AML PDX cells expressing Cas9 were utilized for the transduction with the library-expressing backbone. Previous experiments have demonstrated the effectiveness of puromycin as a selection method for AML PDX samples. Hence, the library backbone contains a puromycin resistance gene and a mTagBFP gene for tracking the entire

screening process. Figure 18 provides an overview of the screening procedure for AML PDX samples.

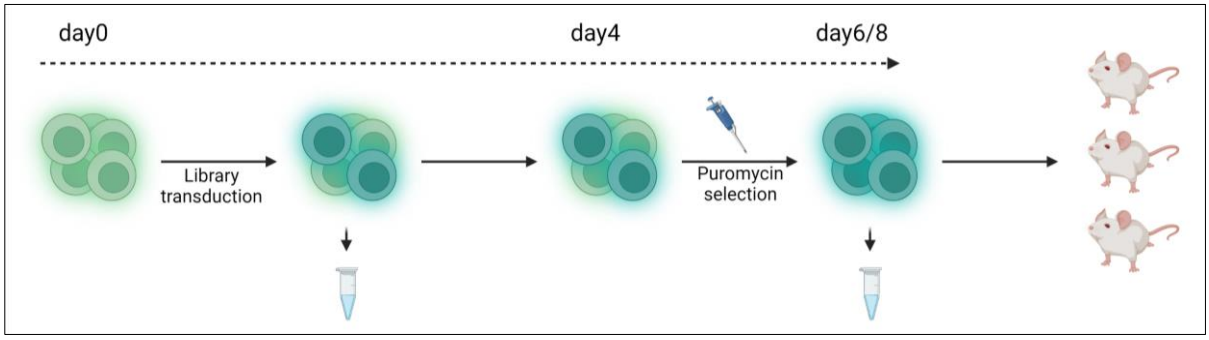

Figure 18: Experimental set-up of *in vivo* screening in AML PDX cells
Tubes represent the time points of DNA sampling (Created with BioRender).

After transduction and collection of Input_1, the cells were kept *in vitro* for four days to enable the expression of the puromycin resistance gene, which is crucial for enriching sgRNA-positive cells later on. The puromycin selection was started on day four post-transduction. Depending on the PDX sample and the initial transduction efficiency, successful selection typically occurred two to four days later. A successful selection was defined as having at least 90% of cells positive for Cas9/eGFP and library (mTagBFP). Following the collection of the second input sample, the cells were prepared for injection into NSG mice as described in the methods (3.2.1).

To control any potential *ex vivo* skewing or loss of library coverage due to cell death, specific time points were chosen for collecting the input samples. The period between the two input sample time points is typically 5-7, depending on the length of puromycin selection. Due to the extended *ex vivo* time, it is expected to see some dropouts of strong candidates in Input_2. Figure 19 shows a correlation of the two collected input samples in the AML388 PDX sample, where the normalized readcounts were compared. The R2 score of 0.6244 shows a low correlation, which suggests that there were knockouts in the Input_2 sample. As a result, only Input_1 was used for MAGeCK analysis of the AML PDX samples. Input_2 serves as a control for library coverage and skewing before being injected into mice.

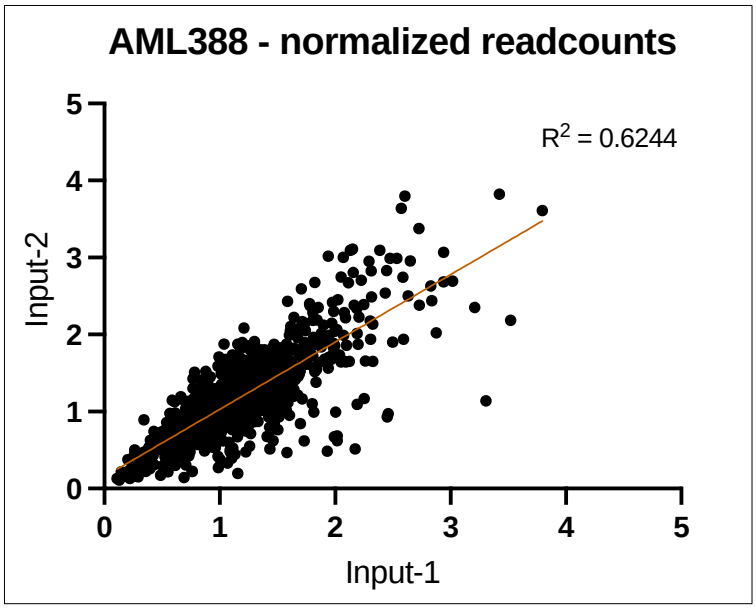

Figure 19: Exclusion of Input_2 from AML PDX sample analysis
The correlation (depicted by the R^2) between the collected input samples.

A representative flow cytometry analysis of the AML388 sample before injection is shown in Figure 20. Before transduction, the cells were checked by flow cytometry for a sufficient Cas9/eGFP expression of over 90%. The initial transduction efficiency of the AML388 sample, measured at day four post-transduction, is represented by a mTagBFP expression of 17%, and therefore low enough to ensure single integrations. Good cell viability and suitable transduction efficiency allowed for puromycin selection. After two days of incubation with puromycin, the enrichment efficiency was measured and monitored through the expression of mTagBFP. With an enrichment rate of over 90%, the library-expressing cells were prepared for injection into NSG mice.

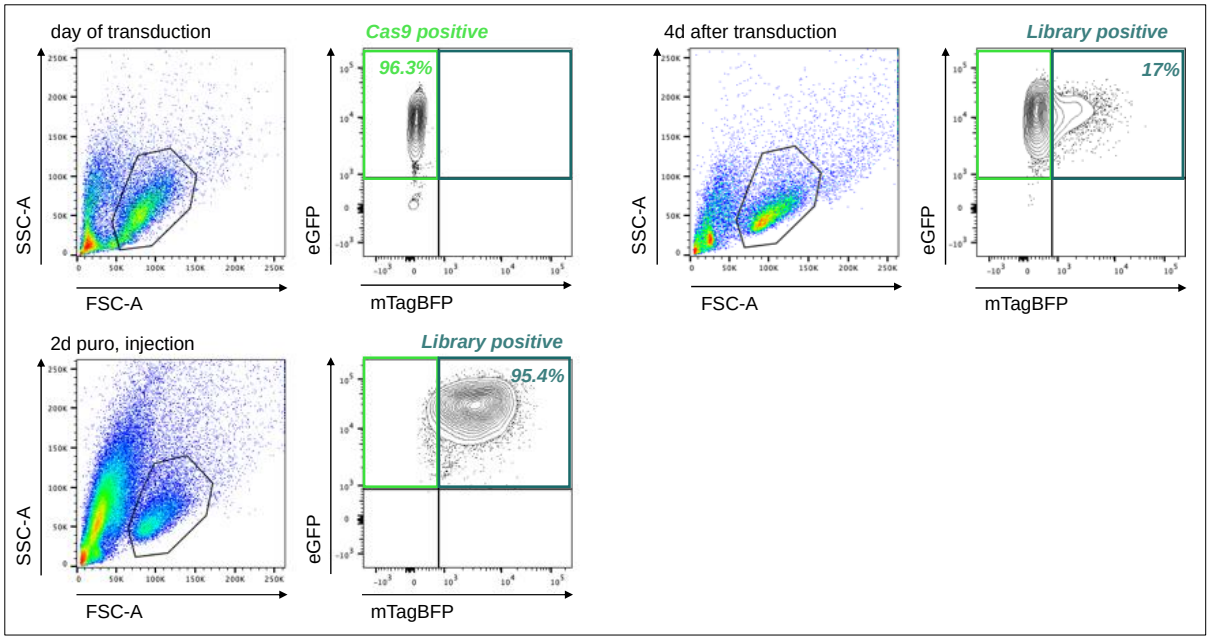

Figure 20: Transduction and enrichment of library expressing AML388 cells
Analysis on the day of transduction showed the number of Cas9-positive cells. Day four after transduction, depicted the initial library transduction efficiency. Two days after puromycin and on the day of injection, the percentage of library-positive cells showed successful enrichment.

Mice were taken down at first signs of leukemia and bone marrow cells were isolated. The expression of Cas9/eGFP and library (mTagBFP) was determined using flow cytometry, measuring the percentage of double-positive cells (see Figure 21).

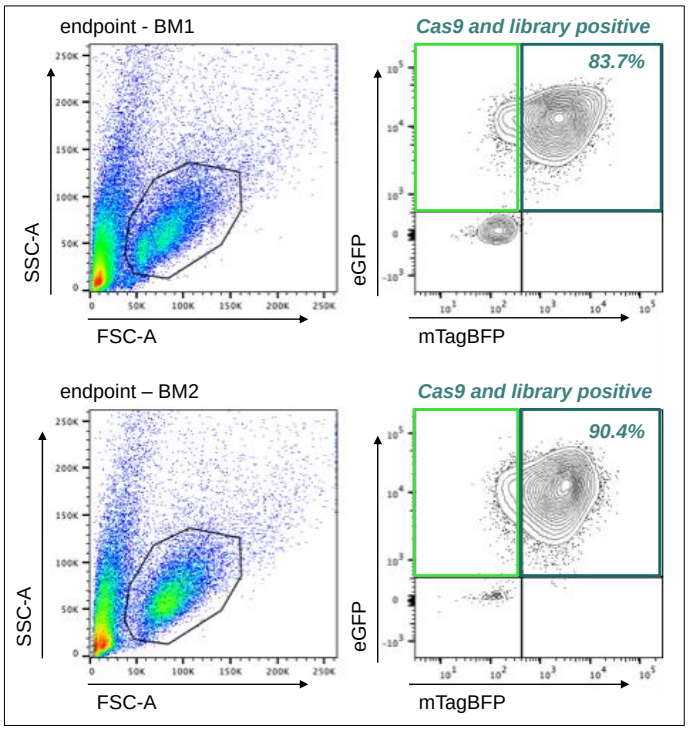

Figure 21: High expression of Cas9 and sgRNA library in BM samples of the AML388 cells after *in vivo* screening
For both samples, the percentage of Cas9 and library-positive cells is shown.

Representative flow cytometry analysis of two bone marrow samples of the AML388 cells shows Cas9/eGFP and library expression on the day of cell isolation. Both samples show more than 80% double positive cells. Collected cells were processed for DNA isolation and used for NGS PCR as the final read-out (3.5.9 and 3.5.12).

4.3.2 Screening procedure in ALL PDX cells

The screening process for ALL PDX is different from that of AML PDX in terms of the selection method and the shorter *ex vivo* time prior to injection into mice (Figure 22).

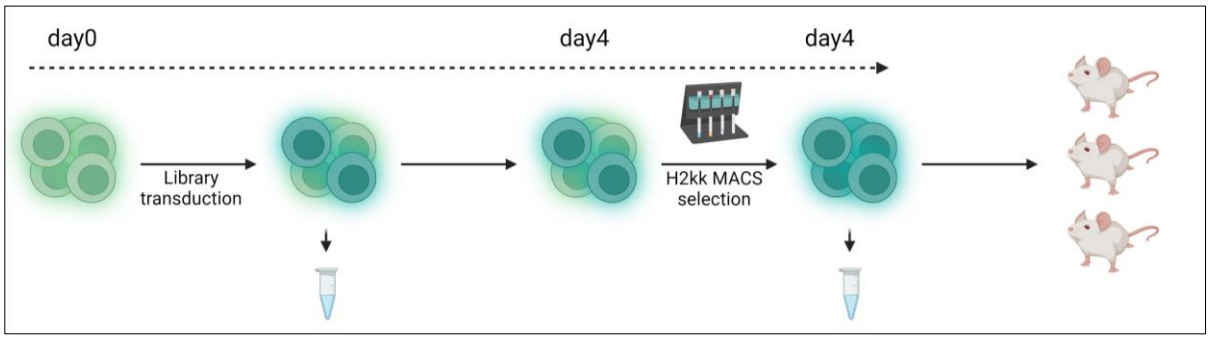

Figure 22: : Experimental set-up of *in vivo* screening in ALL PDX cells
Tubes represent the time points of DNA sampling (Created with BioRender).

On day four after transduction, the selection process began using H2Kk-MACS enrichment, which was previously used in experiments conducted by (Wirth et al. 2022; Bahrami et al. 2023). On the same day, both enrichment and injection were carried out. Prior to selection, the transduced cells were examined for their expression of Cas9/eGFP and library (mTagBFP), as indicated by a double-positive eGFP/mTagBFP cell population in flow cytometry. The representative flow cytometry analysis of ALL1034 revealed an initial library expression of 13.6% and Cas9 expression in over 90% of the cells (see Figure 23). In order to ensure the successful H2Kk-MACS selection, the cells were verified by flow cytometry before being injected into NSG mice. The analyzed data indicated an enrichment of library-expressing cells of over 90%. These enriched cells were prepared for injection into NSG mice after collecting Input_2.

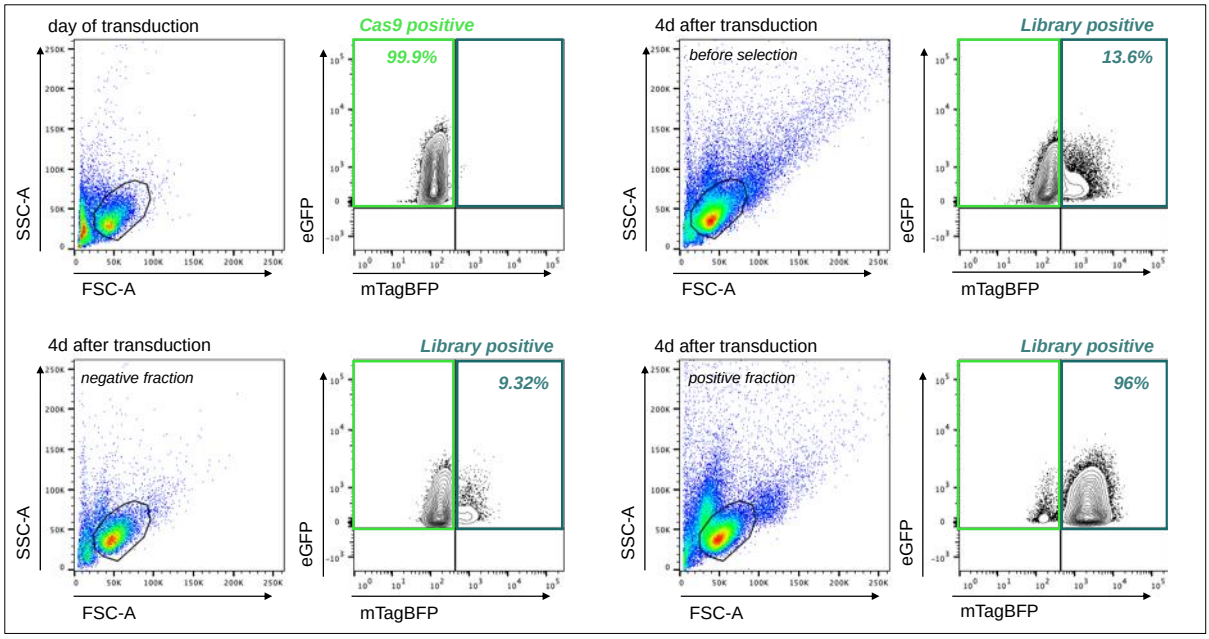

Figure 23: Transduction and enrichment of library expressing ALL1034 cells
Analysis on the day of transduction showed the number of Cas9-positive cells. Day four after transduction, depicted the initial library transduction efficiency and MACS enrichment was started. The negative and positive fractions showed the successful enrichment of the library positive cell fraction.

The ALL PDX samples showed a stronger correlation between Input_1 and Input_2 compared to the AML PDX samples, as shown in Figure 24 through the R^2 score. This difference can be attributed to the shorter *ex vivo* time of three days in the PDX samples screening process, as opposed to 5-7 days in AML PDX samples. This high correlation led to using both input samples in the MAGeCK analysis.

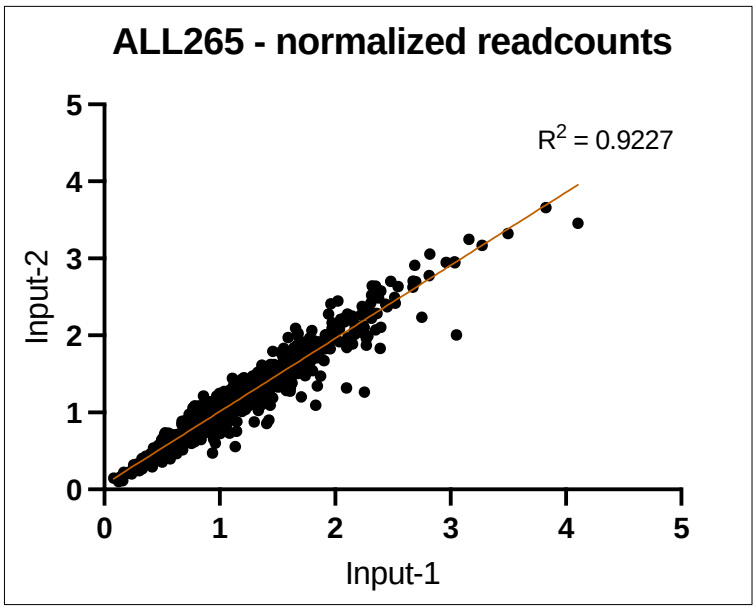

Figure 24: Input_1 and Input_2 were used for ALL sample analysis
The correlation (depicted by the R^2) between the collected input samples.

Mice were taken down at the first sign of disease and the sample handling was carried out as detailed in section 0 for the AML PDX cell. Figure 25 displays a representative FACS analysis of one BM output sample.

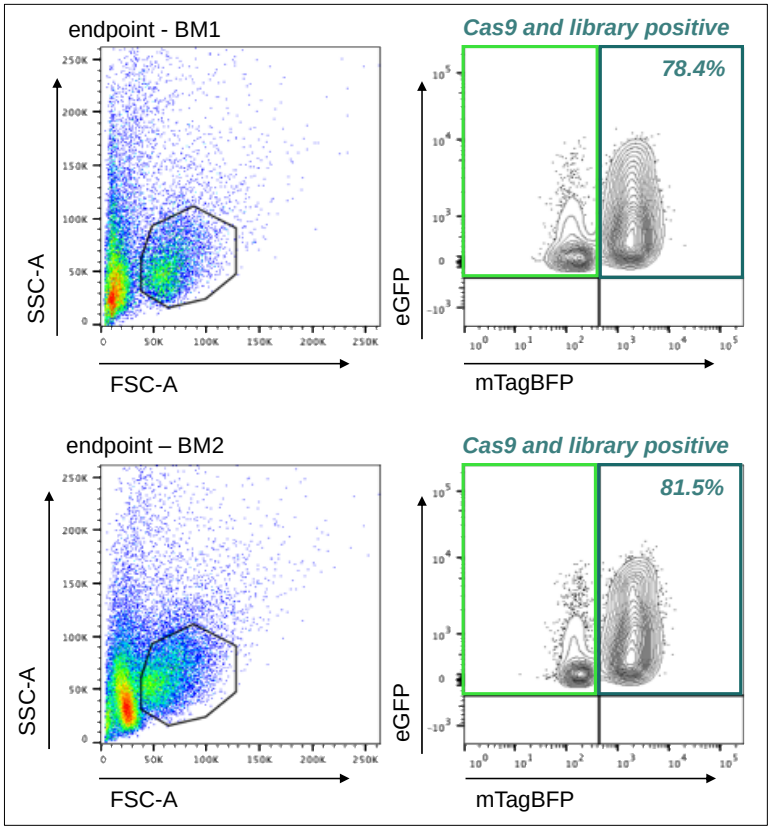

Figure 25: High expression of Cas9 and sgRNA library in BM samples of the ALL1034 cells after *in vivo* screening
For both samples, the percentage of Cas9 and library-positive cells is shown.

The ALL1034 cells showed around 80% of library and Cas9 expressing cells (double positive). We collected and processed quality-checked bone marrow samples for NGS analysis as the final readout.

4.3.3 Mapped reads and zero counts as quality control of generated readcount files

To analyze the screened PDX samples, cells were prepared for NGS. The fastq files obtained were then used to generate readcount tables for each submitted sample and replicate. The detailed method of using a python script to create density plots, Gini indices, and readcount tables is described in sections 3.6.2 and 3.7.1.

The readcount tables were used to check the quality of sequencing and the performed *in vivo* screen. The authors of the MAGeCK algorithm recommend specific values to

evaluate the data quality (Li et al. 2014; 2015), with an important value being the total number of reads in the fasq file. It is recommended to have at least 100-300 times the number of sgRNAs. All the fastq files obtained from the submitted samples passed this threshold (see Table 23 and Table 24).

Additionally, it is recommended that the mapped reads constitute a minimum of 60%. This value represents the number of reads that can be accurately matched to the library compared to the total number of reads. All samples with available data met the criteria, as indicated in Table 23 and Table 24. It is assumed that the quality of the missing samples (ALL50, ALL502, and ALL1034) was comparable.

As a third quality marker, it's important to check the total number of missing sgRNAs (sgRNAs with 0 readcounts). The authors of the MAGeCK algorithm recommend that no more than 1% of sgRNAs should have no assigned readcounts. This value is particularly relevant for whole genome screens in homogeneous cell models, such as established cell lines. However, when using a customized library targeting leukemia-relevant genes in a leukemia background, there will be a larger decrease in readcounts. After reviewing the ALL PDX samples, the recommended threshold of 1% can be underscored by three out of five samples. The highest percentage of zero counts was found in the ALL50 sample, which had 3.84%. The value is still quite low, particularly compared to the average rate of zero counts found in the AML PDX samples. In a study by Yamauchi and colleagues, they used a customized library of 470 genes and ended up with 65.4% of zero counts in their output file (Yamauchi et al. 2018). However, they could still successfully validate one of their dropouts, confirming their data. Based on this information, we decided to proceed with all three AML PDX samples, despite their percentage of zero counts ranging from 7-35%.

Table 23: Quality checks of AML PDX readcounts

	AML388	**AML356**	**AML393**
average reads/sgRNA	312	921	1544
average % of mapped reads	90,56	90,96	91,20
average % of zero reads in output samples	15,45	7,46	34,74

Table 24: Quality checks of ALL PDX readcounts

	ALL265	**ALL199**	**ALL50**	**ALL502**	**ALL1034**
average reads/sgRNA	839	1224	445	2269	2231
average % of mapped reads	88,55	89,34	no data	no data	no data
average % of zero reads in output samples	1,34	0,35	3,86	0,25	0,27

4.3.4 Positive and negative controls as quality control of *in vivo* screen

To ensure the quality and reliability of the generated screen data, positive and non-targeting controls were included and checked. The Drug_all library contained 11 pan-essential genes, while the Drug_sub libraries had six. Additionally, there were 26 or 13 non-targeting sgRNA controls used in the two different types of libraries.

The positive controls should drop out in all samples to confirm the functionality of the Cas9 nuclease. We calculated the average normalized readcounts of all positive controls in both the input and output samples and compared them (see Figure 26). In all eight PDX samples, the positive controls showed a significant reduction in the output compared to the input. This provided clear evidence of the functionality of Cas9.

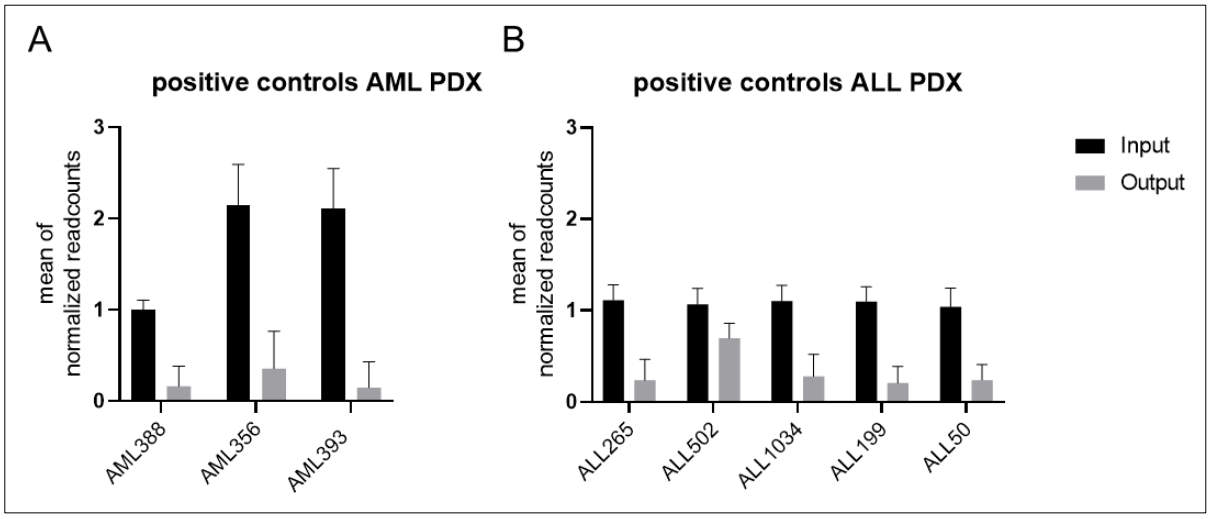

Figure 26: Dropout of positive controls showed the functionality of Cas9
A: Mean of normalized readcounts of positive controls comparing input and output samples of AML PDX cells. **B:** Mean of normalized readcounts of positive controls comparing input and output samples of ALL PDX cells.

The non-targeting sgRNAs were used as a second measure of quality. The readcounts of the non-targeting controls in the ALL PDX samples remained the same or increased due to the absence of DNA damage caused by Cas9, representing the expected results. In the AML388 and AML356 samples, the non-targeting sgRNAs showed similar results. However, in the AML393 sample, most of the non-targeting sgRNAs showed a decrease in readcounts. This could be due to a low number of injected or engrafted cells, resulting in inadequate library coverage. Consequently, we have excluded the AML393 sample from all subsequent analyses.

After completing the screen internal quality control tests, which included checking both non-targeting and positive controls, the final analysis was conducted on seven PDX

samples using the MAGeCK algorithm. This allowed for the prediction of significant dropouts.

4.4 Analysis of CRISPR/Cas9 screen using MAGeCK

In order to identify targets that are crucial for the *in vivo* growth of leukemic cells, the MAGeCK algorithm was utilized, as previously described by (Li et al. 2014). Biological replicates of collected bone marrow samples were used for the MAGeCK analysis. After comparing input and output groups, the algorithm sums up all five sgRNAs of a gene into an overall analysis of each gene, resulting in an overall analysis of each gene and producing an RRA score, a p-value, a false discovery rate (FDR), and a log2-fold change. Significant depleted genes (dropouts) were determined by an RRA score < 0.003, representing a p-value below 0.05 and an FDR below 0.15. In addition to the *in vivo* screening of seven PDX samples, an *in vitro* screening was also conducted in the AML388 and ALL265 samples.

4.4.1 *In vivo* screen in two AML PDX

Romina Ludwig performed the wet lab work for the AML356 screens using the two sub-libraries, while I conducted the analysis and quality checks.

The CRISPR/Cas9 screen has the potential to identify general AML dependencies by depletion of those genes in all or most of the samples or the identification of AML PDX sample-specific genes essential for *in vivo* growth and leukemia maintenance.

After conducting quality controls, we found that only two out of the five AML PDX samples were appropriate for *in vivo* screening (see 4.24.2). Due to the complexity and clonality of AML cells, the total number of sgRNAs is more limited compared to our ALL PDX samples. We tested the different generated libraries (Drug_all or Drug_sub) in PDX cells without Cas9 and found that AML388 is suitable for screening with the Drug_all library. However, AML356 had a lower screening capacity (indicated by a Gini index above 0.4 in the Cas9 negative background). Therefore, we conducted two screening experiments using the two Drug_sub libraries. We screened the same targets in both samples in one or two screening experiments. Mice were taken down at first signs of disease, and isolated from bone marrow cells were used for NGS and MAGeCK analysis.

To analyze the *in vivo* screen, we calculated the average RRA score of each gene in both samples and ranked them from lowest to highest. For easier data presentation, we utilized the log10 of the RRA score (Figure 27).

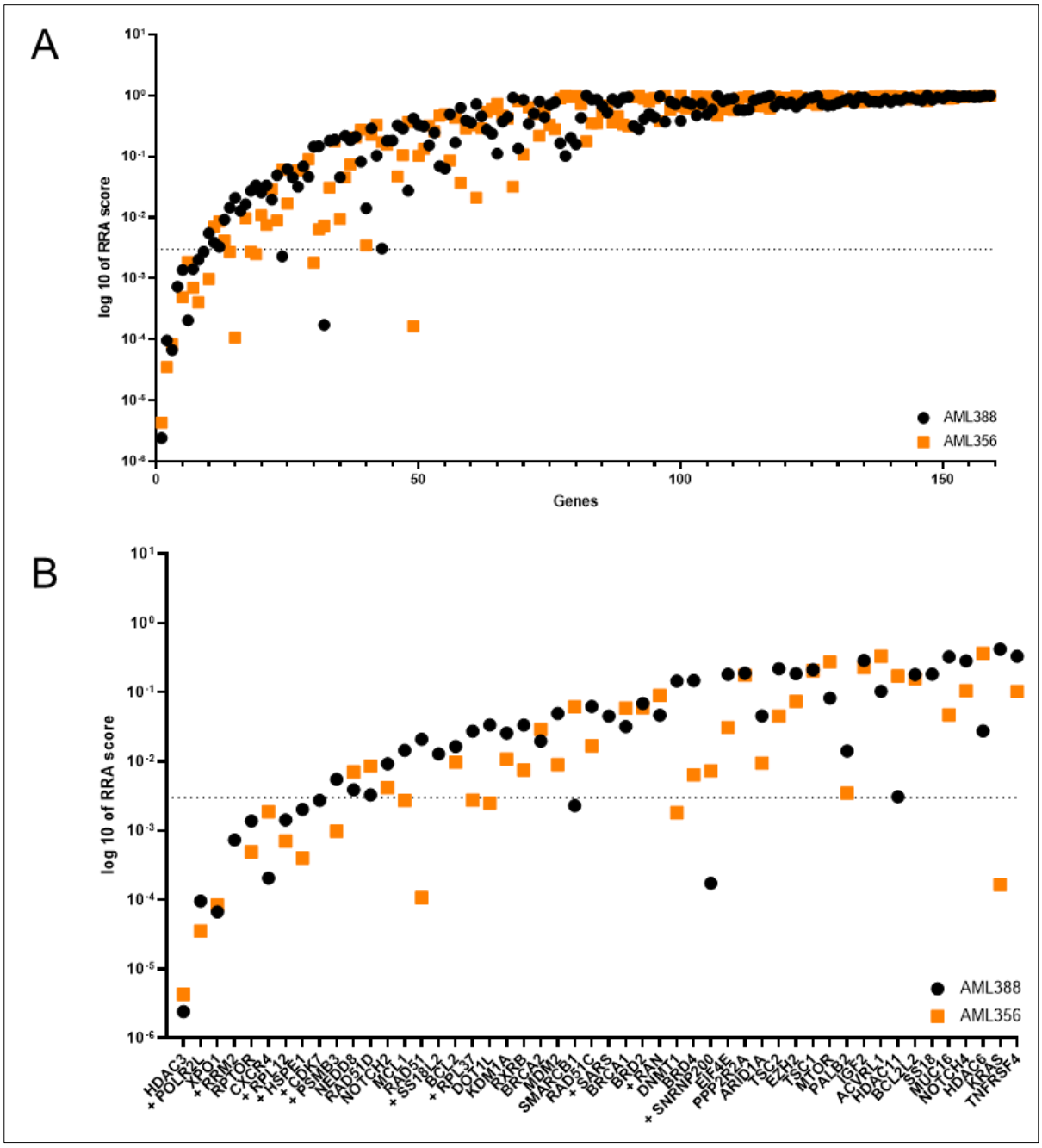

Figure 27: MAGeCK analysis of CRISPR/Cas9 *in vivo* screen in two AML PDX samples. Dropouts are depicted by RRA score. The dotted line represents the threshold of significance of 0.003. **A:** Overview of all dropouts and non-dropouts**. B:** Depiction of 50 strongest depleted genes. Positive controls are marked by "+".

The RRA score of the 50 strongest dropouts is displayed in Figure 27B. Dotted lines are used to mark an RRA score of 0.003. Positive controls are indicated by a "+" before the gene name. Most of the positive controls show a significant dropout, with an RRA

score below 0.003. In sample AML388, six out of 11 positive controls were significantly depleted. In sample AML356, an average of five out of six (Drug_sub = total of six positive controls) had an RRA score below 0.003, indicating successful gene editing by Cas9.

The four most depleted genes in both AML PDX samples were *HDAC3, XPO1, RPTOR*, and *CXCR4*, which suggests that these genes may be essential for the growth of leukemic cells *in vivo.* The Venn diagram in Figure 28 demonstrates the shared and unique dropouts of the AML388 and AML356 samples (Venn diagram generated using the following online tool: https://bioinformatics.psb.ugent.be/webtools/Venn/) *SMARCB1* is only depleted in the AML388 sample, while the AML356 sample has five unique dropouts. It is possible that those distinct dropouts are specific dependencies of the PDX sample.

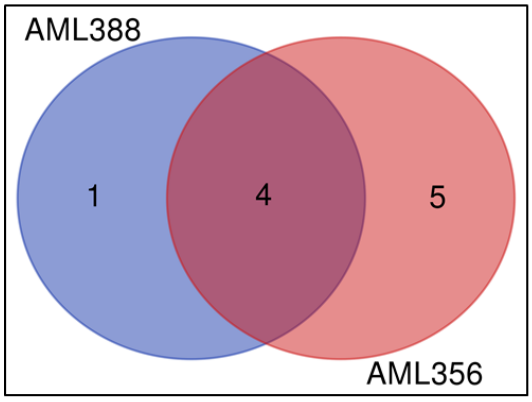

AML *in vivo* data

Names	total	Genes
AML356 AML388	4	XPO1 HDAC3 RPTOR CXCR4
AML388	1	SMARCB1
AML356	5	DOT1L MCL1 RAD51 KRAS DNMT1

Figure 28: Venn diagram of significant dropouts in AML PDX *in vivo* screen showing shared and unique depleted genes

The CRISPR/Cas9 *in vivo* screen quality controls for AML PDX produced the expected results, which suggests that the dropouts identified are dependable candidates.

4.4.2 *In vivo* screen in five ALL PDX

Romina Ludwig conducted the wet lab work for the *in vivo* screen of sample ALL199, while I performed the analysis and quality checks.

By utilizing the CRISPR/Cas9 screening technologies in an *in vivo* approach in ALL PDX samples, we can identify targets that are crucial for the growth of leukemia cells *in vivo*. The dropouts we receive are potential treatment options since all genes used in the libraries are targetable by drugs. If dropouts occur in many ALL PDX samples,

they are potential ALL dependencies, whereas dropouts that arise in one specific PDX sample are more sample-specific targets.

All five ALL samples passed the required quality controls before screening, making it possible to screen all of them. The screening was done as described in chapter 3.3.14. Mice were taken down at the earliest signs of leukemia. For NGS, the DNA samples collected from the bone marrow were processed and prepared for sequencing, followed by MAGeCK analysis. The RRA scores generated by the MAGeCK analysis of the ALL PDX samples were used to analyze the *in vivo* CRISPR/Cas9 screens (Figure 29). To make the data more accessible, the average RRA score of each gene from the five samples was calculated and used to sort the samples according to their average score. The gene with the lowest RRA score on average is depicted as the first gene close to the graph origin, with the log10 of the RRA score used for depiction.

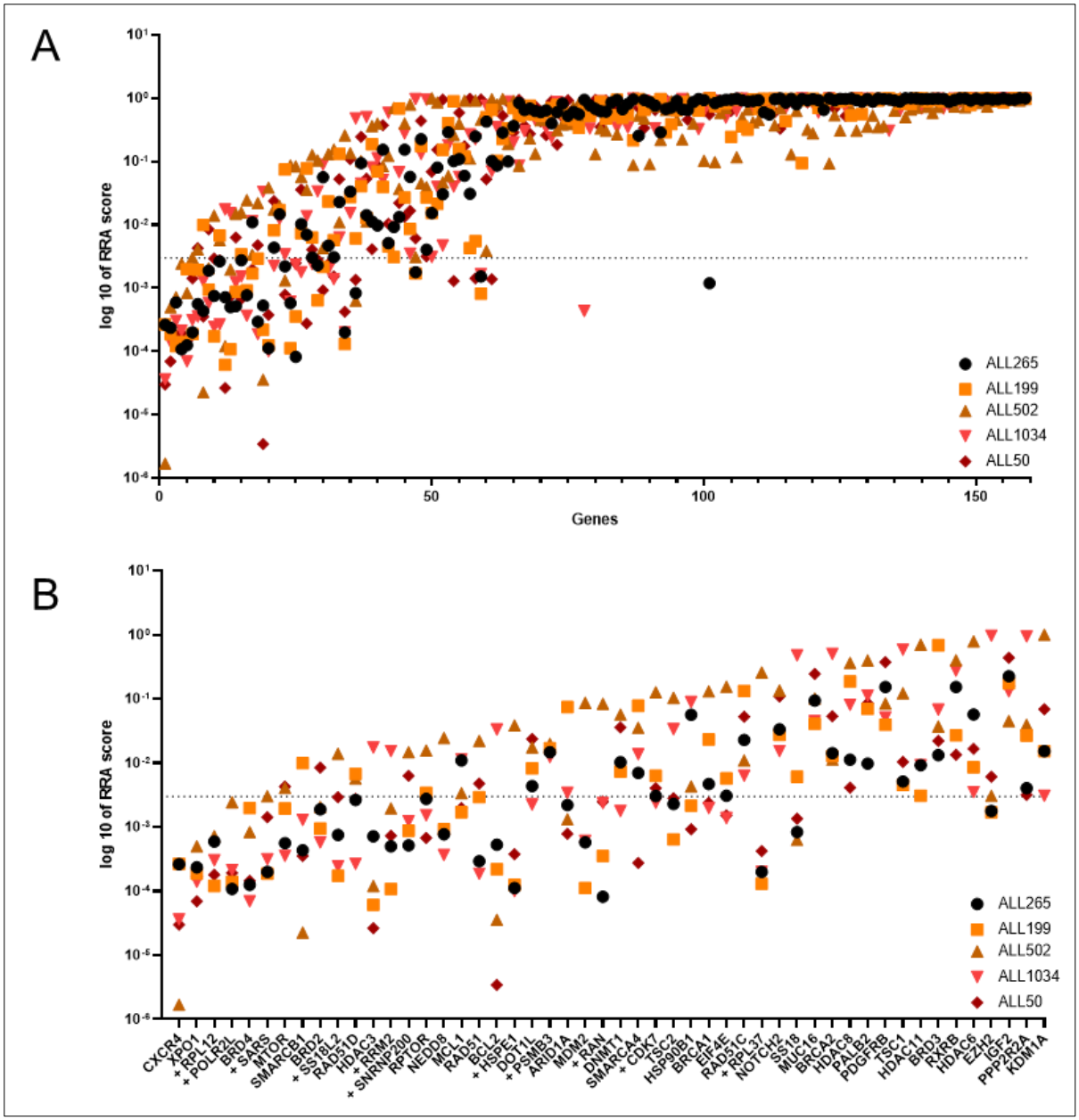

Figure 29: MAGeCK analysis of the CRISPR/Cas9 *in vivo* screens in five ALL PDX samples
Dropouts are depicted by RRA score. The dotted line represents the threshold of significance of 0.003. **A:** Overview of all dropouts and non-dropouts. **B:** Depiction of 50 strongest depleted genes. Positive controls are marked by "+".

The Figure 29B displays the 50 genes with the lowest average RRA score across all five PDX samples. Positive controls are marked by a "+" before their gene name. These positive controls were expected to show significant depletion, which confirmed the functionality of the cas9 nuclease. In all ALL PDX samples, except for ALL502, eight or nine out of the eleven positive controls were significantly depleted. Only three out of the eleven positive controls showed depletion in the ALL502 data, but the sample also showed fewer significant dropouts overall when compared to the other four samples.

The average number of significant dropouts in the remaining four PDX samples is 27, whereas the ALL502 sample only showed 12 significant dropouts.

The two strongest depleted genes are *CXCR4* and *XPO1*, as already seen in the AML PDX *in vivo* screen. Furthermore, in all five ALL PDX samples, the *BRD4* gene is also strongly depleted (see Figure 30). The Venn diagram (Venn diagram generated using the following online tool: https://bioinformatics.psb.ugent.be/webtools/Venn/) displays both unique depleted genes from the five samples and all shared dropouts between them.

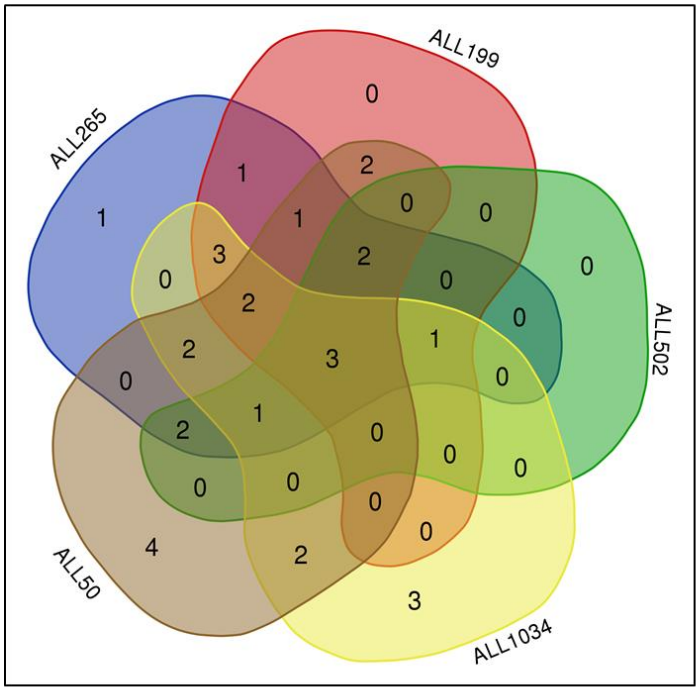

ALL *in vivo* data

Names	total	Genes
ALL1034 ALL199 ALL265 ALL50 ALL502	3	BRD4 XPO1 CXCR4
ALL1034 ALL199 ALL265 ALL502	1	BRD2
ALL199 ALL265 ALL50 ALL502	2	BCL2 HDAC3
ALL1034 ALL199 ALL265 ALL50	2	MDM2 NEDD8
ALL1034 ALL265 ALL50 ALL502	1	SMARCB1
ALL1034 ALL199 ALL265	3	KRAS MTOR RAD51
ALL199 ALL265 ALL50	1	TSC2
ALL265 ALL50 ALL502	2	SS18 ARID1A
ALL1034 ALL265 ALL50	2	RPTOR RAD51D
ALL199 ALL265	1	EZH2
ALL199 ALL50	2	MCL1 HSP90B1
ALL1034 ALL50	2	BRCA1 EIF4E
ALL265	1	ERG
ALL1034	3	HDAC1 DNMT1 DOT1L
ALL50	4	BCL2L1 PTEN PARP1 SMARCA4

Figure 30: Venn diagram of significant dropouts in ALL PDX *in vivo* screens showing shared and unique depleted genes

The CRISPR/Cas9 *in vivo* screen quality controls were successfully passed by all five samples from ALL PDX. It is assumed that the dropouts found can be considered reliable candidates. These dropouts can be used for further testing and analysis.

4.4.3 Correlation of *in vivo* and *in vitro* data shows overlapping *in vivo* specific dropouts between AML and ALL PDX

When using a suitable culture medium, it is possible to cultivate AML PDX samples for a certain period *in vitro*. For the AML388 sample, it was possible to screen *in vivo* and in parallel *in vitro*. These two data sets of the AML388 sample allow the correlation of *in vivo* and *in vitro* generated dropouts. Both screens had the exact duration of screening time, either *in vivo* or in *vitro*.

In vitro cultivation of ALL PDX is more challenging than the AML PDX sample. The cells can be kept for up to 14 days in vitro using an improved culture medium. The preparation of the ALL265 cells for the *in vivo* screen was very efficient, leading to leftover cells that could be used for an additional *in vitro* screen. The endpoint of the *in vitro* screen was after 14 days due to a drop in cell viability.

The two *in vivo – in vitro* data sets of the two PDX samples were compared using the RRA scores from the MAGeCK analysis (Figure 31). The dotted lines represent the threshold of significance (RRA score of 0.003). The orange marked part represents the *in vivo*-only dropouts. The *in vitro*-only depleted genes are in the red square. Shared dropouts are represented in the square located at the graph's origin. Positive controls are marked by a "+". The correlation was calculated by using the R^2 score.

Dropout screening in the AML388 PDX cells (Figure 31A+C) revealed more *in vitro*-only dropouts than *in vivo*-only or shared dropouts. *HDAC3* and *XPO1* are shared dropouts also identified in the AML356 sample *in vivo* screen. *BCL2* and *MDM2* are strong *in vitro*-only depleted genes. A detailed check of the *in vivo*-only genes showed that *SMARCB1, RPTOR*, and *CXCR4* were depleted (Figure 31C). *CXCR4* is a known niche modulator crucial for interaction with *in vivo* environment (Burger and Bürkle 2007). This shows the potential of a CRISPR/Cas9 screen to identify *in vivo* specific targets. Further, the dropout of *CXCR4 in vivo* but not *in vitro* strengthens the validity of this data.

CRISPR/Cas9 *in vivo* and *in vitro* screens in ALL265 cells share the most significant dropouts. No strong *in vitro* depletions can be identified. The depleted genes only seen *in vivo* are depicted in more detail in Figure 31D. *CXCR4, SMARCB1*, and *RPTOR* are *in vivo*-only dropouts like already seen in the AML388. *In vivo* dropout of *CXCR4* again functions as a positive control. The dropout of *SMARCB1* and *RPTOR* in both *in vivo* screens but not in the performed *in vitro* screens suggests they are more critical *in vivo* than *in vitro*.

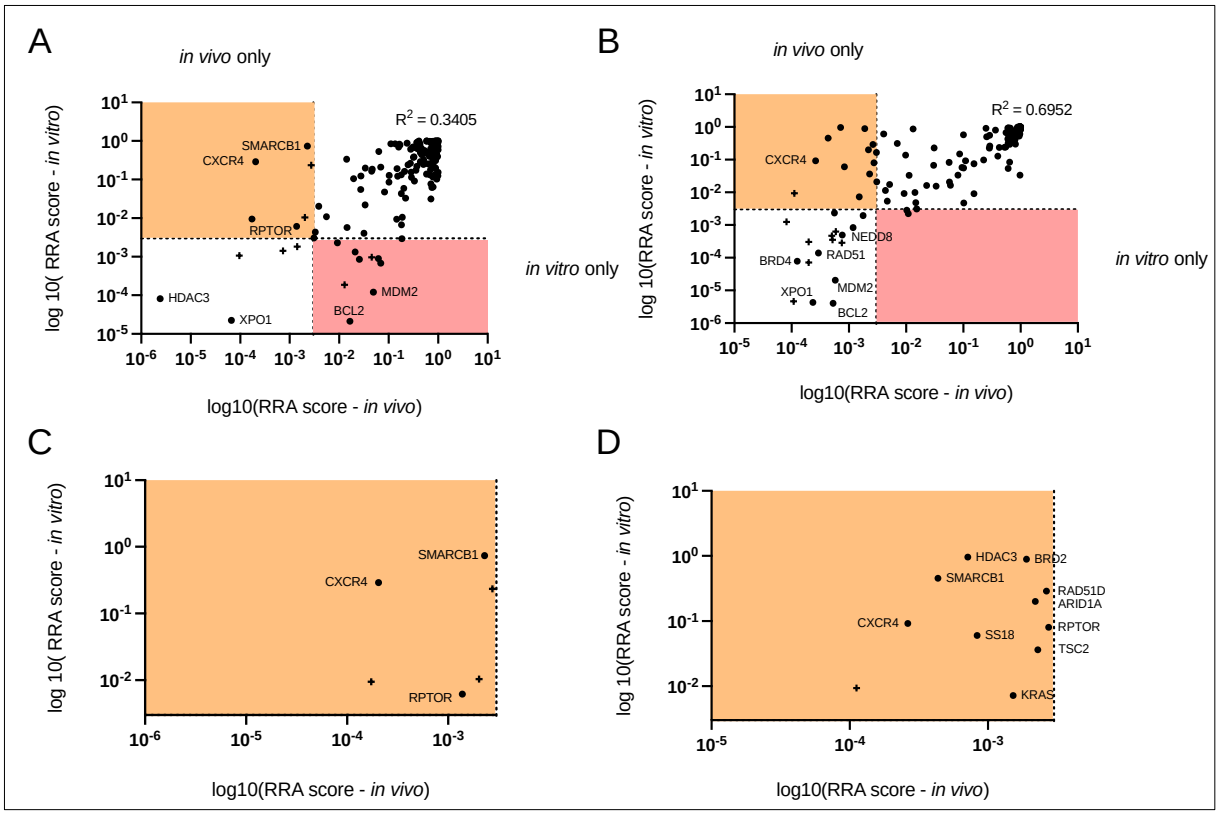

Figure 31: CRISPR/Cas9 screens showed shared dependencies between both leukemia types as well as the importance of *in vivo* screens
A: Comparison of the *in vivo* and *in* vitro screen of the AML388 sample. **B:** Comparison of the *in vivo* and *in vitro* screen of the ALL265 sample. **C:** *in vivo*-only dropouts of the AML388 sample. **D:** *in vivo*-only dropouts of the ALL265 sample. The dotted line represents the threshold of significance of 0.003. The orange square indicates "*in vivo*-only" candidates and the red square "*in vitro*-only" dropouts. Positive controls are marked by "+".

The correlation between these data sets highlights the consistency of dropouts across various types of leukemia. It also emphasizes the significance of an *in vivo* screen to identify essential genes in an *in vivo* environment but not *in vitro*.

4.1 *In vivo* CRISPR/Cas9 screens revealed more common dropouts than sample-specific depleted genes in the seven screened PDX samples

The *in vivo* CRISPR/Cas9 screen in the two AML and five ALL PDX samples led to 24 depleted targets that dropout in at least two PDX samples (Table 25).

Table 25: Shared dropouts in at least two PDX samples

significant dropout in at least two PDX samples	occurrence
CXCR4, XPO1	7/7
HDAC3	6/7
SMARCB1, BRD4	5/7
NEDD8, RPTOR, BRD2, KRAS, RAD51, BCL2, MDM2	4/7
MCL1, ARID1A, MTOR; RAD51D, SS18, TSC2	3/7
DNMT1, DOT1L, EZH2, HSP90B1, BRCA1, EIF4E	2/7

There are unique dropouts present in only three samples of ALL PDX. During the screening, five unique dropouts (*BCL2L1, PTEN, PARP1,* and *SMARCA4*) were discovered in the ALL50 sample, while one unique target (ERG) was found in sample ALL265 (see Figure 30). The ALL1034 sample revealed *HDAC1* as a unique target when comparing the AML and ALL *in vivo* screening data. This means there are no AML-specific dropouts when comparing all the dropouts in the two AML screens with the data of the five ALL screens. However, all screened ALL PDX samples show 20 ALL-only dropouts, concluding that ten shared dropouts exist between the screened AML and ALL PDX samples.

Further analysis of significant dropouts in more than two samples reveals that BRD2 and *BRD4* seem more critical in the ALL PDX samples. *BRD4* drops out significantly in all five screened ALL samples, while *BRD2* is depleted in four out of five ALL PDX samples, and no AML samples. A more detailed look, including all screened Bromodomain and Extra-Terminal Domain (BET) gene family members, confirmed this ALL sample tendency (see Figure 32). Four out of five ALL PDX samples show a less significant dependency on the *BRD3* gene. Additionally, none of the screened samples showed any dependency on the *BRDT* gene.

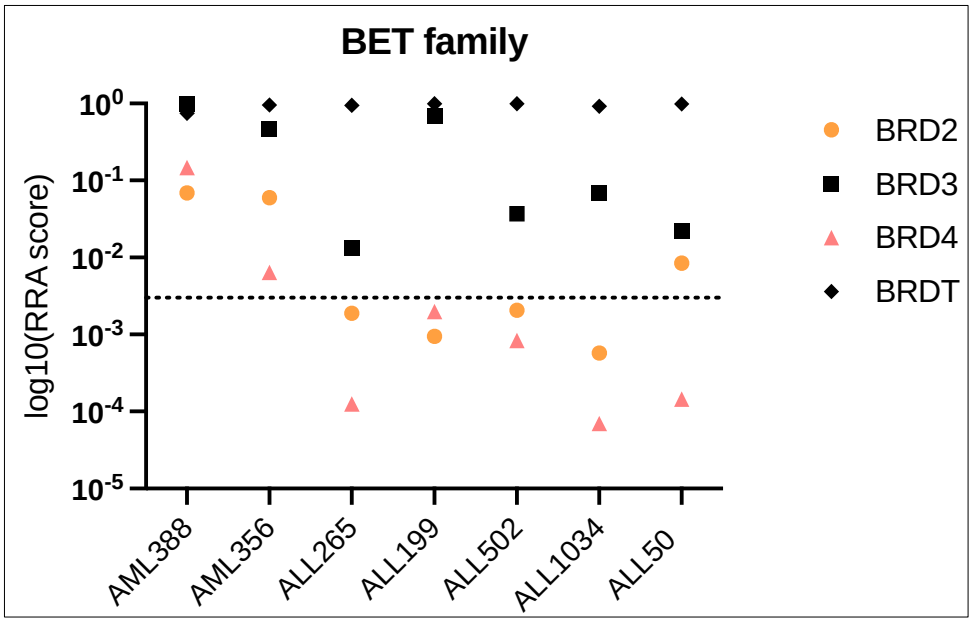

Figure 32: Genes of the BET family are more important in ALL than in AML PDX samples
The dotted line indicates the threshold of significance of a RRA score of 0.003.

While the BET gene family members appear to be primarily important in ALL samples, most of the 24 depleted targets are shared candidates. These shared candidates, listed in Table 25, were utilized for further analysis.

4.2 Pathway analysis of shared dropouts reveals an epigenetic dependency and the importance of the SWI/SNF complex

We analyzed the 24 most significant dropouts in all seven PDX samples (as shown in Table 25) to identify the pathways associated with our target. We conducted a gene set enrichment analysis using the Enrichr online tool (https://maayanlab.cloud/Enrichr/) (Chen et al. 2013; Kuleshov et al. 2016; Xie et al. 2021). The results suggested that the epigenetic pathways were the most important among our 24 target genes (as seen in Table 26). Other significant pathways were DNA repair, PI3K signaling, and apoptosis.

Table 26: Target genes associated with several pathways
*Pathways depicted with at least two associated genes.

Pathway*	**Number of depleted genes**	**Pathway associated genes**
Epigenetic pathways	9/24	*ARID1A, BRD2, BRD4, DNMT1, DOT1L, EZH2, HDAC3, SMARCB1, SS18*
DNA repair	4/24	*BRCA1, MDM2, RAD51, RAD51D*
PI3K signaling	3/24	*MTOR, RPTOR, TSC2*
Apoptosis	2/24	*BCL2, MCL1*

Using the CORUM database as a reference (see Figure 33A), the gene set enrichment analysis identified various enriched protein complexes. The CORUM database contains information about experimentally characterized protein complexes and their biological features, as described by (Tsitsiridis et al. 2023). Out of all the protein complexes, the SWI/SNF complex has the highest number of associated subunits, followed by mTOR-related complexes. As a result, we examined the depletion score of every SWI/SNF component in the library across all seven samples (Figure 33B).

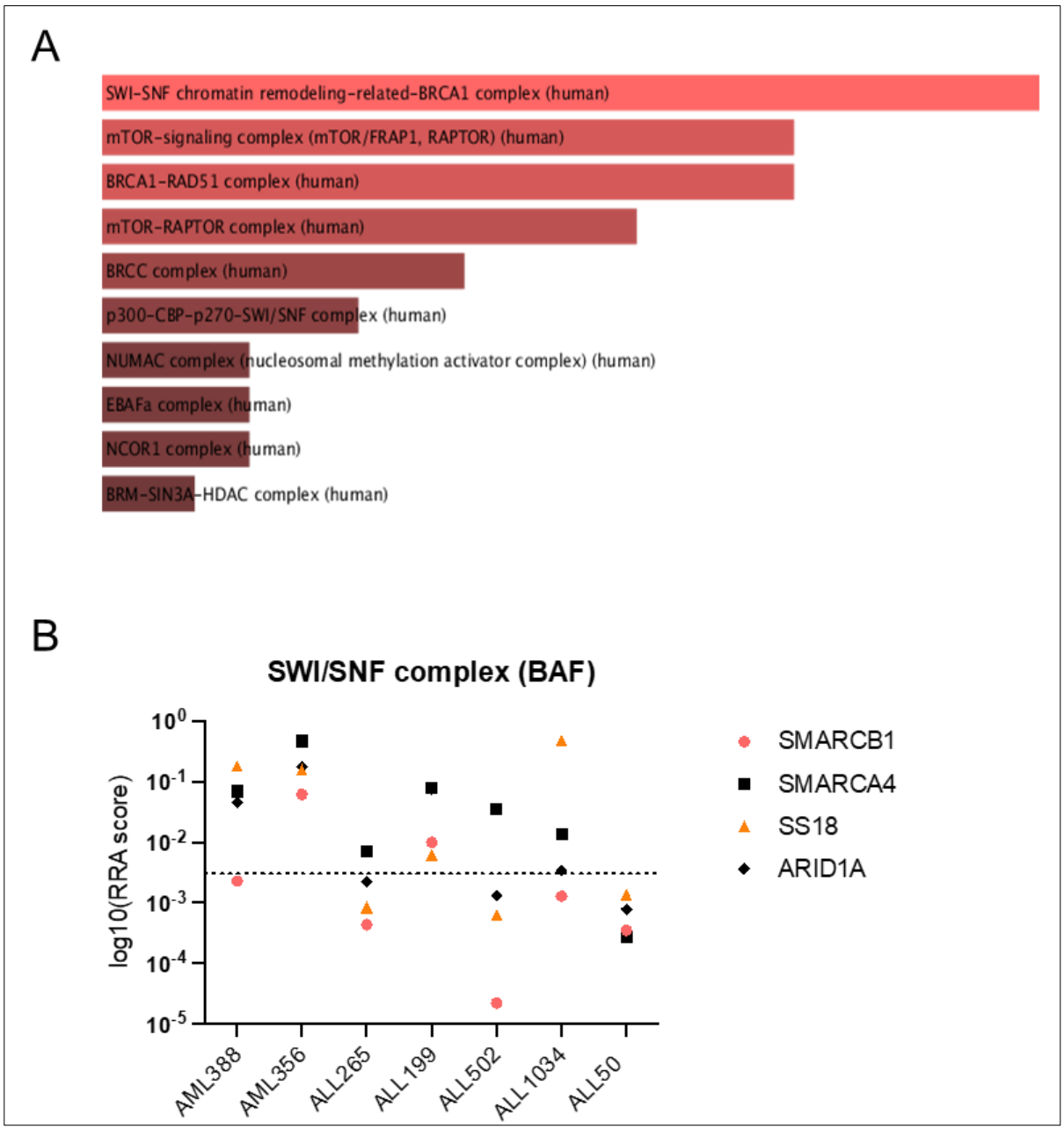

Figure 33: The seven screened PDX samples are dependent on the SWI/SNF complex
A: Enriched protein complexes identified by pathway analysis and comparison of the 24 target genes to the CORUM database. Bars sorted by p-value ranking. **B:** RRA score of all SWI/SNF genes included in the screened library.

Our library includes genes from the SWI/SNF complex*: SMARCB1, SS18, SMARCA4*, and *ARID1A*. However, *SMARCA4* was excluded from the network analysis as it only dropped out in the ALL50 sample. *SMARCB1* was found to be depleted in five out of seven samples. There is no significant depletion of a complex-important gene in the two samples, AML356 and ALL199.

It looks like the SWI/SNF-associated genes play a significant role in most of the screened PDX samples. The ALL50 sample had a depletion in all four genes, while the ALL265 and ALL502 samples had a depletion in three of four genes but not in *SMARCA4*. On the other hand, the ALL1034 and AML388 samples only had a depletion in *SMARCB1*. Overall, these results suggest that the SWI/SNF-associated genes are particularly relevant to the ALL samples.

4.3 Selection of targets for upcoming drug treatment trials as part of our validation process

The CRISPR/Cas9 library comprises genes that can be associated with drugs, allowing for individualized prediction of treatment based on the *in vivo* screening results. Currently, *in vivo* drug trials based on the screening results are ongoing. Katharina Hunt conducted drug treatment trials as part of her doctoral studies.

To choose the targets for the upcoming drug treatment trials, the average RRA score of the top 10 depleted genes was determined and is displayed in Table 27. The average RRA scores are ranked in order of significance, with *XPO1* being the most significant target.

Table 27: Average RRA score of the top depleted genes
First 10 genes are depicted.

Number	Genes	Average RRA score in all seven samples
1	*XPO1*	0,000183404
2	*CXCR4*	0,000381765
3	*HDAC3*	0,002636594
4	*RPTOR*	0,003701259
5	*RAD51D*	0,004287196
6	*NEDD8*	0,005486814
7	*MCL1*	0,0066546
8	*RAD51*	0,007331536
9	*BCL2*	0,008601877
10	*SMARCB1*	0,010842427

We have decided to exclude *RPTOR, RAD51D, RAD51*, and *SMARCB1* from any upcoming drug treatment trials since there are no direct drugs available that target them specifically. Furthermore, we used *CXCR4* as a positive control for in vivo screening and therefore did not take *CXCR4* into account.

Based on the ranking and the excluded genes, we plan preclinical treatment trials using the available specific inhibitors targeting *XPO1, HDAC3, NEDD8, MCL1*, and *BCL2*. We predict that PDX samples with a gene dropout in our CRISPR/Cas9 screens will respond to the respective drug inhibiting the respective protein. The drug treatment trials will test our hypothesis that testing gene function via CRISPR/Cas9 *in vivo* screens in PDX models represents a reliable tool for predicting individual drug responses in acute leukemias.

5. Discussion

For the last decades, classical chemotherapy was the standard of care for patients with acute leukemia. The approval of several targeted therapies improved the therapy options and the overall survival of patients. Nevertheless, personalized treatment of patients is still challenging. Different studies use descriptive methods like NGS for treatment assignment and genome profiling (van Tilburg et al. 2021; Burd et al. 2020). Nevertheless, problems like the establishment of resistance to targeted therapies and the lack of a suitable biomarker for treatment planning remain (Small, Oh, and Platanias 2022). To overcome those challenges functional tools emerged. Studies using *ex vivo* drug screens with primary patient cells are such a functional tool (S. H. R. Lee et al. 2023). However, drug tests performed *ex vivo* do not accurately reflect the clinical situation.

To address this limitation, we established a functional precision medicine tool by performing CRISPR/Cas9 knockout screens in a patient-derived xenograft model of acute leukemias. An additional advantage of using the CRISPR/Cas9 system is the possibility of screening for several dependencies of one sample in only one experiment. With this screen, we aimed at identifying genes that are essential for the *in vivo* growth of leukemia cells, thereby representing putative new therapeutic targets. Since every gene included in our library could be pharmacologically targeted by at least one drug, we planned to use the gene-associated drug to validate the identified dependency.

The CRISPR/Cas9 knockout screen in seven different PDX samples (five ALL, two AML) revealed more shared dependencies than individual dropouts. The seven samples share 24 genes, that were depleted in more than one sample. The shared deleted genes are important for epigenetic regulation, DNA repair, PI3K signaling, and apoptosis. After excluding targets with indirect or unspecific drugs, we could name the PDX sample-specific treatment strategies.

5.1 Quality control measures applied to small-library *in vivo* screens revealed notable differences between AML and ALL samples.

When starting this project, we aimed at generating a robust *in vivo* CRISPR/Cas9 screening pipeline. However, most published studies focused on *in vitro* screens in cell lines. To ensure the quality of our unique screening procedure, we investigated several quality measurements.

As measures, we checked the quality of the NGS sequencing and the resulting redcount tables. All seven PDX samples passed those measures (Table 23 and Table 24). To control the suitability of the used library size we performed an experiment using Cas9-negative PDX cells and the sgRNA library as “barcodes” (Figure 17). As a screen internal quality measure we analyzed the included positive and non-targeting controls (Figure 26). Whereas all ALL samples passed those controls, just two of the five AML samples succeeded.

Although the screening procedure of AML and ALL samples differ in their selection methods, this does not cause the observed discrepancies. The AML388 sample was used for both *in vivo* and *in vitro* screening, originating from the same transduction and puromycin-selection experiment. Although the *in vivo* sample passed quality controls, the *in vitro* screen data was more consistent in quality (data not shown). Therefore, the difference in screening quality between the AML and ALL samples is likely due to an *in vivo* phenomenon. Also, a reduction of homing and/or engraftment due to the puromycin treatment can be excluded since puromycin is a standard selection method and was used in several *in vivo* CRISPR/Cas9 screens in AML samples (S. Lin et al. 2022; Manguso et al. 2017; Mercier et al. 2022).

Besides quality controls, the number of depleted genes appeared different between AML and ALL samples. In the AML PDX *in vivo* screens, eight depleted genes out of 146 (~5%)were found on average. In the five ALL samples, an average of 17 depleted genes (~11,5%) were identified, indicating a difference between the screened AML and ALL PDX samples.

As the screening procedure has been eliminated as the cause of the identified difference, the basic biology of the two ALs may provide a possible explanation. Several studies on AML and ALL demonstrated the importance of leukemia-initiating cells (LICs) for the development and maintenance of leukemia (Tsvee Lapidot et al. 1994; Bonnet and Dick 1997; Senft and Jeremias 2019; Bernt and Armstrong 2009). LICs are defined as cells with the potential to give rise to leukemia in a xenotransplant model (Bonnet and Dick 1997). LIC or leukemic stem cells (LSCs) are well studied and described in AML and CML whereas the concept of LSCs in ALL is less established (Ebinger et al. 2016; Lang, Wojcik, and Rieger 2015; Senft and Jeremias 2019).

The general concept of LSCs is based on the hypothesis of two cancer stem cell (CSC) models. The stochastic model or clonal evolution (CE) model and the hierarchy or CSC model as indicated in Figure 34 (Dick 2008; Rich 2016).

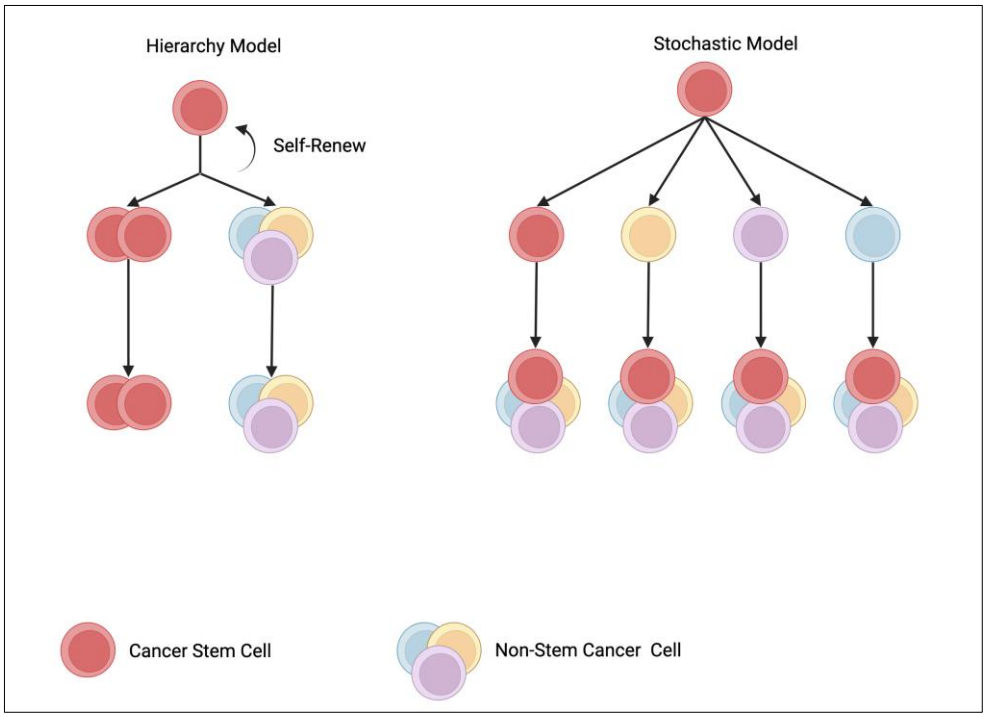

Figure 34: Cancer stem cells model hypothesis..
Adapted from ((Xiao et al. 2017) Created with BioRender).

In the hierarchy model, the LSCs are a rare subset of cells that can perform self-renewal and give rise to clonal daughter cells. This model is hypothesized to be the organization of normal HSCs. The stochastic model is defined by a biological homogeneity, where every cell has the potential to behave like an LSC initiated by intrinsic or extrinsic factors (Dick 2008; Elder et al. 2017; Rich 2016). Intra-tumor heterogeneity of AML cells was shown to be organized in a hierarchical model (Bonnet and Dick 1997; Dick 2008; T. Lapidot et al. 1994). Since leukemia-initiating capacity was identified In various numbers of ALL cells with different immunophenotypes, ALL is suggested to follow a stochastic cancer stem model (Elder et al. 2017; Rehe et al. 2013).

The difference between AML and ALL in their LSC model may cause a different engraftment capacity. For AML samples where just a rare subtype of cells can give rise to leukemia, the step of engraftment is more limiting. This limitation might reduce the number of homed and engrafted cells drastically and could affect the coverage of the library. This could explain the missing of several sgRNAs after the screen (zero readcounts) and the lower quality of the controls in AML samples. For ALL samples, where possibly every cell has the capacity to initiate leukemia, the step of homing and engraftment is less limiting.

To ensure sufficient library coverage during homing and engraftment, it is especially important for AML samples to enhance their homing/engraftment capacity. In most of the published AML *in vivo* screens, the AML cells were injected into irradiated immunocompromised mice (S. Lin et al. 2022; Mercier et al. 2022; Yamauchi et al. 2018). Those researchers claim the importance of irradiation to maximize the engraftment capacity of AML cells. The engraftment of more cells might result in better library coverage during this step. An additional option for enhancing engraftment could be a different mouse model. Krevvata et al. showed enhanced engraftment of primary AML samples when using an NSG-S mouse model, which has transgene expression of human cytokines. They increased the percentage of engraftment (n=77) from 50% to 82% when using NSG-S compared to NSG mice and additionally observed a higher tumor burden and a shorter survival time of the injected mice (Krevvata et al. 2018).
An improvement in the engraftment of AML cells might allow more AML samples to pass the quality controls by ensuring sufficient coverage of the library during the step of homing and engraftment.

5.2 Comparison of *in vivo* and *in vitro* data showed the importance of an *in vivo* screening pipeline

For the AML388 and ALL265 samples, it was possible to perform an *in vivo* and *in vitro* screen in parallel (see Figure 31). When comparing the *in vivo* screen analysis to the obtained *in vitro* data, the AML388 sample showed a weaker correlation between the two screens compared to the ALL265 sample. As mentioned in chapter 5.1, the homing and engraftment of AML PDX samples may be more limited, which can impact the library coverage.
The AML388 screens revealed the most dropouts in the *in vitro*-only square, whereas the ALL265 sample shared most of the depleted genes between the *in vivo* and *in vitro* screen and revealed only three *in vitro*-only dropouts with an RRA value close to the significance threshold of 0.003. The shorter experiment time of the ALL265 *in vitro* screen (14 days) is a possible explanation for the smaller number of dropouts (12 *in vitro* and 19 *in vivo*). In the AML388 sample screen, most dropouts appeared *in vitro*-only. However, some robust *in* vivo-only dropouts were found in the *in vivo* screen, indicating that the AML388 samples is more difficult to screen *in vivo* and adaption of the screening protocol is necessary.

Interestingly both samples share *CXCR4, SMARCB1* and *RPTOR* as *in vivo*-only depleted genes, suggesting them to be important for homing, engraftment and/or i*n vivo* proliferation of leukemic cells.

In normal hematopoiesis *CXCR4* is essential for homing and maintenance of hematopoietic stem cells (HSCs) in the bone marrow (Foudi et al. 2006; Sugiyama et al. 2006). In T-ALL, *CXCR4* was shown to be important for the LIC activity (Passaro et al. 2015). The role of *CXCR4* in AML is discussed controversially, especially its role in homing (Ramakrishnan et al. 2020). A recently published CRISPR/Cas9 screen in an AML mouse model showed *CXCR4* to be important for *in vivo* growth of leukemic cells but seems to be not critical for homing to the bone marrow (Ramakrishnan et al. 2020). Since we injected cells earliest at day four after library transduction, we are able to either identify essential targets for homing, engraftment or *in vivo* growth. Concluding, *CXCR4* is depleted *in vivo*-only due to its described important role in homing, engraftment and or *in vivo* growth, whereas it is not essential *in vitro (Cancilla, Rettig, and DiPersio 2020)*.

SMARCB1 is a core component of the SWI/SNF chromatin remodeling complex which is one of the most commonly mutated chromatin modulators in human cancer (> 20%) and important for gene regulation, maintenance and differentiation of hematopoietic cells (Centore et al. 2020). Three mammalian SWI/SNF complexes have been identified, consisting of at least 29 proteins each: BAF (BRG1/BRM-associated factor), PBAF (polybromo-associated BAF) and the non-canonical BAF (ncBAF) (Wanior et al. 2021) (see Figure 35).

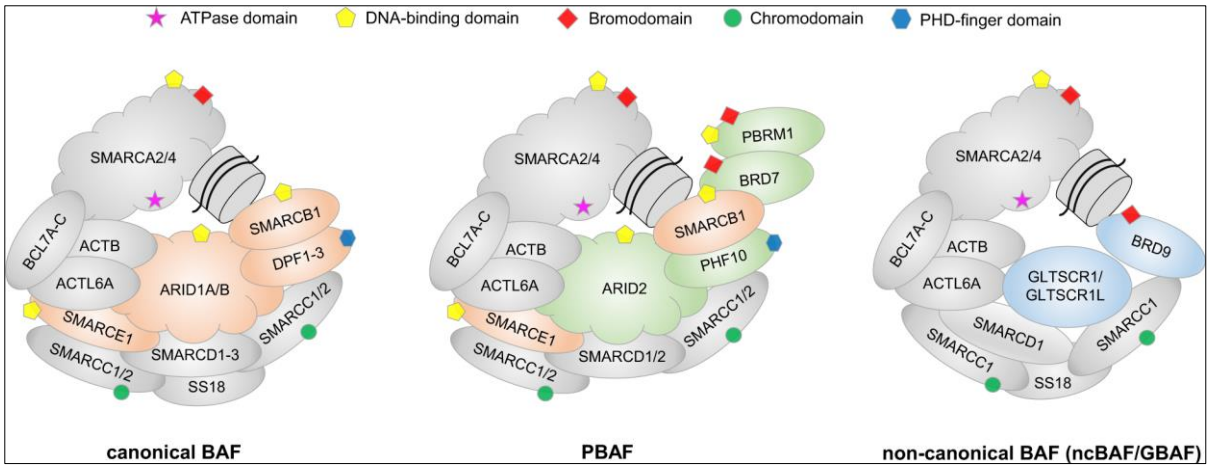

Figure 35: The mammalian SWI/SNF complexes BAF, PBAF and ncBAF and their subunits. (Wanior et al. 2021).

SMARCB1 is described to be essential for different hematological malignancies due to its crucial function as a structural scaffold. The loss of *Smarcb1* was shown to induce the development of T-cell lymphoma in a mouse model (Roberts et al. 2002). Besides this, *SMARCB1* is described as a tumor suppressor in AML and the SWI/SNF complex seems to be crucial for the maintenance of an oncogenic gene expression program in AML. An aberrant *SMARCB1* is associated with Rac GTPase activation and hypermigration of AML cells. Rac GTPases are important for homing, engraftment, survival, and trafficking in the bone marrow in myeloid leukemias (Chatterjee et al. 2018). Although this is just described for AML, a similar role of *SMARCB1* is possible in ALL and therefore would explain the identification of an *in vivo*-only dependency in our CRISPR/Cas9 knockout screen. To close the circle, in normal hematopoiesis *Rac1*, a Rac GTPase is associated with the regulation of the *CXCR4* receptor conformation in HCSs and their progenitor cells and therefore controls the signaling efficiency of the receptor (Zoughlami et al. 2012).

RPTOR (Raptor) is a scaffold subunit of the mTORC1 complex and is important for its stability and assembly. mTORC1 signaling controls proliferation and cell survival and is reported to be a critical pathway in cancer, including AML (Oki et al. 2021). *Raptor*-deficient AML stem cells showed a defective leukemia-initiating capacity, indicating the importance of Raptor/mTORC1 for homing and engraftment (Hoshii et al. 2012; Oki et al. 2021). Although to my knowledge nothing comparable is described in ALL, this suggests Raptor-depleted cells to have a disadvantage for leukemia initiation at least in AML samples and a disadvantage in *in vivo* proliferation.

All three targets can be associated with either leukemia initiation or proliferation *in vivo*, reinforcing our results.

To strengthen the *in vivo*-only targets of the ALL265 screen the dropouts of *SS18* and *ARID1A* need to be mentioned. Both are subunits of the above-described SWI/SNF complex (Andrades et al. 2023; Middeljans et al. 2012).

The importance of *in* vivo screening is highlighted by the comparison of *in vivo* and *in vitro* data. The three *in vivo*-only dropouts, identified in both samples of different types of AL, suggest an *in vivo* dependency in both of them.

5.3 Comparison of the target genes to the DepMap database reinforced the importance of *in vivo* screens

The established *in vivo* CRISPR/Cas9 screening pipeline allowed screening of seven PDX samples, five of them ALL, and two AML samples. The screens resulted in 24 depleted targets in at least two samples (see Table 25). Nineteen of the 24 targets are also described as a dependency in at least one acute leukemias cell line in the DepMap database (Dempster et al. 2019; 2021; 'DepMap 22Q2 Public' 2022; Meyers et al. 2017a; Pacini et al. 2021). The following five genes have no assigned dependency: *CXCR4, ARID1A, BRCA1, BRD2*, and *SS18. ARID1A* and *SS18* are subunits of the epigenetic remodeling complex SWI/SNF (Middeljans et al. 2012). *BRCA1* is a tumor suppressor gene commonly mutated in breast and ovarian cancer. It interacts with *BRG1* (*SMARCA4*), a subunit of the SWI/SNF complex (Bochar et al. 2000). Supporting the possible *in vivo* dependency of the SWI/SNF complex as discussed in chapter 5.2. Besides those epigenetic modulators, *BRD2* a member of the BET (bromodomains and extra terminal domain) family showed no dependency in AL cell lines in the DepMap database (Doroshow, Eder, and LoRusso 2017). *BRD2* exhibits various mechanisms of action, such as transcriptional regulation and control of the cell cycle. There is evidence that BRDs promote aberrant gene expression in leukemia and additionally, a reduction of leukemic cells can be achieved by treatment with BET inhibitors (Lucas and Günther 2014; L. Zhang et al. 2021). The last target without a described AL dependency in the DepMap database is *CXCR4*. The importance of *CXCR4 in vivo* was already discussed in chapter 5.2.

A possible explanation is the experimental setup of the DepMap CRISPR/Cas9 knockout screens. All screens were performed *in vitro*, using several cancer cell lines. *In vitro* cell line screens lack a suitable microenvironment and cannot identify genes important for engraftment, homing, niche interaction, or *in vivo* growth. Four of the five above-mentioned genes were already described in chapter 5.2. as *in vivo*-only depleted genes in the ALL265 sample screen.

The discussed data in this chapter and chapter 5.2.highlights the importance of *in vivo* screens. Relying solely on *in vitro* screens could result in missing out on several potential targets.

5.4 CRISPR/Cas9 screens identified well-described targets and revealed an epigenetic dependency in all seven samples

Besides demonstrating the general importance of *in vivo* screens we were able to reproduce several targets, earlier described as dropouts in other CRISPR/Cas9 knockout screens. *BCL2, SMARCB1*, and *DOT1L* were identified in a whole genome *in vitro* screen in AML cell lines (Tzelepis et al. 2015; 2016). *BCL2*, as well as *DOTL1*, are well-described leukemia-important genes. The expression of *BCL2*, an antiapoptotic factor, is important for the survival of AML cells (Waclawiczek et al. 2023). The H3K79 methyltransferase *DOT1L* participates in key processes like gene expression, DNA repair, and cell cycle progression and is involved in the development of *KTM2A*-rearranged leukemia (McLean, Karemaker, and van Leeuwen 2014). The role of *SMARCB1* in leukemia is described in chapter 5.2.

Additionally, several *in vivo* screens describe targets identified by our screens. The receptor *CXCR4* was earlier described as a dropout in an *in vivo* AML screen (Ramakrishnan et al. 2020). The importance of *CXCR4* in AL is described in chapter 5.2. *KRAS* was recently identified as an *in vivo* dropout in five AML PDX samples by our group (Ghalandary et al. 2023). *KRAS* is one of the most frequently mutated genes in human cancers, including AML (T. Wang et al. 2017). Additionally an *in vivo* CRISPR/Cas9 screen-induced knockout of *BCL2* in treatment-resistant ALL PDX samples was shown to sensitize them toward treatment (Wirth et al. 2022).

The described leukemia importance of these targets and their identification in several other performed CRISPR/Cas9 knockout screens reinforce our identified dropouts.

In addition to comparing our targets to existing literature, we performed a pathway analysis of them. The pathways associated with at least two genes from the 24 targets are depicted in Table 26. The epigenetic pathways have the most associated genes, with 9 out of 24 (*ARID1A, BRD2, BRD4, DNMT1, DOT1L, EZH2, HDAC3, SMARCB1* and *SS18*). The process of epigenetics allows cells with the identical genome to express specific subsets of genes based on their function and development stage, and failure in implementing this process can lead to abnormal gene expression and potentially cancerous outcomes (Sarkies and Sale 2012). This has been shown in different types of leukemia. Epigenetic dysfunction is a hallmark of AML and also in ALL epigenetic dysregulations in DNA methylation, histone modifications and regulation of non-coding RNA have been shown to play a role in leukemia progression (Drożak, Bryliński, and Zawitkowska 2022; Fennell, Bell, and Dawson 2019). Treatments of epigenetic targets are now considered novel and effective treatment

options, aiming at a reduction of abnormal epigenetic modifications in patient cells (Liu et al. 2020).

The number of epigenetic-associated dropouts in our screen reinforces the importance of epigenetic pathways for leukemic cells *in vivo*. The nine epigenetic-related genes include three genes described as subunits of the SWI/SNF complex (*ARID1A, SMARCB1,* and *SS18*). Besides subunits of the SWI/SNF complex, *BRD2* and *BRD4*, belonging to the BET family were depleted in most screens. The BET family is described by *BRD2, BRD3, BRD4*, and the testis-specific *BRDT. BRD4* was identified to be important for leukemia maintenance in AML (Zuber et al. 2011). *BRD4* is widely expressed and was identified as an important functional protein and therefore became one of the most examined epigenetic targets (Feng et al. 2022). In preclinical studies, *BRD4* inhibitors have shown effectiveness against AML and ALL cells. However, in clinical trials, single treatment resulted in limited response and dose-limiting toxicity. Combination with other targeted therapies or classical chemotherapy may show more promise (L. Zhang et al. 2021). Besides the limited response to monotherapy, resistance acquisition is another constraint (Fong et al. 2015).

Although epigenetic targeted therapies are now the new wave of treatment options for AL, they show the same tendency of problems as drugs approved in the first wave of targeted therapies. Patients develop resistance to target therapies, and monotherapies are mainly not effective enough. Perhaps the issue lies not with the drug's efficiency, but with treating the wrong patients. A precise tool for patient-specific treatment prediction might reduce the need for combinatorial treatment, higher doses, and even the development of resistance to the targeted therapy.

5.5 Potential biomarkers identified by the *in vivo* CRISPR/Cas9 screen

Our *in vivo* CRISPR/Cas9 knockout screens identified 24 genes with dropout in at least two PDX samples. The generated dropouts were considered as biomarkers for drug choice. For example, a sample with a *BCL2* dropout was expected to be sensitive to Venetoclax, a *BCL2* inhibitor.

For the final proof of our hypothesis, we aim to validate the targets with an associated direct drug. Among the 146 target genes in our library, 109 can be directly targeted by drugs, while the remaining genes can only be targeted by indirect drugs. An example of an indirect drug-target pair is *SMARCB1*, a subunit of the SWI/SNF complex. The assigned drug for targeting this gene is an *EZH2* inhibitor. *EZH2* is the catalytic subunit of the Polycomb repressor complex 2 (PRC2) and is antagonized by the SWI/SNF

complex (Wilson et al. 2010). Due to our interest in studying the direct effect of a drug on a specific target, we have excluded such dropouts from the study. In addition to the indirect drugs mentioned, our dropouts are also assigned to various unspecified drugs. HDAC inhibitors are an example of an unspecific inhibition since most inhibitors are pan HDAC inhibitors, like Valproic acid and Vorinostat (Suraweera, O'Byrne, and Richard 2018). Nevertheless, several inhibitors with a described specific function exist. For example, RGFP966 targets *HDAC3* without inhibiting other HDACs with a dose below 15 µM (Beyer et al. 2019).

For the final drug treatment experiment, we identified the following target genes*: BCL2, MCL1, XPO1, NEDD8*, and *HDAC3*. Resulting in drug treatments using: (i) Venetoclax as a *BCL2* inhibitor, (ii) S63845 for targeting *MCL1*, (iii) *XPO1* inhibition by Eltanexor, (iv) targeting of *NEDD8* by Pevonedistat and RGFP966 as an inhibitor of *HDAC3*. Venetoclax is an FDA-approved inhibitor for treating AML patients (Guerra, DiNardo and Konopleva, 2019; Griffioen et al., 2022). The *MCL1* inhibitor S63845 showed activity in *in vitro and in vivo* studies of diverse hematological diseases (Kotschy et al., 2016; Carlet et al., 2021). Eltanexor is currently in Phase II clinical trials for AML treatment (NCT02649790). RGFP966 showed activity *in vivo* and *in vitro* in treating AML cells (Long et al., 2017; Beyer et al., 2019). Pevonedistat was tested in clinical trials as a combinatorial treatment with Azacytidine for AML patients (NCT03268954).

Based on the CRISPR/Cas9 screens, we anticipate that all seven samples will be reliant on *XPO1* and therefore show some impact upon Eltanexor treatment. Additionally, we expect that all samples, with the exception of ALL1034, will exhibit a reduction in leukemic cell growth *in vivo* due to *HDAC3* inhibitor treatment. Venetoclax treatment is believed to affect ALL50, ALL199, ALL265, and ALL502 *in vivo* cell growth. Similarly, the *NEDD8* inhibitor should result in an effect on ALL50, ALL199, ALL265, and ALL1034. Finally, the *MCL1* inhibitor is expected to reduce *in vivo* growth for ALL50, ALL199, and AML356 samples but will not affect the remaining four samples.

In summary, we could predict patient-individual drug treatments in all screened samples. The accordance of those predictions will be validated by *in vivo* drug tests of the gene-associated drugs.

5.6 Conclusion and outlook

Our functional, precision medicine tool identified 24 dependencies in the seven screened AL PDX samples. Out of those 24 dependencies, we defined patient-specific drugs for each PDX sample. In conclusion, we generated biomarkers that can be used for further treatment decisions.

Our next step is to validate these results through *in vivo* drug treatments using patient-individual drugs. Furthermore, we intend to molecularly validate our dropouts by single knockout experiments of the target genes. This has proven to be a useful tool for enhancing *in vivo* screening data obtained from AML and ALL PDX samples (Bahrami et al. 2023; Ghalandary et al. 2023).

Additionally, the 24 obtained target genes suggest a shared importance in AML and ALL samples and it is conceivable to use those genes for further screens in more AL PDX samples. The small number of genes would allow screening in more samples since the library size would not exceed 150 sgRNAs including all needed controls. Even screening of primary cells could be an option with this small library. The hurdle of Cas9 transduction could be circumvented by using Guide Swap (Ting et al. 2018). Guide Swap just requires the transduction of the sgRNA library construct followed by an electroporation of the Cas9 protein bound to a non-targeting crRNA that will be swapped by a targeting sgRNAs.

Concluding, the present study showed the potential of a CRISPR/Cas9 knockout screen as a functional tool for the precise prediction of drugs by using an *in vivo* model of ALs.

6. Literature

Abdelhameed, Ali S., Mohamed W. Attwa, and Adnan A. Kadi. 2017. 'An LC–MS/MS Method for Rapid and Sensitive High-Throughput Simultaneous Determination of Various Protein Kinase Inhibitors in Human Plasma'. *Biomedical Chromatography* 31 (2): e3793. https://doi.org/10.1002/bmc.3793.

Agliano, Alice, Ines Martin-Padura, Patrizia Mancuso, Paola Marighetti, Cristina Rabascio, Giancarlo Pruneri, Leonard D. Shultz, and Francesco Bertolini. 2008. 'Human Acute Leukemia Cells Injected in NOD/LtSz-Scid/IL-2Rγ Null Mice Generate a Faster and More Efficient Disease Compared to Other NOD/Scid-Related Strains'. *International Journal of Cancer* 123 (9): 2222–27. https://doi.org/10.1002/ijc.23772.

Almosailleakh, Marwa, and Juerg Schwaller. 2019. 'Murine Models of Acute Myeloid Leukaemia'. *International Journal of Molecular Sciences* 20 (2): 453. https://doi.org/10.3390/ijms20020453.

Alvarnas, Joseph C., Patrick A. Brown, Patricia Aoun, Karen Kuhn Ballen, Stefan K. Barta, Uma Borate, Michael W. Boyer, et al. 2015. 'Acute Lymphoblastic Leukemia, Version 2.2015'. *Journal of the National Comprehensive Cancer Network* 13 (10): 1240–79. https://doi.org/10.6004/jnccn.2015.0153.

Andrades, Alvaro, Paola Peinado, Juan Carlos Alvarez-Perez, Juan Sanjuan-Hidalgo, Daniel J. García, Alberto M. Arenas, Ana M. Matia-González, and Pedro P. Medina. 2023. 'SWI/SNF Complexes in Hematological Malignancies: Biological Implications and Therapeutic Opportunities'. *Molecular Cancer* 22 (1): 39. https://doi.org/10.1186/s12943-023-01736-8.

Arber, Daniel A., Attilio Orazi, Robert Hasserjian, Jürgen Thiele, Michael J. Borowitz, Michelle M. Le Beau, Clara D. Bloomfield, Mario Cazzola, and James W. Vardiman. 2016. 'The 2016 Revision to the World Health Organization Classification of Myeloid Neoplasms and Acute Leukemia'. *Blood* 127 (20): 2391–2405. https://doi.org/10.1182/blood-2016-03-643544.

Bahrami, Ehsan, Jan Philipp Schmid, Vindi Jurinovic, Martin Becker, Anna-Katharina Wirth, Romina Ludwig, Sophie Kreissig, et al. 2023. 'Combined Proteomics and CRISPR–Cas9 Screens in PDX Identify ADAM10 as Essential for Leukemia in Vivo'. *Molecular Cancer* 22 (1): 107. https://doi.org/10.1186/s12943-023-01803-0.

Barrangou, Rodolphe, Christophe Fremaux, Hélène Deveau, Melissa Richards, Patrick Boyaval, Sylvain Moineau, Dennis A. Romero, and Philippe Horvath. 2007. 'CRISPR Provides Acquired Resistance Against Viruses in Prokaryotes'. *Science* 315 (5819): 1709–12. https://doi.org/10.1126/science.1138140.

Becker, Martin, Heidi Noll-Puchta, Diana Amend, Florian Nolte, Christiane Fuchs, Irmela Jeremias, and Christian J. Braun. 2020. 'CLUE: A Bioinformatic and Wet-Lab Pipeline for Multiplexed Cloning of Custom SgRNA Libraries'. *Nucleic Acids Research* 48 (13): e78. https://doi.org/10.1093/nar/gkaa459.

Bendari, Mounia, Nisrine Khoubila, Siham Cherkaoui, Nezha Hda, Meryem Qachouh, Mouna Lamchahab, Asmaa Quessar, et al. 2020. *Current Cytogenetic Abnormalities in Acute Myeloid Leukemia*. *Chromosomal Abnormalities*. IntechOpen. https://doi.org/10.5772/intechopen.91425.

Bernt, Kathrin M., and Scott A. Armstrong. 2009. 'Leukemia Stem Cells and Human Acute Lymphoblastic Leukemia'. *Seminars in Hematology* 46 (1): 33. https://doi.org/10.1053/j.seminhematol.2008.09.010.

Bertoli, Sarah, Emilie Bérard, Françoise Huguet, Anne Huynh, Suzanne Tavitian, François Vergez, Sophie Dobbelstein, et al. 2013. 'Time from Diagnosis to Intensive Chemotherapy Initiation Does Not Adversely Impact the Outcome of Patients with Acute Myeloid Leukemia'. *Blood* 121 (14): 2618–26. https://doi.org/10.1182/blood-2012-09-454553.

Beyer, Mandy, Annette Romanski, Al-Hassan M. Mustafa, Miriam Pons, Iris Büchler, Anja Vogel, Andrea Pautz, et al. 2019. 'HDAC3 Activity Is Essential for Human Leukemic Cell Growth and the Expression of β-Catenin, MYC, and WT1'. *Cancers* 11 (10): 1436. https://doi.org/10.3390/cancers11101436.

Blachly, James S., Roland B. Walter, and Christopher S. Hourigan. 2022. 'The Present and Future of Measurable Residual Disease Testing in Acute Myeloid Leukemia'. *Haematologica* 107 (12): 2810–22. https://doi.org/10.3324/haematol.2022.282034.

Blackburn, Lisa M., Sarah Bender, and Shelly Brown. 2019. 'Acute Leukemia: Diagnosis and Treatment'. *Seminars in Oncology Nursing* 35 (6): 150950. https://doi.org/10.1016/j.soncn.2019.150950.

Bochar, Daniel A., Lai Wang, Hideo Beniya, Alexander Kinev, Yutong Xue, William S. Lane, Weidong Wang, Fatah Kashanchi, and Ramin Shiekhattar. 2000. 'BRCA1 Is Associated with a Human SWI/SNF-Related Complex: Linking Chromatin Remodeling to Breast Cancer'. *Cell* 102 (2): 257–65. https://doi.org/10.1016/S0092-8674(00)00030-1.

Bonnet, Dominique, and John E. Dick. 1997. 'Human Acute Myeloid Leukemia Is Organized as a Hierarchy That Originates from a Primitive Hematopoietic Cell'. *Nature Medicine* 3 (7): 730–37. https://doi.org/10.1038/nm0797-730.

Burd, Amy, Ross L. Levine, Amy S. Ruppert, Alice S. Mims, Uma Borate, Eytan M. Stein, Prapti Patel, et al. 2020. 'Precision Medicine Treatment in Acute Myeloid Leukemia Using Prospective Genomic Profiling: Feasibility and Preliminary Efficacy of the Beat AML Master Trial'. *Nature Medicine* 26 (12): 1852–58. https://doi.org/10.1038/s41591-020-1089-8.

Burd, Amy, Ross L. Levine, Abigail Shoben, Alice S. Mims, Uma Borate, Eytan M. Stein, Prapti A. Patel, et al. 2018. 'Initial Report of the Beat AML Umbrella Study for Previously Untreated AML: Evidence of Feasibility and Early Success in Molecularly Driven Phase 1 and 2 Studies'. *Blood* 132 (November): 559. https://doi.org/10.1182/blood-2018-99-118494.

Burger, Jan A., and Andrea Bürkle. 2007. 'The CXCR4 Chemokine Receptor in Acute and Chronic Leukaemia: A Marrow Homing Receptor and Potential Therapeutic Target'. *British Journal of Haematology* 137 (4): 288–96. https://doi.org/10.1111/j.1365-2141.2007.06590.x.

Cancilla, Daniel, Michael P. Rettig, and John F. DiPersio. 2020. 'Targeting CXCR4 in AML and ALL'. *Frontiers in Oncology* 10 (September): 1672. https://doi.org/10.3389/fonc.2020.01672.

Centore, Richard C., Gabriel J. Sandoval, Luis Miguel Mendes Soares, Cigall Kadoch, and Ho Man Chan. 2020. 'Mammalian SWI/SNF Chromatin Remodeling Complexes: Emerging Mechanisms and Therapeutic Strategies'. *Trends in Genetics* 36 (12): 936–50. https://doi.org/10.1016/j.tig.2020.07.011.

Chatterjee, Shankha, Mayukh Biswas, Liberalis Boila, Debasis Banerjee, and Amitava Sengupta. 2018. 'SMARCB1 Deficiency Integrates Epigenetic Signals to Oncogenic Gene Expression Program Maintenance in Human Acute Myeloid Leukemia'. *Molecular Cancer Research* 16 (February): molcanres.0493.2017. https://doi.org/10.1158/1541-7786.MCR-17-0493.

Chen, Edward Y., Christopher M. Tan, Yan Kou, Qiaonan Duan, Zichen Wang, Gabriela Vaz Meirelles, Neil R. Clark, and Avi Ma'ayan. 2013. 'Enrichr: Interactive and Collaborative HTML5 Gene List Enrichment Analysis Tool'. *BMC Bioinformatics* 14 (April): 128. https://doi.org/10.1186/1471-2105-14-128.

De Kouchkovsky, I., and M. Abdul-Hay. 2016. '"Acute Myeloid Leukemia: A Comprehensive Review and 2016 Update"'. *Blood Cancer Journal* 6 (7): e441. https://doi.org/10.1038/bcj.2016.50.

Deak, Dalma, Nicolae Gorcea-Andronic, Valentina Sas, Patric Teodorescu, Catalin Constantinescu, Sabina Iluta, Sergiu Pasca, et al. 2021. 'A Narrative Review of Central Nervous System Involvement in Acute Leukemias'. *Annals of Translational Medicine* 9 (1): 68. https://doi.org/10.21037/atm-20-3140.

Dempster, Joshua M., Isabella Boyle, Francisca Vazquez, David E. Root, Jesse S. Boehm, William C. Hahn, Aviad Tsherniak, and James M. McFarland. 2021. 'Chronos: A Cell Population Dynamics Model of CRISPR Experiments That Improves Inference of Gene Fitness Effects'. *Genome Biology* 22 (1): 343. https://doi.org/10.1186/s13059-021-02540-7.

Dempster, Joshua M., Jordan Rossen, Mariya Kazachkova, Joshua Pan, Guillaume Kugener, David E. Root, and Aviad Tsherniak. 2019. 'Extracting Biological Insights from the Project Achilles Genome-Scale CRISPR Screens in Cancer Cell Lines'. bioRxiv. https://doi.org/10.1101/720243.

'DepMap 22Q2 Public'. 2022. figshare. https://doi.org/10.6084/m9.figshare.19700056.v2.

Dick, John E. 2008. 'Stem Cell Concepts Renew Cancer Research'. *Blood* 112 (13): 4793–4807. https://doi.org/10.1182/blood-2008-08-077941.

DiNardo, Courtney D., and Alexander E. Perl. 2019. 'Acute Myeloid Leukaemia in 2018: Advances in Patient Care through Increasingly Individualized Therapy'. *Nature Reviews. Clinical Oncology* 16 (2): 73. https://doi.org/10.1038/s41571-018-0156-2.

Doench, John G. 2018. 'Am I Ready for CRISPR? A User's Guide to Genetic Screens'. *Nature Reviews. Genetics* 19 (2): 67–80. https://doi.org/10.1038/nrg.2017.97.

Doench, John G., Nicolo Fusi, Meagan Sullender, Mudra Hegde, Emma W. Vaimberg, Katherine F. Donovan, Ian Smith, et al. 2016. 'Optimized SgRNA Design to Maximize Activity and Minimize Off-Target Effects of CRISPR-Cas9'. *Nature Biotechnology* 34 (2): 184–91. https://doi.org/10.1038/nbt.3437.

Döhner, Hartmut, Andrew H. Wei, and Bob Löwenberg. 2021. 'Towards Precision Medicine for AML'. *Nature Reviews Clinical Oncology* 18 (9): 577–90. https://doi.org/10.1038/s41571-021-00509-w.

Doroshow, D. B., J. P. Eder, and P. M. LoRusso. 2017. 'BET Inhibitors: A Novel Epigenetic Approach'. *Annals of Oncology* 28 (8): 1776–87. https://doi.org/10.1093/annonc/mdx157.

Dozzo, Annachiara, Aoife Galvin, Jae-Won Shin, Santo Scalia, Caitriona M. O'Driscoll, and Katie B. Ryan. 2022. 'Modelling Acute Myeloid Leukemia (AML): What's New? A Transition from the Classical to the Modern'. *Drug Delivery and Translational Research*, August. https://doi.org/10.1007/s13346-022-01189-4.

Drożak, Paulina, Łukasz Bryliński, and Joanna Zawitkowska. 2022. 'A Comprehensive Overview of Recent Advances in Epigenetics in Pediatric Acute Lymphoblastic Leukemia'. *Cancers* 14 (21): 5384. https://doi.org/10.3390/cancers14215384.

Duan, Linna, and Eric Mukherjee. 2016. 'Janeway's Immunobiology, Ninth Edition'. *The Yale Journal of Biology and Medicine* 89 (3): 424–25. https://www.ncbi.nlm.nih.gov/pmc/articles/PMC5045153/.

Ebinger, Sarah, Erbey Ziya Özdemir, Christoph Ziegenhain, Sebastian Tiedt, Catarina Castro Alves, Michaela Grunert, Michael Dworzak, et al. 2016. 'Characterization of Rare, Dormant, and Therapy-Resistant Cells in Acute Lymphoblastic Leukemia'. *Cancer Cell* 30 (6): 849–62. https://doi.org/10.1016/j.ccell.2016.11.002.

Ebinger, Sarah, Christina Zeller, Michela Carlet, Daniela Senft, Johannes W. Bagnoli, Wen-Hsin Liu, Maja Rothenberg-Thurley, et al. 2020. 'Plasticity in Growth Behavior of Patients' Acute Myeloid Leukemia Stem Cells Growing in Mice'. *Haematologica* 105 (12): 2855–60. https://doi.org/10.3324/haematol.2019.226282.

Ehninger, A., M. Kramer, C. Röllig, C. Thiede, M. Bornhäuser, M. von Bonin, M. Wermke, et al. 2014. 'Distribution and Levels of Cell Surface Expression of CD33 and CD123 in Acute Myeloid Leukemia'. *Blood Cancer Journal* 4 (6): e218–e218. https://doi.org/10.1038/bcj.2014.39.

Elder, A., S. Bomken, I. Wilson, H. J. Blair, S. Cockell, F. Ponthan, K. Dormon, D. Pal, O. Heidenreich, and J. Vormoor. 2017. 'Abundant and Equipotent Founder Cells Establish and Maintain Acute Lymphoblastic Leukaemia'. *Leukemia* 31 (12): 2577–86. https://doi.org/10.1038/leu.2017.140.

Feng, Lu, Guan Wang, Yi Chen, Gu He, Bo Liu, Jie Liu, Cheng-Ming Chiang, and Liang Ouyang. 2022. 'Dual-Target Inhibitors of Bromodomain and Extra-Terminal Proteins in Cancer: A Review from Medicinal Chemistry Perspectives'. *Medicinal Research Reviews* 42 (2): 710–43. https://doi.org/10.1002/med.21859.

Fennell, Katie A., Charles C. Bell, and Mark A. Dawson. 2019. 'Epigenetic Therapies in Acute Myeloid Leukemia: Where to from Here?' *Blood* 134 (22): 1891–1901. https://doi.org/10.1182/blood.2019003262.

Follini, Elena, Matteo Marchesini, and Giovanni Roti. 2019. 'Strategies to Overcome Resistance Mechanisms in T-Cell Acute Lymphoblastic Leukemia'. *International Journal of Molecular Sciences* 20 (12): 3021. https://doi.org/10.3390/ijms20123021.

Fong, Chun Yew, Omer Gilan, Enid Y. N. Lam, Alan F. Rubin, Sarah Ftouni, Dean Tyler, Kym Stanley, et al. 2015. 'BET Inhibitor Resistance Emerges from Leukaemia Stem Cells'. *Nature* 525 (7570): 538–42. https://doi.org/10.1038/nature14888.

Foudi, Adlen, Peggy Jarrier, Yanyan Zhang, Monika Wittner, Jean-Francois Geay, Yann Lecluse, Takashi Nagasawa, William Vainchenker, and Fawzia Louache. 2006. 'Reduced Retention of Radioprotective Hematopoietic Cells within the Bone Marrow Microenvironment in CXCR4–/– Chimeric Mice'. *Blood* 107 (6): 2243–51. https://doi.org/10.1182/blood-2005-02-0581.

'Genomic and Epigenomic Landscapes of Adult De Novo Acute Myeloid Leukemia'. 2013. *The New England Journal of Medicine* 368 (22): 2059–74. https://doi.org/10.1056/NEJMoa1301689.

Ghalandary, Maryam, Yuqiao Gao, Diana Amend, Ginte Kutkaite, Binje Vick, Karsten Spiekermann, Maja Rothenberg-Thurley, et al. 2023. 'WT1 and DNMT3A Play Essential Roles in the Growth of Certain Patient AML Cells in Mice'. *Blood* 141 (8): 955–60. https://doi.org/10.1182/blood.2022016411.

Gimeno, Marian, Edurne San José-Enériz, Sara Villar, Xabier Agirre, Felipe Prosper, Angel Rubio, and Fernando Carazo. 2022. 'Explainable Artificial Intelligence for Precision Medicine in Acute Myeloid Leukemia'. *Frontiers in Immunology* 13. https://www.frontiersin.org/articles/10.3389/fimmu.2022.977358.

Gleditzsch, Daniel, Patrick Pausch, Hanna Müller-Esparza, Ahsen Özcan, Xiaohan Guo, Gert Bange, and Lennart Randau. 2018. 'PAM Identification by CRISPR-Cas Effector Complexes: Diversified Mechanisms and Structures'. *RNA Biology* 16 (4): 504–17. https://doi.org/10.1080/15476286.2018.1504546.

Grupp, Stephan A., Michael Kalos, David Barrett, Richard Aplenc, David L. Porter, Susan R. Rheingold, David T. Teachey, et al. 2013. 'Chimeric Antigen Receptor–Modified T Cells for Acute Lymphoid Leukemia'. *The New England Journal of Medicine* 368 (16): 1509–18. https://doi.org/10.1056/NEJMoa1215134.

He, Xiaoyuan, Xia Xiao, Qing Li, Yanyu Jiang, Yaqing Cao, Rui Sun, Xin Jin, et al. 2019. 'Anti-CD19 CAR-T as a Feasible and Safe Treatment against Central Nervous System Leukemia after Intrathecal Chemotherapy in Adults with Relapsed or Refractory B-ALL'. *Leukemia* 33 (8): 2102–4. https://doi.org/10.1038/s41375-019-0437-5.

Heuser, Michael, Sylvie D. Freeman, Gert J. Ossenkoppele, Francesco Buccisano, Christopher S. Hourigan, Lok Lam Ngai, Jesse M. Tettero, et al. 2021. '2021 Update on MRD in Acute Myeloid Leukemia: A Consensus Document from the European LeukemiaNet MRD Working Party'. *Blood* 138 (26): 2753–67. https://doi.org/10.1182/blood.2021013626.

Hidalgo, Manuel, Frederic Amant, Andrew V. Biankin, Eva Budinská, Annette T. Byrne, Carlos Caldas, Robert B. Clarke, et al. 2014. 'Patient Derived Xenograft Models: An Emerging Platform for Translational Cancer Research'. *Cancer Discovery* 4 (9): 998–1013. https://doi.org/10.1158/2159-8290.CD-14-0001.

Hoshii, Takayuki, Yuko Tadokoro, Kazuhito Naka, Takako Ooshio, Teruyuki Muraguchi, Naoyuki Sugiyama, Tomoyoshi Soga, Kimi Araki, Ken-Ichi Yamamura, and Atsushi Hirao. 2012. 'MTORC1 Is Essential for Leukemia Propagation but Not Stem Cell Self-Renewal'. *The Journal of Clinical Investigation* 122 (6): 2114–29. https://doi.org/10.1172/JCI62279.

Hou, Hsin-An, and Hwei-Fang Tien. 2020. 'Genomic Landscape in Acute Myeloid Leukemia and Its Implications in Risk Classification and Targeted Therapies'. *Journal of Biomedical Science* 27 (1): 81. https://doi.org/10.1186/s12929-020-00674-7.

Hutter, Grit, Christina Nickenig, Henk Garritsen, Frank Hellenkamp, Andre Hoerning, Wolfgang Hiddemann, and Martin Dreyling. 2004. 'Use of Polymorphisms in the Noncoding Region of the Human Mitochondrial Genome to Identify Potential Contamination of Human Leukemia-Lymphoma Cell Lines'. *The Hematology Journal: The Official Journal of the European Haematology Association* 5 (1): 61–68. https://doi.org/10.1038/sj.thj.6200317.

Hwang, Sang Mee. 2020. 'Classification of Acute Myeloid Leukemia'. *Blood Research* 55 (Suppl): S1–4. https://doi.org/10.5045/br.2020.S001.

Inaba, Hiroto, Mel Greaves, and Charles G. Mullighan. 2013. 'Acute Lymphoblastic Leukaemia'. *Lancet* 381 (9881). https://doi.org/10.1016/S0140-6736(12)62187-4.

Ishino, Y, H Shinagawa, K Makino, M Amemura, and A Nakata. 1987. 'Nucleotide Sequence of the Iap Gene, Responsible for Alkaline Phosphatase Isozyme Conversion in Escherichia Coli, and Identification of the Gene Product.' *Journal of Bacteriology* 169 (12): 5429–33. https://www.ncbi.nlm.nih.gov/pmc/articles/PMC213968/.

Ishino, Yoshizumi, Mart Krupovic, and Patrick Forterre. 2018. 'History of CRISPR-Cas from Encounter with a Mysterious Repeated Sequence to Genome Editing Technology'. *Journal of Bacteriology* 200 (7): e00580-17. https://doi.org/10.1128/JB.00580-17.

Jansen, Ruud, Jan D. A. van Embden, Wim Gaastra, and Leo M. Schouls. 2002. 'Identification of Genes That Are Associated with DNA Repeats in Prokaryotes'. *Molecular Microbiology* 43 (6): 1565–75.

Jędraszek, Krzysztof, Marta Malczewska, Karolina Parysek-Wójcik, and Monika Lejman. 2022. 'Resistance Mechanisms in Pediatric B-Cell Acute Lymphoblastic Leukemia'. *International Journal of Molecular Sciences* 23 (6): 3067. https://doi.org/10.3390/ijms23063067.

Kantarjian, Hagop M., Daniel J. DeAngelo, Matthias Stelljes, Giovanni Martinelli, Michaela Liedtke, Wendy Stock, Nicola Gökbuget, et al. 2016. 'Inotuzumab Ozogamicin versus Standard Therapy for Acute Lymphoblastic Leukemia'. *New England Journal of Medicine* 375 (8): 740–53. https://doi.org/10.1056/NEJMoa1509277.

Kantarjian, Hagop, Anthony Stein, Nicola Gökbuget, Adele K. Fielding, Andre C. Schuh, Josep-Maria Ribera, Andrew Wei, et al. 2017. 'Blinatumomab versus Chemotherapy for Advanced Acute Lymphoblastic Leukemia'. *New England Journal of Medicine* 376 (9): 836–47. https://doi.org/10.1056/NEJMoa1609783.

Khwaja, Asim, Magnus Bjorkholm, Rosemary E. Gale, Ross L. Levine, Craig T. Jordan, Gerhard Ehninger, Clara D. Bloomfield, et al. 2016. 'Acute Myeloid Leukaemia'. *Nature Reviews Disease Primers* 2 (1): 1–22. https://doi.org/10.1038/nrdp.2016.10.

Kiyoi, Hitoshi, Naomi Kawashima, and Yuichi Ishikawa. 2020. 'FLT3 Mutations in Acute Myeloid Leukemia: Therapeutic Paradigm beyond Inhibitor Development'. *Cancer Science* 111 (2): 312–22. https://doi.org/10.1111/cas.14274.

Kohnken, Rebecca, Pierluigi Porcu, and Anjali Mishra. 2017. 'Overview of the Use of Murine Models in Leukemia and Lymphoma Research'. *Frontiers in Oncology* 7. https://www.frontiersin.org/articles/10.3389/fonc.2017.00022.

Koike-Yusa, Hiroko, Yilong Li, E-Pien Tan, Martin Del Castillo Velasco-Herrera, and Kosuke Yusa. 2014. 'Genome-Wide Recessive Genetic Screening in Mammalian Cells with a Lentiviral CRISPR-Guide RNA Library'. *Nature Biotechnology* 32 (3): 267–73. https://doi.org/10.1038/nbt.2800.

Komor, Alexis C., Yongjoo B. Kim, Michael S. Packer, John A. Zuris, and David R. Liu. 2016. 'Programmable Editing of a Target Base in Genomic DNA without Double-Stranded DNA Cleavage'. *Nature* 533 (7603): 420–24. https://doi.org/10.1038/nature17946.

Krevvata, Maria, Xiaochuan Shan, Chenghui Zhou, Cedric Dos Santos, Georges Habineza Ndikuyeze, Anthony Secreto, Joshua Glover, et al. 2018. 'Cytokines Increase Engraftment of Human Acute Myeloid Leukemia Cells in Immunocompromised Mice but Not Engraftment of Human Myelodysplastic Syndrome Cells'. *Haematologica* 103 (6): 959–71. https://doi.org/10.3324/haematol.2017.183202.

Kruse, Aaron, Nour Abdel-Azim, Hye Na Kim, Yongsheng Ruan, Valerie Phan, Heather Ogana, William Wang, et al. 2020. 'Minimal Residual Disease Detection in Acute Lymphoblastic Leukemia'. *International Journal of Molecular Sciences* 21 (3): 1054. https://doi.org/10.3390/ijms21031054.

Kuleshov, Maxim V., Matthew R. Jones, Andrew D. Rouillard, Nicolas F. Fernandez, Qiaonan Duan, Zichen Wang, Simon Koplev, et al. 2016. 'Enrichr: A Comprehensive Gene Set Enrichment Analysis Web Server 2016 Update'. *Nucleic Acids Research* 44 (W1): W90-97. https://doi.org/10.1093/nar/gkw377.

Lai, Yunxin, Xinru Wei, Shouheng Lin, Le Qin, Lin Cheng, and Peng Li. 2017. 'Current Status and Perspectives of Patient-Derived Xenograft Models in Cancer Research'. *Journal of Hematology & Oncology* 10 (1): 106. https://doi.org/10.1186/s13045-017-0470-7.

Lang, Fabian, Bartosch Wojcik, and Michael A. Rieger. 2015. 'Stem Cell Hierarchy and Clonal Evolution in Acute Lymphoblastic Leukemia'. *Stem Cells International* 2015 (July): e137164. https://doi.org/10.1155/2015/137164.

Lapidot, T., C. Sirard, J. Vormoor, B. Murdoch, T. Hoang, J. Caceres-Cortes, M. Minden, B. Paterson, M. A. Caligiuri, and J. E. Dick. 1994. 'A Cell Initiating Human Acute Myeloid Leukaemia after Transplantation into SCID Mice'. *Nature* 367 (6464): 645–48. https://doi.org/10.1038/367645a0.

Lapidot, Tsvee, Christian Sirard, Josef Vormoor, Barbara Murdoch, Trang Hoang, Julio Caceres-Cortes, Mark Minden, Bruce Paterson, Michael A. Caligiuri, and John E. Dick. 1994. 'A Cell Initiating Human Acute Myeloid Leukaemia after Transplantation into SCID Mice'. *Nature* 367 (6464): 645–48. https://doi.org/10.1038/367645a0.

Lau, Loretta M S, Chelsea Mayoh, Jinhan Xie, Paulette Barahona, Karen L MacKenzie, Marie Wong, Alvin Kamili, et al. 2022. 'In Vitro and in Vivo Drug Screens of Tumor Cells Identify Novel Therapies for High-Risk Child Cancer'. *EMBO Molecular Medicine* 14 (4): e14608. https://doi.org/10.15252/emmm.202114608.

Lee, Shawn H. R., Wenjian Yang, Yoshihiro Gocho, August John, Lauren Rowland, Brandon Smart, Hannah Williams, et al. 2023. 'Pharmacotypes across the Genomic Landscape of Pediatric Acute Lymphoblastic Leukemia and Impact on Treatment Response'. *Nature Medicine* 29 (1): 170–79. https://doi.org/10.1038/s41591-022-02112-7.

Lee, Su-In, Safiye Celik, Benjamin A. Logsdon, Scott M. Lundberg, Timothy J. Martins, Vivian G. Oehler, Elihu H. Estey, et al. 2018. 'A Machine Learning Approach to Integrate Big Data for Precision Medicine in Acute Myeloid Leukemia'. *Nature Communications* 9 (January): 42. https://doi.org/10.1038/s41467-017-02465-5.

Li, Wei, Johannes Köster, Han Xu, Chen-Hao Chen, Tengfei Xiao, Jun S. Liu, Myles Brown, and X. Shirley Liu. 2015. 'Quality Control, Modeling, and Visualization of CRISPR Screens with MAGeCK-VISPR'. *Genome Biology* 16 (1): 281. https://doi.org/10.1186/s13059-015-0843-6.

Li, Wei, Han Xu, Tengfei Xiao, Le Cong, Michael I Love, Feng Zhang, Rafael A Irizarry, Jun S Liu, Myles Brown, and X Shirley Liu. 2014. 'MAGeCK Enables Robust Identification of Essential Genes from Genome-Scale CRISPR/Cas9 Knockout Screens'. *Genome Biology* 15 (12): 554. https://doi.org/10.1186/s13059-014-0554-4.

Lieber, Michael R. 2010. 'The Mechanism of Double-Strand DNA Break Repair by the Nonhomologous DNA End Joining Pathway'. *Annual Review of Biochemistry* 79: 181–211. https://doi.org/10.1146/annurev.biochem.052308.093131.

Lin, Pei, Lei Chen, Rajyalakshmi Luthra, Sergej N. Konoplev, Xuemei Wang, and L. Jeffrey Medeiros. 2008. 'Acute Myeloid Leukemia Harboring t(8;21)(Q22;Q22): A Heterogeneous Disease with Poor Outcome in a Subset of Patients Unrelated to Secondary Cytogenetic Aberrations'. *Modern Pathology* 21 (8): 1029–36. https://doi.org/10.1038/modpathol.2008.92.

Lin, Shan, Clément Larrue, Nastassja K. Scheidegger, Bo Kyung A. Seong, Neekesh V. Dharia, Miljan Kuljanin, Caroline S. Wechsler, et al. 2022. 'An in Vivo CRISPR Screening Platform for Prioritizing Therapeutic Targets in AML'. *Cancer Discovery* 12 (2): 432–49. https://doi.org/10.1158/2159-8290.CD-20-1851.

Liu, Xiao-liang, Huan-qiu Liu, Ji Li, Cui-ying Mao, Jin-ting He, and Xin Zhao. 2020. 'Role of Epigenetic in Leukemia: From Mechanism to Therapy'. *Chemico-Biological Interactions* 317 (February): 108963. https://doi.org/10.1016/j.cbi.2020.108963.

Lucas, Xavier, and Stefan Günther. 2014. 'Targeting the BET Family for the Treatment of Leukemia'. *Epigenomics* 6 (2): 153–55. https://doi.org/10.2217/epi.14.5.

Malani, Disha, Ashwini Kumar, Oscar Brück, Mika Kontro, Bhagwan Yadav, Monica Hellesøy, Heikki Kuusanmäki, et al. 2022. 'Implementing a Functional Precision Medicine Tumor Board for Acute Myeloid Leukemia'. *Cancer Discovery* 12 (2): 388–401. https://doi.org/10.1158/2159-8290.CD-21-0410.

Manguso, Robert T., Hans W. Pope, Margaret D. Zimmer, Flavian D. Brown, Kathleen B. Yates, Brian C. Miller, Natalie B. Collins, et al. 2017. 'In Vivo CRISPR Screening

Identifies Ptpn2 as a Cancer Immunotherapy Target'. *Nature* 547 (7664): 413–18. https://doi.org/10.1038/nature23270.

Maude, S.L., T.W. Laetsch, J. Buechner, S. Rives, M. Boyer, H. Bittencourt, P. Bader, et al. 2018. 'Tisagenlecleucel in Children and Young Adults with B-Cell Lymphoblastic Leukemia'. *The New England Journal of Medicine* 378 (5): 439–48. https://doi.org/10.1056/NEJMoa1709866.

McLean, C M, I D Karemaker, and F van Leeuwen. 2014. 'The Emerging Roles of DOT1L in Leukemia and Normal Development'. *Leukemia* 28 (11): 2131–38. https://doi.org/10.1038/leu.2014.169.

MD, David A. Sallman, Ateefa Chaudhury MD, Johnny Nguyen MD, and Ling Zhang MD. 2020. *Handbook of Hematologic Malignancies, Second Edition*. Springer Publishing Company.

Mecklenbrauck, Rabea, and Michael Heuser. 2022. 'Resistance to Targeted Therapies in Acute Myeloid Leukemia'. *Clinical & Experimental Metastasis*, November. https://doi.org/10.1007/s10585-022-10189-0.

Medinger, Michael, Claudia Lengerke, and Jakob Passweg. 2016a. 'Novel Therapeutic Options in Acute Myeloid Leukemia'. *Leukemia Research Reports* 6 (October): 39–49. https://doi.org/10.1016/j.lrr.2016.09.001.

Mercier, Francois E., Jiantao Shi, David B. Sykes, Toshihiko Oki, Maja Jankovic, Cheuk Him Man, Youmna S. Kfoury, et al. 2022. 'In Vivo Genome-Wide CRISPR Screening in Murine Acute Myeloid Leukemia Uncovers Microenvironmental Dependencies'. *Blood Advances* 6 (17): 5072–84. https://doi.org/10.1182/bloodadvances.2022007250.

Meyers, Robin M., Jordan G. Bryan, James M. McFarland, Barbara A. Weir, Ann E. Sizemore, Han Xu, Neekesh V. Dharia, et al. 2017a. 'Computational Correction of Copy Number Effect Improves Specificity of CRISPR-Cas9 Essentiality Screens in Cancer Cells'. *Nature Genetics* 49 (12): 1779–84. https://doi.org/10.1038/ng.3984.

Middeljans, Evelien, Xi Wan, Pascal W. Jansen, Vikram Sharma, Hendrik G. Stunnenberg, and Colin Logie. 2012. 'SS18 Together with Animal-Specific Factors Defines Human BAF-Type SWI/SNF Complexes'. *PLOS ONE* 7 (3): e33834. https://doi.org/10.1371/journal.pone.0033834.

Mojica, F. J. M., G. Juez, and F. Rodriguez-Valera. 1993. 'Transcription at Different Salinities of Haloferax Mediterranei Sequences Adjacent to Partially Modified PstI Sites'. *Molecular Microbiology* 9 (3): 613–21. https://doi.org/10.1111/j.1365-2958.1993.tb01721.x.

Mojica, Francisco J.M., Chc)sar Díez-Villaseñor, Jesús García-Martínez, and Elena Soria. 2005. 'Intervening Sequences of Regularly Spaced Prokaryotic Repeats Derive from Foreign Genetic Elements'. *Journal of Molecular Evolution* 60 (2): 174–82. https://doi.org/10.1007/s00239-004-0046-3.

Mroczek, Anna, Joanna Zawitkowska, Jerzy Kowalczyk, and Monika Lejman. 2021. 'Comprehensive Overview of Gene Rearrangements in Childhood T-Cell Acute Lymphoblastic Leukaemia'. *International Journal of Molecular Sciences* 22 (2): 808. https://doi.org/10.3390/ijms22020808.

Oki, Toshihiko, Francois Mercier, Hiroki Kato, Yookyung Jung, Thomas O. McDonald, Joel A. Spencer, Michael C. Mazzola, et al. 2021. 'Imaging Dynamic MTORC1 Pathway Activity in Vivo Reveals Marked Shifts That Support Time-Specific Inhibitor Therapy in AML'. *Nature Communications* 12 (1): 245. https://doi.org/10.1038/s41467-020-20491-8.

Pacini, Clare, Joshua M. Dempster, Isabella Boyle, Emanuel Gonçalves, Hanna Najgebauer, Emre Karakoc, Dieudonne van der Meer, et al. 2021. 'Integrated Cross-Study Datasets of Genetic Dependencies in Cancer'. *Nature Communications* 12 (1): 1661. https://doi.org/10.1038/s41467-021-21898-7.

Papaemmanuil, Elli, Moritz Gerstung, Lars Bullinger, Verena I. Gaidzik, Peter Paschka, Nicola D. Roberts, Nicola E. Potter, et al. 2016. 'Genomic Classification and Prognosis in Acute Myeloid Leukemia'. *New England Journal of Medicine* 374 (23): 2209–21. https://doi.org/10.1056/NEJMoa1516192.

Passaro, Diana, Marta Irigoyen, Claire Catherinet, Stéphanie Gachet, Cindy Da Costa De Jesus, Charlène Lasgi, Christine Tran Quang, and Jacques Ghysdael.

2015. ‘CXCR4 Is Required for Leukemia-Initiating Cell Activity in T Cell Acute Lymphoblastic Leukemia’. *Cancer Cell* 27 (6): 769–79. https://doi.org/10.1016/j.ccell.2015.05.003.

Passweg, J R, H Baldomero, P Bader, C Bonini, S Cesaro, P Dreger, R F Duarte, et al. 2016. ‘Hematopoietic Stem Cell Transplantation in Europe 2014: More than 40 000 Transplants Annually’. *Bone Marrow Transplantation* 51 (6): 786–92. https://doi.org/10.1038/bmt.2016.20.

Quessada, Julie, Wendy Cuccuini, Paul Saultier, Marie Loosveld, Christine J. Harrison, and Marina Lafage-Pochitaloff. 2021. ‘Cytogenetics of Pediatric Acute Myeloid Leukemia: A Review of the Current Knowledge’. *Genes* 12 (6): 924. https://doi.org/10.3390/genes12060924.

Ramakrishnan, Ramprasad, Pablo Peña-Martínez, Puneet Agarwal, Maria Rodriguez-Zabala, Marion Chapellier, Carl Högberg, Mia Eriksson, et al. 2020. ‘CXCR4 Signaling Has a CXCL12-Independent Essential Role in Murine MLL-AF9-Driven Acute Myeloid Leukemia’. *Cell Reports* 31 (8): 107684. https://doi.org/10.1016/j.celrep.2020.107684.

Rehe, Klaus, Kerrie Wilson, Simon Bomken, Daniel Williamson, Julie Irving, Monique L. den Boer, Martin Stanulla, et al. 2013. ‘Acute B Lymphoblastic Leukaemia-Propagating Cells Are Present at High Frequency in Diverse Lymphoblast Populations’. *EMBO Molecular Medicine* 5 (1): 38–51. https://doi.org/10.1002/emmm.201201703.

Rich, Jeremy N. 2016. ‘Cancer Stem Cells: Understanding Tumor Hierarchy and Heterogeneity’. *Medicine* 95 (Suppl 1): S2–7. https://doi.org/10.1097/MD.0000000000004764.

Roberts, Charles W. M., Monique M. Leroux, Mark D. Fleming, and Stuart H. Orkin. 2002. ‘Highly Penetrant, Rapid Tumorigenesis through Conditional Inversion of the Tumor Suppressor Gene Snf5’. *Cancer Cell* 2 (5): 415–25. https://doi.org/10.1016/s1535-6108(02)00185-x.

Rose-Inman, Hayley, and Damon Kuehl. 2014. ‘Acute Leukemia’. *Emergency Medicine Clinics of North America* 32 (3): 579–96. https://doi.org/10.1016/j.emc.2014.04.004.

Salvaris, Ross, and Pasquale Luke Fedele. 2021. ‘Targeted Therapy in Acute Lymphoblastic Leukaemia’. *Journal of Personalized Medicine* 11 (8): 715. https://doi.org/10.3390/jpm11080715.

Samra, Bachar, Elias Jabbour, Farhad Ravandi, Hagop Kantarjian, and Nicholas J. Short. 2020. ‘Evolving Therapy of Adult Acute Lymphoblastic Leukemia: State-of-the-Art Treatment and Future Directions’. *Journal of Hematology & Oncology* 13 (1): 70. https://doi.org/10.1186/s13045-020-00905-2.

Sarkies, Peter, and Julian E. Sale. 2012. ‘Cellular Epigenetic Stability and Cancer’. *Trends in Genetics* 28 (3): 118–27. https://doi.org/10.1016/j.tig.2011.11.005.

Saygin, Caner, Joseph Cannova, Wendy Stock, and Lori Muffly. 2022. ‘Measurable Residual Disease in Acute Lymphoblastic Leukemia: Methods and Clinical Context in Adult Patients’. *Haematologica* 107 (12): 2783–93. https://doi.org/10.3324/haematol.2022.280638.

Scholl, Sebastian, Maximilian Fleischmann, Ulf Schnetzke, and Florian H. Heidel. 2020. ‘Molecular Mechanisms of Resistance to FLT3 Inhibitors in Acute Myeloid Leukemia: Ongoing Challenges and Future Treatments’. *Cells* 9 (11): 2493. https://doi.org/10.3390/cells9112493.

Schuster, Stephen J., Jakub Svoboda, Elise A. Chong, Sunita D. Nasta, Anthony R. Mato, Özlem Anak, Jennifer L. Brogdon, et al. 2017. ‘Chimeric Antigen Receptor T Cells in Refractory B-Cell Lymphomas’. *The New England Journal of Medicine* 377 (26): 2545–54. https://doi.org/10.1056/NEJMoa1708566.

Senft, Daniela, and Irmela Jeremias. 2019. ‘Tumor Cell Dormancy-Triggered by the Niche’. *Developmental Cell* 49 (3): 311–12. https://doi.org/10.1016/j.devcel.2019.04.022.

Shalem, Ophir, Neville E. Sanjana, Ella Hartenian, Xi Shi, David A. Scott, Tarjei S. Mikkelsen, Dirk Heckl, et al. 2014. ‘Genome-Scale CRISPR-Cas9 Knockout Screening in Human Cells’. *Science* 343 (6166): 84–87. https://doi.org/10.1126/science.1247005.

Sheykhhasan, Mohsen, Hamed Manoochehri, and Paola Dama. 2022. ‘Use of CAR T-Cell for Acute Lymphoblastic Leukemia (ALL) Treatment: A Review Study’. *Cancer Gene Therapy* 29 (8): 1080–96. https://doi.org/10.1038/s41417-021-00418-1.

Short, Nicholas J., Marina Konopleva, Tapan M. Kadia, Gautam Borthakur, Farhad Ravandi, Courtney D. DiNardo, and Naval Daver. 2020. 'Advances in the Treatment of Acute Myeloid Leukemia: New Drugs and New Challenges'. *Cancer Discovery* 10 (4): 506–25. https://doi.org/10.1158/2159-8290.CD-19-1011.

Siegel, Rebecca L., Kimberly D. Miller, Hannah E. Fuchs, and Ahmedin Jemal. 2022. 'Cancer Statistics, 2022'. *CA: A Cancer Journal for Clinicians* 72 (1): 7–33. https://doi.org/10.3322/caac.21708.

Singh, Pirthipal, Benedict J. Harden, Benjamin J. Lillywhite, and Peter M. Broad. 2004. 'Identification of Kinase Inhibitors By An ATP Depletion Method'. *ASSAY and Drug Development Technologies* 2 (2): 161–69. https://doi.org/10.1089/154065804323056503.

Small, Sara, Timothy S. Oh, and Leonidas C. Platanias. 2022. 'Role of Biomarkers in the Management of Acute Myeloid Leukemia'. *International Journal of Molecular Sciences* 23 (23): 14543. https://doi.org/10.3390/ijms232314543.

Stock, Wendy, Selina M. Luger, Anjali S. Advani, Jun Yin, Richard C. Harvey, Charles G. Mullighan, Cheryl L. Willman, et al. 2019. 'A Pediatric Regimen for Older Adolescents and Young Adults with Acute Lymphoblastic Leukemia: Results of CALGB 10403'. *Blood* 133 (14): 1548–59. https://doi.org/10.1182/blood-2018-10-881961.

Stone, Richard M., Sumithra J. Mandrekar, Ben L. Sanford, Kristina Laumann, Susan Geyer, Clara D. Bloomfield, Christian Thiede, et al. 2017. 'Midostaurin plus Chemotherapy for Acute Myeloid Leukemia with a FLT3 Mutation'. *The New England Journal of Medicine* 377 (5): 454–64. https://doi.org/10.1056/NEJMoa1614359.

Sugiyama, Tatsuki, Hiroshi Kohara, Mamiko Noda, and Takashi Nagasawa. 2006. 'Maintenance of the Hematopoietic Stem Cell Pool by CXCL12-CXCR4 Chemokine Signaling in Bone Marrow Stromal Cell Niches'. *Immunity* 25 (6): 977–88. https://doi.org/10.1016/j.immuni.2006.10.016.

Suraweera, Amila, Kenneth J. O'Byrne, and Derek J. Richard. 2018. 'Combination Therapy With Histone Deacetylase Inhibitors (HDACi) for the Treatment of Cancer: Achieving the Full Therapeutic Potential of HDACi'. *Frontiers in Oncology* 8 (March): 92. https://doi.org/10.3389/fonc.2018.00092.

Teachey, David T, and Ching-Hon Pui. 2019. 'Comparative Features and Outcomes between Paediatric T-Cell and B-Cell Acute Lymphoblastic Leukaemia'. *The Lancet. Oncology* 20 (3): e142–54. https://doi.org/10.1016/S1470-2045(19)30031-2.

Terwilliger, T., and M. Abdul-Hay. 2017. 'Acute Lymphoblastic Leukemia: A Comprehensive Review and 2017 Update'. *Blood Cancer Journal* 7 (6): e577. https://doi.org/10.1038/bcj.2017.53.

Thastrup, Maria, Alasdair Duguid, Christian Mirian, Kjeld Schmiegelow, and Christina Halsey. 2022. 'Central Nervous System Involvement in Childhood Acute Lymphoblastic Leukemia: Challenges and Solutions'. *Leukemia* 36 (12): 2751–68. https://doi.org/10.1038/s41375-022-01714-x.

'The Nobel Prize in Chemistry 2020'. n.d. NobelPrize.Org. Accessed 30 March 2023. https://www.nobelprize.org/prizes/chemistry/2020/summary/.

Thol, Felicitas, and Arnold Ganser. 2020. 'Treatment of Relapsed Acute Myeloid Leukemia'. *Current Treatment Options in Oncology* 21 (8): 66. https://doi.org/10.1007/s11864-020-00765-5.

Tilburg, Cornelis M. van, Elke Pfaff, Kristian W. Pajtler, Karin P.S. Langenberg, Petra Fiesel, Barbara C. Jones, Gnana Prakash Balasubramanian, et al. 2021. 'The Pediatric Precision Oncology INFORM Registry: Clinical Outcome and Benefit for Patients with Very High-Evidence Targets'. *Cancer Discovery* 11 (11): 2764–79. https://doi.org/10.1158/2159-8290.CD-21-0094.

Ting, Pamela Y., Albert E. Parker, J. Scott Lee, Chris Trussell, Orzala Sharif, Fabio Luna, Glenn Federe, et al. 2018. 'Guide Swap Enables Genome-Scale Pooled CRISPR–Cas9 Screening in Human Primary Cells'. *Nature Methods* 15 (11): 941–46. https://doi.org/10.1038/s41592-018-0149-1.

Truong, Dong-Jiunn Jeffery, Karin Kühner, Ralf Kühn, Stanislas Werfel, Stefan Engelhardt, Wolfgang Wurst, and Oskar Ortiz. 2015. 'Development of an Intein-Mediated Split-

Cas9 System for Gene Therapy'. *Nucleic Acids Research* 43 (13): 6450–58. https://doi.org/10.1093/nar/gkv601.

Tsherniak, Aviad, Francisca Vazquez, Phil G. Montgomery, Barbara A. Weir, Gregory Kryukov, Glenn S. Cowley, Stanley Gill, et al. 2017. 'Defining a Cancer Dependency Map'. *Cell* 170 (3): 564-576.e16. https://doi.org/10.1016/j.cell.2017.06.010.

Tsitsiridis, George, Ralph Steinkamp, Madalina Giurgiu, Barbara Brauner, Gisela Fobo, Goar Frishman, Corinna Montrone, and Andreas Ruepp. 2023. 'CORUM: The Comprehensive Resource of Mammalian Protein Complexes–2022'. *Nucleic Acids Research* 51 (D1): D539–45. https://doi.org/10.1093/nar/gkac1015.

Tzelepis, Konstantinos, Hiroko Koike-Yusa, Etienne De Braekeleer, Yilong Li, Emmanouil Metzakopian, Oliver M. Dovey, Annalisa Mupo, et al. 2015. 'A Crispr/Cas9 Drop-out Screen Identifies Genome-Wide Genetic Valnerubilities in Acute Myeloid Leukaemia'. *Blood* 126 (23): 554. https://doi.org/10.1182/blood.V126.23.554.554.

Uy, Geoffrey L., Sumithra J. Mandrekar, Kristina Laumann, Guido Marcucci, Weiqiang Zhao, Mark J. Levis, Heidi D. Klepin, et al. 2017. 'A Phase 2 Study Incorporating Sorafenib into the Chemotherapy for Older Adults with FLT3-Mutated Acute Myeloid Leukemia: CALGB 11001'. *Blood Advances* 1 (5): 331–40. https://doi.org/10.1182/bloodadvances.2016003053.

Valent, Peter, Alberto Orfao, Stefan Kubicek, Philipp Staber, Torsten Haferlach, Michael Deininger, Karoline Kollmann, et al. 2021. 'Precision Medicine in Hematology 2021: Definitions, Tools, Perspectives, and Open Questions'. *HemaSphere* 5 (3): e536. https://doi.org/10.1097/HS9.0000000000000536.

Vick, Binje, Maja Rothenberg, Nadine Sandhöfer, Michela Carlet, Cornelia Finkenzeller, Christina Krupka, Michaela Grunert, et al. 2015. 'An Advanced Preclinical Mouse Model for Acute Myeloid Leukemia Using Patients' Cells of Various Genetic Subgroups and in Vivo Bioluminescence Imaging'. *PloS One* 10 (3): e0120925. https://doi.org/10.1371/journal.pone.0120925.

Waclawiczek, Alexander, Aino-Maija Leppa, Simon Renders, Karolin Stumpf, Cecilia Reyneri, Barbara Betz, Maike Janssen, et al. 2023. 'Combinatorial BCL-2 Family Expression in Acute Myeloid Leukemia Stem Cells Predicts Clinical Response to Azacitidine/Venetoclax'. *Cancer Discovery*, March, CD-22-0939. https://doi.org/10.1158/2159-8290.CD-22-0939.

Wang, Dong. 2018. 'Some Further Thoughts about Spectral Kurtosis, Spectral L2/L1 Norm, Spectral Smoothness Index and Spectral Gini Index for Characterizing Repetitive Transients'. *Mechanical Systems and Signal Processing* 108 (August): 360–68. https://doi.org/10.1016/j.ymssp.2018.02.034.

Wang, Joy Y., and Jennifer A. Doudna. 2023. 'CRISPR Technology: A Decade of Genome Editing Is Only the Beginning'. *Science* 379 (6629): eadd8643. https://doi.org/10.1126/science.add8643.

Wang, Tim, Kıvanç Birsoy, Nicholas W. Hughes, Kevin M. Krupczak, Yorick Post, Jenny J. Wei, Eric S. Lander, and David M. Sabatini. 2015. 'Identification and Characterization of Essential Genes in the Human Genome'. *Science (New York, N.Y.)* 350 (6264): 1096–1101. https://doi.org/10.1126/science.aac7041.

Wang, Tim, Jenny J. Wei, David M. Sabatini, and Eric S. Lander. 2014. 'Genetic Screens in Human Cells Using the CRISPR-Cas9 System'. *Science* 343 (6166): 80–84. https://doi.org/10.1126/science.1246981.

Wang, Tim, Haiyan Yu, Nicholas W. Hughes, Bingxu Liu, Arek Kendirli, Klara Klein, Walter W. Chen, Eric S. Lander, and David M. Sabatini. 2017. 'Gene Essentiality Profiling Reveals Gene Networks and Synthetic Lethal Interactions with Oncogenic Ras'. *Cell* 168 (5): 890-903.e15. https://doi.org/10.1016/j.cell.2017.01.013.

Wanior, Marek, Andreas Krämer, Stefan Knapp, and Andreas C. Joerger. 2021. 'Exploiting Vulnerabilities of SWI/SNF Chromatin Remodelling Complexes for Cancer Therapy'. *Oncogene* 40 (21): 3637–54. https://doi.org/10.1038/s41388-021-01781-x.

Wieduwilt, Matthew J., Wendy Stock, Anjali Advani, Selina Luger, Richard A. Larson, Martin Tallman, Frederick Appelbaum, et al. 2021. 'Superior Survival with Pediatric-Style Chemotherapy Compared to Myeloablative Allogeneic Hematopoietic Cell Transplantation in Older Adolescents and Young Adults with Ph-Negative Acute

Lymphoblastic Leukemia in First Complete Remission: Analysis from CALGB 10403 and the CIBMTR'. *Leukemia* 35 (7): 2076–85. https://doi.org/10.1038/s41375-021-01213-5.

Wilson, Boris G., Xi Wang, Xiaohua Shen, Elizabeth S. McKenna, Madeleine E. Lemieux, Yoon-Jae Cho, Edward C. Koellhoffer, Scott L. Pomeroy, Stuart H. Orkin, and Charles W. M. Roberts. 2010. 'Epigenetic Antagonism between Polycomb and SWI/SNF Complexes during Oncogenic Transformation'. *Cancer Cell* 18 (4): 316–28. https://doi.org/10.1016/j.ccr.2010.09.006.

Wirth, Anna-Katharina, Lucas Wange, Sebastian Vosberg, Kai-Oliver Henrich, Christian Rausch, Erbey Özdemir, Christina M. Zeller, et al. 2022. 'In Vivo PDX CRISPR/Cas9 Screens Reveal Mutual Therapeutic Targets to Overcome Heterogeneous Acquired Chemo-Resistance'. *Leukemia* 36 (12): 2863–74. https://doi.org/10.1038/s41375-022-01726-7.

Worst, Barbara C., Cornelis M. van Tilburg, Gnana Prakash Balasubramanian, Petra Fiesel, Ruth Witt, Angelika Freitag, Miream Boudalil, et al. 2016. 'Next-Generation Personalised Medicine for High-Risk Paediatric Cancer Patients – The INFORM Pilot Study'. *European Journal of Cancer* 65 (September): 91–101. https://doi.org/10.1016/j.ejca.2016.06.009.

Xiao, Jing, Jiasheng Mu, Tian-Run Liu, and Haineng Xu. 2017. 'Dig the Root of Cancer: Targeting Cancer Stem Cells Therapy'. *Journal of Medical Discovery* 2 (April): JMD17003. https://doi.org/10.24262/jmd.2.2.17003.

Xie, Zhuorui, Allison Bailey, Maxim V. Kuleshov, Daniel J. B. Clarke, John E. Evangelista, Sherry L. Jenkins, Alexander Lachmann, et al. 2021. 'Gene Set Knowledge Discovery with Enrichr'. *Current Protocols* 1 (3): e90. https://doi.org/10.1002/cpz1.90.

Xue, Liang, Wen-Horng Wang, Anton Iliuk, Lianghai Hu, Jacob A. Galan, Shuai Yu, Michael Hans, Robert L. Geahlen, and W. Andy Tao. 2012. 'Sensitive Kinase Assay Linked with Phosphoproteomics for Identifying Direct Kinase Substrates'. *Proceedings of the National Academy of Sciences* 109 (15): 5615–20. https://doi.org/10.1073/pnas.1119418109.

Yamauchi, Takuji, Takeshi Masuda, Matthew C. Canver, Michael Seiler, Yuichiro Semba, Mohammad Shboul, Mohammed Al-Raqad, et al. 2018. 'Genome-Wide CRISPR-Cas9 Screen Identifies Leukemia-Specific Dependence on a Pre-MRNA Metabolic Pathway Regulated by DCPS'. *Cancer Cell* 33 (3): 386-400.e5. https://doi.org/10.1016/j.ccell.2018.01.012.

Zhang, Jing, Yan Gu, and Baoan Chen. 2019. 'Mechanisms of Drug Resistance in Acute Myeloid Leukemia'. *OncoTargets and Therapy* 12 (March): 1937–45. https://doi.org/10.2147/OTT.S191621.

Zhang, Lu, Tianyu Cai, Xiaoyu Lin, Xiaoli Huang, Mai H. Bui, Joshua P. Plotnik, Richard J. Bellin, et al. 2021. 'Selective Inhibition of the Second Bromodomain of BET Family Proteins Results in Robust Antitumor Activity in Preclinical Models of Acute Myeloid Leukemia'. *Molecular Cancer Therapeutics* 20 (10): 1809–19. https://doi.org/10.1158/1535-7163.MCT-21-0029.

Zoughlami, Younes, Carlijn Voermans, Kim Brussen, Karel A. van Dort, Neeltje A. Kootstra, David Maussang, Martine J. Smit, Peter L. Hordijk, and Paula B. van Hennik. 2012. 'Regulation of CXCR4 Conformation by the Small GTPase Rac1: Implications for HIV Infection'. *Blood* 119 (9): 2024–32. https://doi.org/10.1182/blood-2011-06-364828.

Zuber, Johannes, Junwei Shi, Eric Wang, Amy R. Rappaport, Harald Herrmann, Edward A. Sison, Daniel Magoon, et al. 2011. 'RNAi Screen Identifies Brd4 as a Therapeutic Target in Acute Myeloid Leukaemia'. *Nature* 478 (7370): 524–28. https://doi.org/10.1038/nature10334.

7. Danksagung

Zuerst möchte ich mich bei Prof. Irmela Jeremias für die Betreuung und Unterstützung bedanken. Liebe Irmela, von Herzen vielen lieben Dank für deine Hilfe in allen Lebenslagen. Das ist nicht selbstverständlich und ich bin dir wirklich sehr dankbar für alles.

Ebenfalls einen großen Dank an Prof. Marc Schmidt-Supprian für die Betreuung meiner Doktorarbeit und den wissenschaftlichen Austausch und die Anregungen während unserer Treffen.
Ein herzliches Dankeschön auch an die weiteren Mitglieder meines Thesis Advisory Committees, Prof. Dr. Arnd Kieser, Dr. Christian Braun und Dr. Martin Becker. Euch allen vielen Dank für die anregenden Meetings und die Unterstützung.

Besonders möchte ich mich bei Dr. Martin Becker bedanke, der mir mit seiner hervorragenden Vorarbeit, Unterstützung und seinen Ideen diese tolle Doktorarbeit möglich gemacht hat. Lieber Martin, ich höre immer noch „Go big, or go home!“. Danke für die tolle Zeit, auch wenn sie viel zu kurz war.

Ein weiteres großes Dankeschön an Dr. Maryam Ghalandary für die Hilfe mit der S2 Arbeit als es mir nicht mehr möglich war und der Korrektur dieser Arbeit. Thank you so much, Maryam!

Vielen lieben Dank auch der ganzen restlichen AHS Gruppe und ganz besonders Romina Ludwig. Liebe Romina, vielen Dank für deine Hilfe bei der ganzen S2 Arbeit und deiner Unterstützung während dem Mutterschutz/Elternzeit.
Liebes 002 Büro, es war mir eine riesige Freude und ein Fest. Danke für die tolle Zeit inklusive unserer Stammtische und sozialen Events.

Und da das Beste bekanntlich zum Schluss kommt. Danke an meine Eltern und meine Schwester sowie meine Schwiegereltern für die Unterstützung und Hilfe. Liebe Mama, lieber Papa, liebe Eva, danke dass ihr die weite Strecke zu uns immer wieder auf euch genommen habt um uns zu besuchen und zu helfen.
Liebe Rita danke, dass du dich so toll um Tamina gekümmert hast und ich beruhigt arbeiten konnte.

Und dir Blacky danke ich für alles. Danke für deine Unterstützung in der teils doch harten Zeit, den wissenschaftlichen Diskussionen auf dem Balkon in Bayerisch Gmain und nicht zu Letzt für den Satz: „Geh erstmal studieren“. Here I am :D ♥♥